The Branched Chain Amino Acids in Autism Spectrum Disorders

by

Dora Clara Tărlungeanu

February, 2018

A thesis presented to the
Graduate School
of the
Institute of Science and Technology Austria, Klosterneuburg, Austria
in partial fulfillment of the requirements
for the degree of
Doctor of Philosophy

IST AUSTRIA
Institute of Science and Technology

The dissertation of Dora Clara Tărlungeanu, titled *The Branched Chain Amino Acids in Autism Spectrum Disorder*, is approved by

Supervisor: Gaia Novarino, IST Austria, Klosterneuburg, Austria

Signature: _____

Committee Member: Harald Janovjak, IST Austria, Klosterneuburg, Austria

Signature: _____

Committee Member: Michael Schmeisser, Otto-von-Guericke-Universität, Magdeburg, Germany

Signature: _____

Exam Chair: Daria Siekhaus, IST Austria, Klosterneuburg, Austria

Signature: _____

I hereby declare that this dissertation is my own work and that it does not contain other people's work without this being so stated; this thesis does not contain my previous work without this being stated, and the bibliography contains all the literature that I used in writing the dissertation.

I declare that this is a true copy of my thesis, including any final revisions, as approved by my thesis committee, and that this thesis has not been submitted for a higher degree to any other university or institution.

I certify that any republication of materials presented in this thesis has been approved by the relevant publishers and co-authors.

Signature: _____

Dora Clara Tărlungeanu

March 16, 2018

Abstract

Autism spectrum disorders (ASD) are a group of genetic disorders often overlapping with other neurological conditions. Despite the remarkable number of scientific breakthroughs of the last 100 years, the treatment of neurodevelopmental disorders (e.g. autism spectrum disorder, intellectual disability, epilepsy) remains a great challenge. Recent advancements in genomics, like whole-exome or whole-genome sequencing, have enabled scientists to identify numerous mutations underlying neurodevelopmental disorders. Given the few hundred risk genes that were discovered, the etiological variability and the heterogeneous phenotypic outcomes, the need for genotype- along with phenotype-based diagnosis of individual patients becomes a requisite.

Driven by this rationale, in a previous study our group described mutations, identified via whole-exome sequencing, in the gene *BCKDK* – encoding for a key regulator of branched chain amino acid (BCAA) catabolism - as a cause of ASD. Following up on the role of BCAAs, in the study described here we show that the *solute carrier transporter 7a5* (*SLC7A5*), a large neutral amino acid transporter localized mainly at the blood brain barrier (BBB), has an essential role in maintaining normal levels of brain BCAAs. In mice, deletion of *Slc7a5* from the endothelial cells of the BBB leads to atypical brain amino acid profile, abnormal mRNA translation and severe neurological abnormalities. Additionally, deletion of *Slc7a5* from the neural progenitor cell population leads to microcephaly. Interestingly, we demonstrate that BCAA intracerebroventricular administration ameliorates abnormal behaviors in adult mutant mice. Furthermore, whole-exome sequencing of patients diagnosed with neurological disorders helped us identify several patients with autistic traits, microcephaly and motor delay carrying deleterious homozygous mutations in the *SLC7A5* gene.

In conclusion, our data elucidate a neurological syndrome defined by *SLC7A5* mutations and support an essential role for the BCAAs in human brain function. Together with recent studies (described in chapter two) that have successfully made the transition into clinical practice, our findings on the role of BCAAs might have a crucial impact on the development of novel individualized therapeutic strategies for ASD.

Acknowledegements

The work presented here was carried out in the Neuroscience Department at IST Austria and was financially supported by NICHD (P01HD070494) and SFARI (grant 275275) to Joseph G.Gleeson and FWF (SFB35_3523) to Gaia Novarino; by CIDR for genome-wide SNP analysis (X01HG008823) and Broad Institute Center for Mendelian Disorders (UM1HG008900 to D. MacArthur); the Yale Center for Mendelian Disorders (U54HG006504 to Michele Galluccio); the Gregory M. Kiez and Mehmet Kutman Foundation; the Italian Ministry of Instruction University and Research (PON01_00937 to Cesare Indiveri) and NIH (R01-GM108911 to Avner Schlessinger). I am thankful to the MolTag Doctoral Program for offering me financial support to participate at conferences and workshops and I gratefully thank all the children with ASD and their families for participating in this study, without them this research would not have been possible.

I am very grateful to my supervisor, Dr. Gaia Novarino, for running this project with enthusiasm and giving me the opportunity to work on it and to contribute our findings to the scientific community. Working in her lab I learnt to overcome challenges and to adapt quickly to a dynamic environment, I developed a sharp attention to detail and I honed my critical thinking ability, which I am thankful and grateful for.

I would like to address a warm thank you to the members of my thesis committee (Dr. Gaia Novarino, Dr. Harald Janovjak, Dr. Michael Schmeisser, Dr. Cătălin Guet and Dr. Daria Siekhaus) for their time, guidance, friendship and support. I have been privileged to perform rotations in two other great labs before joining the Novarino group, thus I want to thank again Dr. Daria Siekhaus and Dr. Harald Janovjak for their invaluable patience and trust in me when I was just at the beginning of my journey at IST Austria and I had to learn concepts from scratch, and for their honest friendship, support and constant encouragements to pursue a scientific career.

Of our international collaborators, I would like to thank Kent E. Duncan and Philipp Christoph Janiesch for helping us with the polysome profiling experiments; Majdi Kara, Fatma Mujgan Sonmez, Kaya Bilguvar, Seham Esharif, Tawfeg Ben-Omran, Meral Topcu, Ahmet Okay Caglayan, Murat Gunel and Joseph G. Gleeson for recruiting and characterizing patients; Mariafrancesca Scalise, Michele Galluccio and Cesare Indiveri for performing proteoliposome experiments and Avner Schlessinger for the in silico analysis.

Of our internal collaborators at IST Austria, I would like to thank the Preclinical Facility for their help and support with animal experiments; Professor Ryuichi Shigemoto and the Electron Microscopy (EM) Facility for assistance with the EM experiments; Albert C. Manzano, Mike Liu and Florian Marr for technical assistance and the Bioimaging Facility for support with microscopy experiments.

I have been lucky to work with a number of wonderful colleagues and good friends. I want to thank all the past and present group members: Emanuela Morelli, Roberto Sacco, Ximena Contreras, Eva Reinthaler, Elena Deliu, Jasmin Morandell, Christoph Dotter, Mateja Tesulov, Rachele Danti and Lisa Knaus for all the nice and sometimes challenging times we spent together in the lab and for their friendship. I also want to thank Miroslava Spanova, Alvaro

Ingles, Inma Sanchez, Aparna Ratheesh and Damaris Rangel for their technical and moral support during my rotations and throughout my entire PhD. Special thanks goes to my colleagues Saritah, Justine and Dama who started their thesis in the same time as I did, with whom I spent lots of unforgettable moments and became good friends for life.

I want to thank all my friends back home for their moral support, advices and for not letting me forget the important things in life outside of the lab. I especially want to thank Delia, Roxi, Roxana and Simi for amazing moments together like trips abroad, EC or simple phone calls that made me realize that I can always count on them.

I warmly acknowledge my parents, my relatives and family friends for advices, support and relaxing/fun moments throughout my life.

Last but not least, I would like to thank my friend Reinhard for all his patience, especially when I was working late or on weekends and couldn't spend enough time together, support, kindness and for becoming the "voice of reason" in my ongoing life changes especially after my mom has passed away. Thank you for being there.

Vienna, January 3rd, 2018

Dora Clara Tărlungeanu

About the Author

Dora Clara Tărlungeanu completed a BSc and an MSc in Pharmacy at the University of Medicine and Pharmacy "Iuliu Hatieganu" in Cluj-Napoca (Romania) before joining IST Austria in September 2013. Her main research interests include understanding the role of genetics in the onset of autism spectrum disorder (ASD) and challenging the irreversibility aspects of ASD by employing mouse models. She worked on the research project "The Branched Chain Amino Acids in Autism Spectrum Disorders " with the Novarino group at IST Austria, and has published these results in the high-impact journal *Cell*. During her PhD studies, Dora has also presented her research results at several conferences and has earned a best poster award at the BioParadigms conference in Lausanne, Switzerland in 2017. Besides her scientific research interests, she was also part of organizing committees for scientific symposia at IST Austria like the Young Scientist Symposium 2016 and the Science Industry Day 2017.

List of Publications Appearing in Thesis

1. Dora C. Tărlungeanu et al. 2016. Impaired Amino Acid Transport at the Blood Brain Barrier is a Cause of Autism Spectrum Disorder. ***Cell***, 167, 1481-1494.

Table of Contents

Abstract v

Acknowledegements vi

About the Author viii

List of Publications Appearing in Thesis ix

List of Figures xiii

List of Tables xiv

List of Symbols/Abbreviations xv

1 Chapter 1 – Introduction 1

1.1 Autism Spectrum Disorders 1
1.1.1 Social and Communication Impairment 1
1.1.2 Repetitive and Restricted Behavior 2
1.2 Comorbidities 2
1.2.1 Intellectual Disability (ID) 2
1.2.2 Epilepsy 3
1.2.3 Motor abnormalities 3
1.3 Prevalence 3
1.4 Neuroanatomical Abnormalities in ASD 4
1.4.1 Cerebellar Dysfunction 4
1.4.2 Regional brain structures 5
1.4.3 Macrocephaly and microcephaly 5
1.5 The etiological landscape of ASD 5
1.6 Reversibility of ASD 7
1.7 Pathophysiological hypothesis underlying ASD 8
1.7.1 Excitation/inhibition (E/I) imbalance hypothesis 8
1.7.2 Protein synthesis defects in ASD 10
1.8 Discussion 12

2 Chapter 2 - Genomics in neurodevelopmental disorders: an avenue to personalized medicine 13

2.1 Introduction 13
2.2 Dissecting the genetics of NDDs 13
2.3 The promise of genetics 14
2.4 Modeling NDDs: potentials and limitations 15
2.5 Bridging the gap between research and clinic – personalized therapeutic approaches for NDDs 16
2.6 Discussion 18

3 Chapter 3 - Impaired amino acid transport at the blood brain barrier is a cause of autism spectrum disorder 20

3.1 Summary 20
3.2 Introduction 20
3.3 Methods 21
3.4 Results 37
3.4.1 SLC7A5 mediates BCAA flux at the BBB 37
3.4.2 Deletion of Slc7a5 from the BBB activates the AAR signal transduction pathway in the brain 39
3.4.3 Altered mRNA translation in Slc7a5 mutant mice 41
3.4.4 Slc7a5 conditional knock out animals show motor delay and autism-related phenotypes 41
3.4.5 Inhibitory activity defects in $Tie2^{Cre};Slc7a5^{fl/fl}$ mice 44

3.4.6 Tie2^{Cre};Slc7a5$^{fl/fl}$ mutant mice resemble Bckdk knock out animals 46
3.4.7 SLC7A5 mutations in patients with ASD and motor delay 46
3.4.8 Functional assessment of SLC7A5 A246V and P375L mutations 48
3.4.9 BCAA intracerebroventricular injections rescue neurological abnormalities in adult Slc7a5 mutant mice……. 50
3.4.10 Conditional deletion of Slc7a5 in the neuroprogenitor cells leads to microcephaly 52
3.5 DISCUSSION 56
4 Chapter 4 - Conclusions and future directions 58
5 References 60
6 Appendix 1. Supplemental figures and tables 74

List of Figures

Figure 1. ASD core symptoms with comorbidities and associated disorders. 2
Figure 2. Anatomical and functional brain areas affected in ASD, that are relevant to social behavior, communication and repetitive movements. 4
Figure 3. Genetic architecture of ASD depicting the variance in autism liability as determined by genetic and environmental factors. Non-additive effects: dominant, recessive or epistatic 6
Figure 4. Neuronal signaling pathways in translational regulation. 11
Figure 5. Genomic sequencing guides the way from patient DNA to personalized medicine. 18
Figure 6. Slc7a5 mediates BCAA flux at the BBB**.** 38
Figure 7. Activation of the amino acid response pathway in the brain of Slc7a5 mutant mice. 40
Figure 8. Neurobehavioral abnormalities in the $Tie2^{Cre}$;$Slc7a5^{fl/fl}$ mice. 43
Figure 9. Excitation/inhibition imbalance in $Tie2^{Cre}$;$Slc7a5^{fl/fl}$ somatosensory cortex. 45
Figure 10. Mutations in the human SLC7A5 lead to ASD and motor deficits. 47
Figure 11. A246V and P375L mutations compromise SLC7A5 function. 49
Figure 12. Normalization of $Tie2^{Cre}$;$Slc7a5^{fl/fl}$ mouse behavior after leucine and isoleucine i.c.v. administration. 51
Figure 13. Slc7a5 deletion from neural progenitor cells leads to microcephaly. 54

Figure S 1. Slc7a5 and Tie2Cre expression at the BBB, Related to Figure 6 74
Figure S 2. Slc7a5 does not transport neurotransmitters, Related to Figure 6 76
Figure S 3. Behavioral and electrophysiological alterations in Tie^{2Cre};$Slc7a5^{fl/fl}$ mice, Related to Figure 8 and 9 77
Figure S 4. Absence of gross alterations in brain architecture of Tie^{2Cre};$Slc7a5^{fl/fl}$ mice, Related to Figure 9. 80
Figure S 5. Phenotypic characterization of $Bckdk^{-/-}$ animals, Related to Figure 9. 81
Figure S 6. Genotyping information of Family 1426 and 1465, Related to Figure 10. 83
Figure S 7. Characterization of SLC7A5-A246V, -A246G and SLC7A5-P375L mutants, Related to Figure 11. 84

List of Tables

Table 1. Monogenic disorders with increased autism rate. 8

Table S 1. 85
Table S 2. 85
Table S 3. 86
Table S 4. 87
Table S 5. 88

List of Symbols/Abbreviations

ADHD – Attention Deficit Hyperactivity Disorder

ACC – Anterior Cingulate Cortex

Amy - Amygdala

AS – Angelman Syndrome

ASD – Autism Spectrum Disorder

BBB – Blood Brain Barrier

BCAA – Branched Chain Amino Acid

BDNF – Brain Derived Neurotrophic Factor

Cb – Cerebellum

CMA – Chromosome Microarray

CNS – Central Nervous System

DNM – *de novo* mutation

DS – Dravet Syndrome

FXS – Fragile X Syndrome

GWAS – Genome Wide Association Study

I.C.V. – Intracerebroventricular

IGF1 – Insulin Growth Factor 1

iPSC – induced Pluripotent Stem Cells

ID – Intellectual Disability

KO - Knockout

LTP – Long Term Potentiation

LTD – Long Term Depression

mPFC – medial Prefrontal Cortex

NDD – Neurodevelopmental Disorder

PMDS – Phelan-McDermid Syndrome

RS – Rett Syndrome

SNV – Single Nucleotide Variant

STR – Striatum

TS – Tuberous Sclerosis

WES – Whole Exome Sequencing

WGS – Whole Genome Sequencing

Chapter 1 – Introduction

1.1 Autism Spectrum Disorders

The term autism was employed for the first time in the early 1940s by Leo Kanner and Hans Asperger to describe a group of children that displayed unusual behavior and preference for isolation instead of social interaction. Nowadays, clinicians and researchers have replaced the term autism with "autism spectrum disorders" (ASD) to indicate a group of syndromes that share a heterogeneous pattern of inheritance and a constellation of symptoms which include early dysfunction in social interactions, communication deficits and the presence of repetitive and restricted behaviors (Figure 1) (Elsabbagh et al., 2012). Although in recent years a strong scientific and public interest has been directed towards ASD, making a diagnosis of autism is challenging due to the absence of early clinical manifestations and biomarkers (Daniels & Mandell, 2014). Thus, diagnosis is predominantly made after two years of age and it's mainly phenotype-driven endorsed by the Diagnostic and Statistical Manual of Mental Disorders (DSM) (Sharma, Mishra, & Mishra, 2015). Patients diagnosed with ASD often present with other comorbidities (see section 1.2.) like intellectual disability (ID – 35-40%) (Matson & Shoemaker, 2009), epilepsy (20-25%) (Canitano, 2007), motor abnormalities or language delay. Typically ASD has been classified into syndromic (when ASD occurs in conjunction with additional phenotypes) - Rett syndrome (RS) (Amir et al., 1999), Fragile X syndrome (FXS) (Verkerk et al., 1991), tuberous sclerosis (TS) (Kandt et al., 1992) and nonsyndromic (classic autism or idiopathic autism when ASD occurs with no additional symptoms). Evidence suggests that the causes involve both genetic and environmental factors (Y. S. Kim & Leventhal, 2015).

1.1.1 Social and Communication Impairment

One of the most essential and complex behaviors that define human interactions is social behavior. Social behavior relies on the ability of people to properly communicate with each other (verbally, non-verbally, via gestures or mimics), to sense, process and interpret social cues, to predict what someone will do next and respond with the appropriate behavior. Several brain areas, such as the medial prefrontal cortex, the amygdala or the anterior cingulate cortex are at interplay making up the so called "social brain" which mediates the social outcome (Frith, 2007) (Figure 2). Conversely, in ASD patients the social behavior is drastically impaired ranging from lack of basic communication skills, inability to initiate interactions or develop relationships, to lack of social or emotional reciprocity, to absence of interest in others' emotions and to impairments in nonverbal social interactions (Lord et al., 2000). In newborns the first signs of impaired social behavior are represented by the lack of innate preference for human voices and faces over other stimuli (Mills & Melhuish, 1974). Autistic infants display altered joint attention and inability to share eye gaze (Young, Merin, Rogers, & Ozonoff, 2009), while in older children lack of play with peers and isolation (Bauminger, Shulman, & Agam, 2003) are the common alerts for testing them for ASD. Language onset in ASD children is usually very late and is characterized by stereotyped phrases, echolalia (repetition of the same word/sound), intonation and rhythm problems. Non-verbal communication is also affected with an inability to express feelings, thoughts or even point at objects. At the other end of the spectrum are the ASD children that develop an uneven language (i.e. monologue) in a very narrow, restricted area of interest (e.g.

memorization, calendar calculation, music, math) without being able though to have a dialog about the same topics (Tager-Flusberg & Kasari, 2013). The neurophysiological substrates underlying social abnormalities are still an enigma, but based on human and animal model studies the excitatory-inhibitory activity imbalance theory, which leads to hyper- or hypo-activation of certain brain structures, could explain the mechanism behind social behavior abnormalities (Gogolla, Takesian, Feng, Fagiolini, & Hensch, 2014; Yizhar et al., 2011).

1.1.2 Repetitive and Restricted Behavior

The third dimension of the ASD core symptom triad describes the tendency of the patients to insist on sameness with adherence to routines (e.g. eating the same food in the same order, never taking a detour form a route) and display of a restricted pattern of behavior with repetitive motor movements, use of objects or speech. The highly fixated interests include also unusual interest in sensory environmental cues with hyper- or hyporeactivity and limited interest in spontaneous activities (Kanner, 1968). Although the exact neurobiological mechanism leading to this peculiar phenotype is still not completely understood, several recent studies in ASD animal models managed to narrow down the onset of a specific repetitive behavior to the dopaminergic medium spiny neural circuits within the striatum (Figure 2) (Rothwell et al., 2014) thus paving the road for future discoveries.

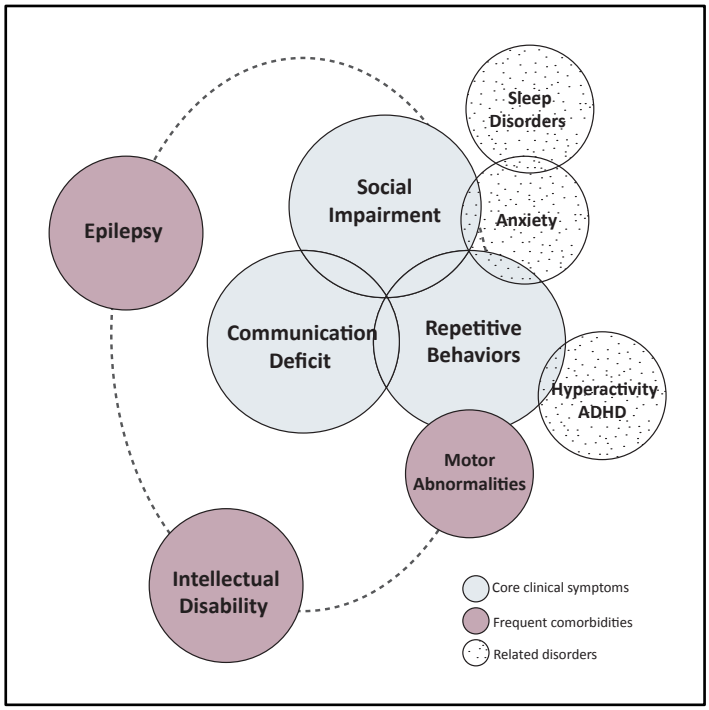

Figure 1. ASD core symptoms with comorbidities and associated disorders.

1.2 Comorbidities

1.2.1 Intellectual Disability (ID)

Is a neurodevelopmental disorder also referred to as cognitive impairment or mental retardation and it affects approximately 1.5-2% of the Western population (Mefford,

Batshaw, & Hoffman, 2012). ID ranges from mild to profound, and it can be associated with other clinical findings (syndromic ID) or it occurs isolated (non-syndromic ID). Clinical diagnosis is based on significant limitations in daily activities and an IQ below 70, which means that the diagnosis is not made until early adulthood. During early childhood the diagnosis is based on substantial motor, cognitive and speech delays. The severe forms of ID are thought to have a genetic origin, but in at least 50% of cases the cause remains elusive. Genetic research in ID has increased over the past decade and thus many autosomal or X-linked mental retardation genes, both inherited or *de novo (*variants that occur for the first time in the proband without being present in the parental genome), have been identified (Topper, Ober, & Das, 2011), with *FMR1* (FXS) being one of the most common inherited monogenic causes of ID and ASD in male patients (Bagni, Tassone, Neri, & Hagerman, 2012).

1.2.2 Epilepsy

Is a neurological condition characterized by recurrent spontaneous seizures that are due to abnormal neuronal activity, such as excessive excitation or hypersynchronization, and can occur as a result of developmental defects or due to insults (e.g. trauma, stress, etc) later on in life. With over 65 million people affected worldwide, epilepsy is the most common, chronic neurological disorder (Thurman et al., 2011). Epilepsy can be observed as comorbidity with other disorders or as an individual condition that comes in many different forms. Although in many cases seizures can be controlled, the treatment gap is still immense either due to costs or reduced accessibility or due to lack of response to medication (Cameron et al., 2012). Genetic underpinnings for epilepsies have been long recognized and over the past twenty years significant discoveries have been made such as: the large number of epilepsy risk genes, the complexities of phenotype-genotype relationships and the contribution of somatic mutations and noncoding microRNAs to epilepsy onset (Noebels, 2015; Poduri, Evrony, Cai, & Walsh, 2013).

1.2.3 Motor abnormalities

Motor symptomatology in autism is poorly understood and has received less attention than the classical ASD triad of symptoms even though already in 1943, in his early observations, Kanner mentioned that children with ASD presented with a “clumsy” gait and gross motor patterns (Kindregan, Gallagher, & Gormley, 2015). In recent years several studies have focused on the motor and sensory-motor behaviors of children with ASD, providing evidence that children diagnosed with ASD displayed less coordination and fewer motor capabilities (Fournier, Hass, Naik, Lodha, & Cauraugh, 2010). The most frequently reported motor behaviors range from imitation disorders, static and dynamic postural balance issues, decreased postural control and gait deviations (Paquet, Olliac, Golse, & Vaivre-Douret, 2016).

1.3 Prevalence

Over the past twenty years there has been a steady increase in the ASD cases mainly due to increased access to diagnostic services and increased awareness of the condition (Lenoir et al., 2009). Consequently, ASD represents an issue of public concern, as the estimated prevalence in the USA is 1 in 68 births, making ASD one of the most common neurodevelopmental disorders (Autism, Developmental Disabilities Monitoring Network Surveillance Year Principal, Centers for Disease, & Prevention, 2012). In addition, there is

also an uneven distribution between sexes, with a male to female ratio of approximately 4:1 (Fombonne, 2009). This strong male bias has been investigated and genetic studies suggested that females are protected from the effects of heritable and *de novo* ASD risk variants due to sex chromosomal genes (Lu & Cantor, 2012; Stone et al., 2004) or sex hormones (Sarachana, Xu, Wu, & Hu, 2011), which are regulating the effects of genetic variation on the onset of an ASD phenotype.

1.4 Neuroanatomical Abnormalities in ASD

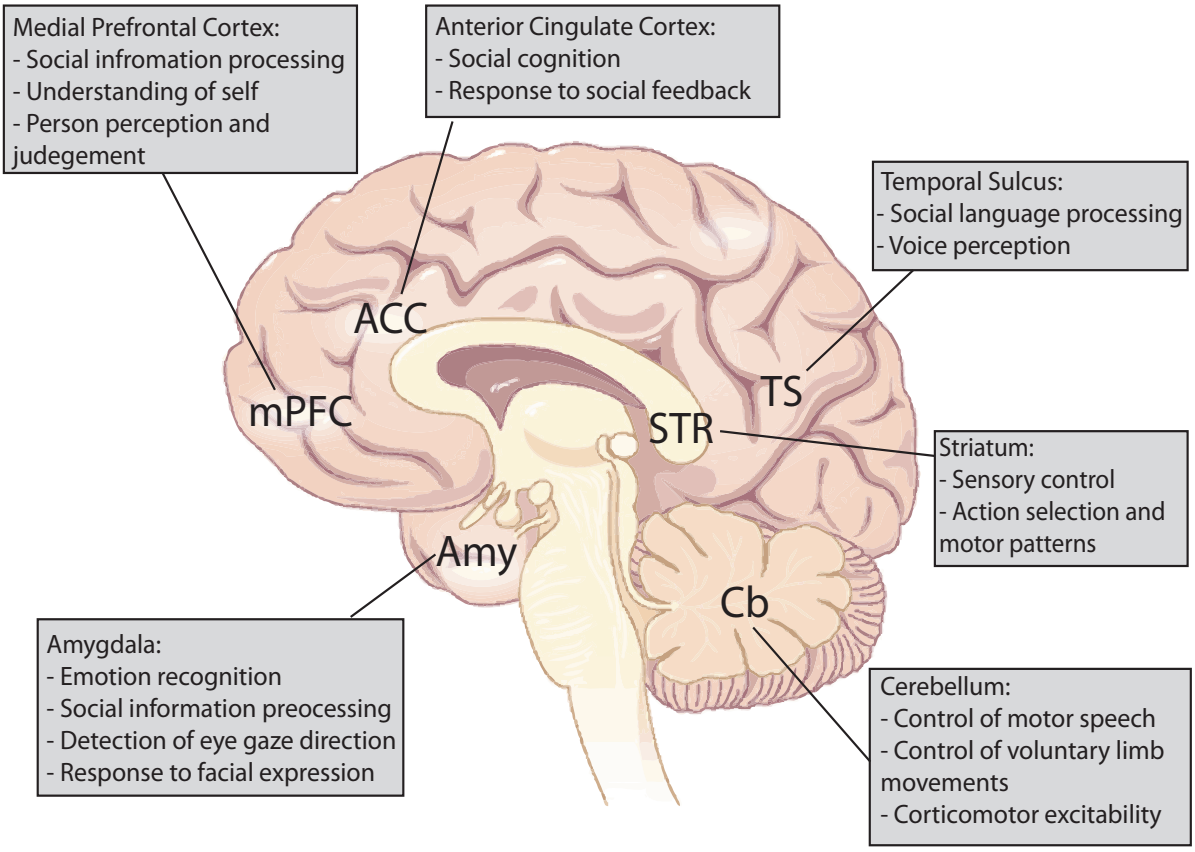

Figure 2. Anatomical and functional brain areas affected in ASD, that are relevant to social behavior, communication and repetitive movements (adapted from (Barak & Feng, 2016)).

1.4.1 Cerebellar Dysfunction

Motor abnormalities are a common observation among ASD patients (see section 1.2.3.) and their symptomatology is reminiscent of patients diagnosed with cerebellar deficits. Therefore, researchers have focused on these aspects revealing that cerebellar deficiencies are common in ASD and are often characterized by reduced Purkinje and granule cells (Whitney, Kemper, Bauman, Rosene, & Blatt, 2008). Neuroimaging studies revealed that the cerebellum (Figure 2) is involved in motor deficits via connections with the parietal lobe and

cortical and subcortical brain regions as well as via a lack of sensory integration of external stimuli (Rinehart et al., 2006; Schmahmann, Rosene, & Pandya, 2004).

1.4.2 Regional brain structures

Neuroimaging studies have revealed a series of core regions that mediate clinical phenotypes of ASD. The temporal sulcus and Broca's area seem to be related to deficits in language processing (Redcay, 2008) (Figure 2); the frontal lobe, parietal cortex and the amygdala mediate impairments of social behavior (J. E. Kim et al., 2010) (Figure 2) while the orbitofrontal cortex and the caudate nucleus have been associated with repetitive behaviors (Atmaca, Yildirim, Ozdemir, Tezcan, & Poyraz, 2007) (Figure 2). Interestingly, these key regions are not only specific for ASD manifestation but also for other disorders such as obsessive-compulsive disorder, anxiety and schizophrenia (Zarei et al., 2011).

1.4.3 Macrocephaly and microcephaly

In his initial findings, Kanner mentioned already that five out of the eleven children studied presented with larger heads. This feature was later observed in several other studies (Courchesne, Campbell, & Solso, 2011), revealing that one out of six autistic subjects displayed macrocephaly (Fombonne, Roge, Claverie, Courty, & Fremolle, 1999). Indeed, autism appears to be associated with either macrocephaly or microcephaly thus recent studies focused on understanding the pathological mechanism behind abnormal head growth. It has been shown that early overgrowth is caused by an increased expansion of cortical surface area rather than thickness before two years of age (Hazlett et al., 2011). Genome wide association studies (GWAS) of head size have shown a polygenic architecture in the general population. One of the main regulators of normal brain development is the evolutionarily conserved Ser/Thr protein kinase Mammalian Target of Rapamycin (mTOR). MTOR signaling is essential for the maintenance and differentiation of neuronal progenitors (i.e. soma size, neurite outgrowth), neuronal migration and synapse formation (Figure 4). Mutations in a series of upstream and downstream effectors of mTOR have been investigated and the outcomes were similar: macrocephaly, seizures and behavioral abnormalities (Kwon et al., 2006; Reijnders et al., 2017). A subset of ASD cases with increased head size (> 3 standard deviations) and overall somatic overgrowth have been associated with mutations in the phosphatase tensin homolog (PTEN) gene – mTOR upstream effector - which antagonizes the phosphoinositol-3-kinase/AKT signaling pathway and suppresses cell proliferation (Klein, Sharifi-Hannauer, & Martinez-Agosto, 2013; McBride et al., 2010). Additionally, a study investigating large ID & ASD cohorts indicated that mTOR variation contributes significantly to macrocephaly and identified *de novo* mutations in a key upstream mTOR regulator, *RHEB* (Reijnders et al., 2017). Conversely, several cases of autism with microcephaly have been reported (Fombonne et al., 1999; Miles, 2011). Irrespective of head over/undergrowth, how this physical abnormality relates to the behavioral and neuroanatomical features of ASD remains elusive.

1.5 The etiological landscape of ASD

On average a newborn acquires between 50-100 new genetic variants, resulting in 0.86 new amino acid altering mutations per individual (Lynch, 2010) and the recurrence of developing ASD in siblings of an affected individual range from 7-19% (Gronborg, Schendel, & Parner, 2013) with a heritability estimate of 31-71% (Gaugler et al., 2014). Given such a high

individual liability, a plethora of variants associated with ASD have been found in hundreds of different genes based on an extensive series of twin studies (Tick, Bolton, Happe, Rutter, & Rijsdijk, 2016) and GWAS (Gaugler et al., 2014), making ASD one of the most heritable neurodevelopmental disorder.

The identified variants range from chromosomal abnormalities, to recessive mutations, to single nucleotide changes (single nucleotide variants (SNV)) and to loss or gain of up to thousands of nucleotides (copy number variants (CNV)). Several studies identified rare combinations of common variants and many *de novo* germline variants with a large effect size as contributors to the total ASD genetic risk (Figure 3) (Iossifov et al., 2014; Sanders et al., 2015; Sanders et al., 2012). *De novo* germline mutations (DNM) occur usually in probands that posses also a normal allele (haploinssuficiency) and they are mostly represented by missense mutations – in general have gain-of–function effects and contribute to 12% of diagnoses; and by likely gene disrupting (LGD) mutations – comprising nonsense, frameshift or splice site variants that have predominantly a loss-of-function effect and contribute to 9% of diagnoses (Geisheker et al., 2017; Iossifov et al., 2014). Furthermore, rare genetic variants, both *de novo* and inherited, are causal in approximately 11% of the simplex cases (Sanders et al., 2015). Common genetic variants contribute to ASD risk in a high percentage (49%) (Figure 3) but the net effect to the individual liability is higher in the case of rare genetic events (Gaugler et al., 2014). However, germline mutations do not explain a considerable portion of ASD risk pointing out that other genetic contributions must be investigated. For instance, postzygotic (i.e. somatic) mutations explain a significant proportion of ASD cases, as shown by two studies published earlier this year (Krupp et al., 2017; Lim et al., 2017).

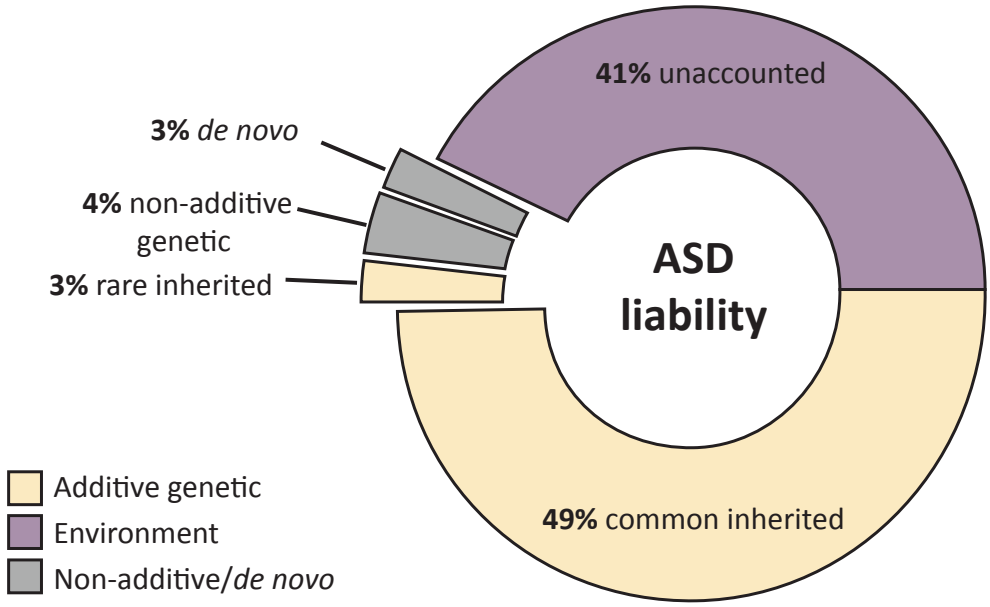

Figure 3. Genetic architecture of ASD depicting the variance in autism liability as determined by genetic and environmental factors. Non-additive effects: dominant, recessive or epistatic (adapted from (Gaugler et al., 2014)).

The combination of genetic and functional analyses has shown that a great number of the genes involved in such neurological disorders could ultimately converge along a small number of biological pathways. Indeed, many of the genes implicated in ASD encode for

proteins involved in synaptic function, excitation/inhibition balance, amino acid metabolism, transcriptional regulation and chromatin remodeling pathways (de la Torre-Ubieta, Won, Stein, & Geschwind, 2016); (Pinto et al., 2014); (De Rubeis et al., 2014; Novarino et al., 2012a). Knowing the genetic basis of a disorder makes it possible to generate accurate models that would allow to study the effects of any given mutation and to investigate the underlying mechanisms.

Even though the proportion of the phenotypic variance due to genetic factors is very high for autism, one should not disregard the importance of the environmental factors (e.g. viral infections) that may contribute to the etiology of autism (Figure 3). Furthermore, the possibility that a genetic defect alters features of brain development by affecting the immune system is receiving more and more attention. Several studies have shown that mediators of immune functions such as cytokines and chemokines also play a role in brain development (e.g. synaptogenesis) (Edmonson, Ziats, & Rennert, 2016).

In addition to the already complex etiology of ASD, research has focused also on epigenetics, a prime mediator of the environmental effects on genomes and phenotypes, in order to characterize changes in ASD that are due to a molecular level on top of the DNA sequence, without modifications to the sequence itself. Epigenetic changes occur due to the recruitment of specific epigenetic "modifiers" that add specific small molecules (e.g. methyl/acetyl) to DNA or to its packaging proteins - the histones. Methylation is one of the most widely studied epigenetic marks and involves the addition of a methyl group to the cytosine in a CpG dinucleotide. Such CpG domains are reccurent in promoter and enhancer regions of the genome, and an increased methylation leads to a local closed chromatin structure which in many cases is associated with silencing of the associated gene thus the net effect will lead to the lack of the corresponding functional protein. Epigenetic changes are influenced both by genetic (e.g. local DNA sequence variation destroys binding affinity) and environmental (e.g. smoking, stress) variations and represent important etiological triggers for ASD onset (Loke, Hannan, & Craig, 2015; Zhubi, Cook, Guidotti, & Grayson, 2014).

Thus, given the complex architecture of autism, deciphering the various etiologies and their role in the pathophysiology of the disease is very challenging due to the high number of risk genes and the dynamic gene-environment interplay.

1.6 Reversibility of ASD

Although approaches like DNA microarrays and WGS or WES have revealed many mutations that are potentially causative for ASD onset, there are still no definitive cures or therapies available for this group of disorders. In addition, ASD is described as a neurodevelopmental disorder, most often attributed to abnormalities that occur in one or more critical developmental periods, implying that once one of these critical windows is closed it might be difficult or even impossible to develop certain abilities (Espinosa & Stryker, 2012). In other words this means that if a gene is required for a very specific developmental stage, restoring its activity at a later time point might not be sufficient to repair the consequences of its early absence. Therefore, ASD have always been considered to be non-curable/non-reversible disorders. Conversely, there are genes whose protein products are required throughout the entire lifespan, highlighting the potential for a later time point restoration. Recently, several studies have challenged this view, thus implying that correction of underlying genetic defects in certain cases may allow a molecular and behavioral plasticity

mechanism in the adult brain that would compensate or even correct developmental defects (Novarino et al., 2012a; Rothwell et al., 2014; Sztainberg et al., 2015; Tillotson et al., 2017).

1.7 Pathophysiological hypothesis underlying ASD

Despite accumulating extensive genetic information on the factors predisposing to ASD, the neurophysiological substrates leading to the onset remain poorly understood. Attempts to elucidate these substrates have led to the emergence of several theories/hypothesis speculating that different genetic glitches can give rise to a similar phenotype thus unifying genetic factors under a common pathophysiological umbrella (Markram & Markram, 2010). Some of these hypotheses are discussed below.

1.7.1 Excitation/inhibition (E/I) imbalance hypothesis

More than a decade ago an influential study postulated that autism and related disorders may arise due to a changed ratio between excitation and inhibition leading to an increased excitability of cortical circuitry (Rubenstein & Merzenich, 2003). Supportive evidence for this hypothesis stems from a series of studies that modeled monogenic ASD syndromes in animals (Table1).

Table 1. Monogenic disorders with increased autism rate.

Gene ..	Disorder	Rate of Autism	MR	Function
FMR1	FXS	15-30%	+	Translational repressor
TSC1/2	TS	20-60%	+	mTOR inhibitor
PTEN	Hamartoma Syndrome (ASD&macrocephaly)	ND	+	PI3K/mTOR inhibitor
MECP2	Rett syndrome	100%	+	Transcriptional repressor
UBE3A	Angelman syndrome	40%	+	E3 ubiquitin ligase
CACNA1C	Timothy syndrome	60%	+	L-type voltage-gated calcium channel (CaV1.2)
SCN1A	Dravet syndrome	ND	+	Sodium channel (NaV1.1)
NLGN3/4	Familial ASD	ND	+	Synaptic adhesion
NRXN1	Familial ASD	ND	+	Synaptic adhesion
SHANK3	Familial ASD	ND	+	PSD scaffolding

Many monogenic disorders are associated with autism and cognitive impairment. This table illustrates the estimated rate of ASD in each disease and the presence/absence of mental retardation (MR). ND – prevalence of autism association with the disorder not determined (adapted from (Kelleher & Bear, 2008)).

Particularly, heterozygous loss of function mutation of the sodium channel subunit *SCN1A* is causing Dravet syndrome (DS), which is a severe form of childhood epilepsy associated with

ASD. Generation of a mouse model lacking one copy of the *Scn1a* gene selectively in the GABAergic forebrain neurons (the main cell type affected by this mutation) recapitulates all major symptoms like seizures, hyperactivity or social dysfunction (Han et al., 2012; Tai, Abe, Westenbroek, Scheuer, & Catterall, 2014). Interestingly, in this case a channelopathy (dysfunction of a sodium channel) leads to an interneuronopathy since the NaV1.1 (the protein product of the *Scn1a* gene) is mainly present on the axon initial segments of parvalbumin-positive (Pv+) fast-spiking and somatostatin –positive interneurons in the neocortex and hippocampus (Ogiwara et al., 2007; Tai et al., 2014). Hence, loss of its one copy prevents inhibitory activity of the Pv+ neurons and leads to the E/I imbalance.

Another disorder associated with both epilepsy and autistic behavior (20-60% of cases) (Numis et al., 2011) is TS, named after the presence of cortical malformations that resemble tubers. TS is an autosomal dominant disorder caused by mutations in the genes *TSC1* and *TSC2* which are both part of an upstream complex that is inhibiting mTORC1 (mammalian target of rapamycin complex 1) signaling, thus controlling processes like translation and growth in many tissues. In order to understand the underlying pathophysiology mouse models were generated in which the *Tsc1* gene was deleted selectively in glia/neural progenitor cells/forebrain excitatory neurons and they all presented with epilepsy highlighting multiple potential pathways for seizure onset (Carson, Van Nielen, Winzenburger, & Ess, 2012; Wong & Crino, 2012). Conditional deletion of *Tsc1* selectively from hippocampal pyramidal neurons revealed that the primary, cell-autonomous effect was a weakened inhibition caused by defective mTOR activity which in turn altered the excitatory and inhibitory synaptic transmission leading to hippocampal hyperexcitability (Bateup et al., 2013).

A particular disorder where both enhanced inhibition and reduced excitation have been reported in mouse models is the RS. RS is a neurodevelopmental syndrome characterized by mental retardation, autism and seizures. It is caused by mutations in *MECP2*, one of the most dosage-sensitive genes involved in neuronal functional integrity, covering a wide range of phenotypes based on deletion/duplication/truncation mutations (Amir et al., 1999). Although both types of defects have been reported, reduced excitation had a larger effect and it has been recapitulated across several studies including neocortical neurons from KO mice (Dani & Nelson, 2009), hippocampal neurons cultured from KO mice (E. D. Nelson, Kavalali, & Monteggia, 2006) and induced pluripotent stem cells from RS patients (Marchetto et al., 2010).

Thanks to technological advancements made in the field of optogenetics the E/I imbalance hypothesis could be tested in freely moving animals. By building a series of optogenetic tools that enabled a combinatorial interrogation of E/I imbalance, scientists were able to increase inhibitory cell excitability in the medial prefrontal cortex of mice and consequently rescue social deficits caused by E/I balance elevation in real-time (Yizhar et al., 2011).

Even though such hypothesis represent a very minimalistic concept because different brain circuits may be characterized by different excitation and inhibition requirements in order to maintain a proper function (i.e. social behavior), they are useful for explaining specific misregulations of brain circuits involved in developmental disorders (S. B. Nelson & Valakh, 2015). Namely, this hypothesis unifies evidences like the observation that many ASD risk genes are linked to gain-of-function phenotypes in ion channels and synaptic proteins (Bourgeron, 2009), the hyperactivity of the frontal brain regions (J. E. Kim et al., 2010) and the fact that approximately 30% of ASD patients present with clinically apparent seizures (Canitano, 2007).

1.7.2 Protein synthesis defects in ASD

Modeling monogenic disorders (Table 1) associated with ASD in animals revealed not only altered excitation/inhibition balance, as seen in 1.7.1, but also a set of negative regulators of synaptic protein synthesis which eventually may lead to defective synaptic development, altered plasticity and autistic phenotypes (Figure 4).

A supportive evidence in this sense is the FXS, an X-linked form of mental retardation associated with ASD (15-30%) caused by the silencing of the *FMR1* gene, whose protein product, the fragile X mental retardation protein (FMRP), binds to specific mRNAs and represses their translation (Figure 4). FMRP interacts with approximately 400 mRNAs and in FXS its absence leads to a translational de-repression of the targets with exaggerated protein synthesis (Brown et al., 2001). Knockout mouse models of the FXS recapitulate the human phenotype and display an increase in cerebral protein synthesis explaining one prominent theory of FXS which states that a consequence of the increased protein translation leads to an exaggerated long-term depression (LTD) of excitatory synapses via enhanced mGluR5 signaling (Darnell & Klann, 2013).

In the same vein, the altered protein translation hypothesis is also supported by TS disorder. Already mentioned in section 1.7.1, TS leads to an excitation/inhibition imbalance via excessive mTORC1 activation. One of the main effector mechanisms of mTORC1 is activation of the eukaryotic cap-dependent translation via binding of elongation initiation factor 4E (eIF4E) to the 5' mRNA cap which in turn allows recruitment of other elongation proteins and initiates translation (Richter & Sonenberg, 2005). The translation process is impeded by a family of unphosphorylated elongation binding proteins (4EBPs). Active mTORC1 phosphorylates 4EBPs making them unable to stall translation thus allowing cap-dependent initiation. Inactivation of *Tsc1/2* in hippocampal neurons upregulates mTORC1 activity supporting thus enhanced 4EBPs phosphorylation and increased protein translation (Figure 4).

Loss-of-function mutations in *PTEN,* another negative regulator of mTORC1 signaling, leads to hamartoma-tumor syndromes which include in their clinical spectrum ASD and macrocephaly (McBride et al., 2010). It is interesting to observe the association between *PTEN* and macrocephaly especially in view of the role of the mTOR pathway in regulating cell proliferation and cell growth, effect most likely mediated via translational control (Figure 4). To support this, mouse KO models of *Pten* cause neuronal hypertrophy and macrocephaly (Tilot, Frazier, & Eng, 2015).

In addition to the mTORC1 upstream effects of *TSC1/2* deletion, downstream mutations in genes like elongation initiation factor 4E-binding protein 2 (*EIF4EBP2)* – an eIF4E repressor downstream of mTORC1, led to altered protein translation. Deletion of mouse *Eif4ebp2* engenders ASD-like behavior, an enhanced translation of neuroligin (synaptic adhesion protein) mRNAs and augmented excitatory synaptic activity. Moreover, pharmacologically adjusting the eIF4E activity leads to correction of E/I imbalance and rescue of social behavior deficits of the *Eif4ebp2* knockout mice (Gkogkas et al., 2013).

Taken together, the association of mutations in *FMR1*, *TSC1/2*, *PTEN* and *EIF4EBP2* with ASD indicates that indeed alterations in translational repression may serve as a plausible mechanism leading to autistic phenotypes.

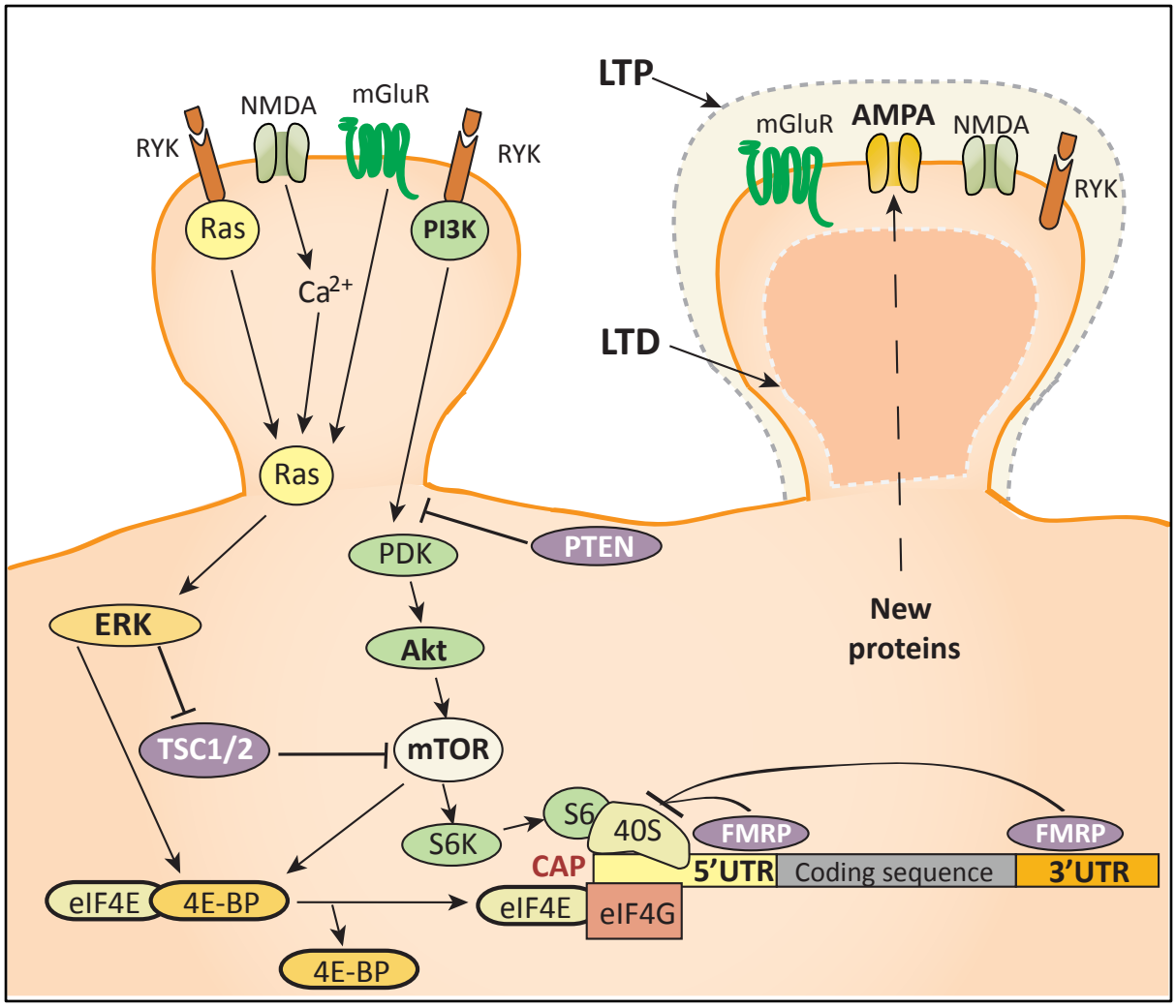

Figure 4. Neuronal signaling pathways in translational regulation.

The PI3K/mTOR and Ras/ERK pathways couple synaptic activity to downstream translational processes and play key roles in protein synthesis-dependent LTP (long-term potentiation) and LTD (long-term depression). These signaling pathways get recruited downstream of the activation of NMDA receptors, group I metabotropic glutamate receptors (mGluR) and neurotrophin Trk receptors (RYK). Availability of cap-binding elongation factor eIF4E via phosphorylation of 4E-BP is a main mechanism through which these pathways regulate protein translation. Depicted are also main repressors of these pathways (PTEN, TSC1/2 or FMRP). When mutated, the repressors cannot fulfill their normal constraints on synaptic activity-induced protein synthesis leading to an excessive translation that could explain one of the pathophysiological mechanisms behind ASD. → - phosphorylation; ----| - dephosphorylation (adapted from (Kelleher & Bear, 2008)).

1.8 Discussion

From the first description back in the early ‘40s the understanding of ASD has changed substantially. Based on the evidence provided in this chapter, one can conclude that ASD research has achieved much: it reached a consensus about behavioral definition; acknowledged the increased prevalence; clarified specific comorbidities that accompany ASD; discovered numerous rare and common genetic variants together with potential epigenetic and environmental factors contributing to the overall ASD risk; challenged the irreversibility concept; postulated the potential of convergence along common biological pathways for many risk genes and used a systems-level approach to understand neurobiology and pathophysiology.

However, the advances in ASD understanding brought also an increased complexity. Addressing the wide genetic heterogeneity and the possible treatments still remain a major challenge. Recent endeavors aimed at using genotype- along with phenotype- driven diagnosis will be presented in the next chapters, highlighting the current state of the field and paving potential avenues for individualized interventions.

2 Chapter 2 - Genomics in neurodevelopmental disorders: an avenue to personalized medicine

2.1 Introduction

The past decade has seen a rapid development of precise technological and methodological advancements in genetics and genomics, thus allowing an unprecedented identification of mutations that are involved in complex neurodevelopmental conditions. Neurodevelopmental disorders (NDDs) are characterized by mental impairments that persist throughout life, hampering development and learning, they affect more than 3% of children worldwide and they can be attributed to mutations at over 1000 loci (Shashi et al., 2014).
Understanding the etiology of NDDs faces many challenges that range from delineating the heritable genetic components, to defining individual factors that predispose to NDD risk and to establishing whether the hundreds of risk genes implicated might converge along a few biological pathways (de la Torre-Ubieta et al., 2016). In addition, the clinical and genetic heterogeneity of NDDs make diagnosing a lengthy and costly process complicating the quest for personalized medicine. However, the identification of bona fide genetic risk factors and the use of functional genomics to progress from mutation to phenotype represent a solid foundation for the development of individualized therapeutic approaches. In the previous chapter (See chapter 1) some features of these disorders were already mentioned and here the importance of genomics in elucidating the etiology of NDDs is further emphasized. In addition, advantages and limitations in the use of animal or stem cell models to study patient-specific genetic mutations are described. Eventually, the gap between research and translational medicine is bridged with a series of preclinical (See chapter 3) and clinical findings that created an evidence-based framework of how personalized medicine can advance the treatment of NDDs.

2.2 Dissecting the genetics of NDDs

Sequencing of the human and other mammalian genomes has provided an important set of tools to start understanding the human genetic variation. The first steps to elucidate the genetic heterogeneity of NDDs were done by using karyotyping or fluorescence in situ hybridization (FISH). As the need for more accurate detection of nucleotide variations in the context of developmental disabilities grew, chromosome microarray (CMA) technology was developed and rapidly implemented as part of first-line evaluation for children with a NDDs (Manning, Hudgins, Professional, & Guidelines, 2010; Volkmar et al., 2014). CMA has set the stage for genetic variation detection but it was the advent of WGS and WES that led to the identification of many inherited and *de novo* germline variants significantly contributing to the total NDD risk (Figure 5a,b).
The study of 1133 children with severe, undiagnosed developmental disorders, and their parents, using a combination of WES and array-based detection of chromosomal rearrangements, revealed 12 novel genes associated with NDDs. These results are of importance as they increase the proportion of children that could be diagnosed, from 28% to 31%. Moreover they encourage nationwide studies and the sharing of plausibly pathogenic variants observed in undiagnosed patients on web portals such as DECIPHER (Deciphering Developmental Disorders, 2015). In a similar fashion, WES of families (parents, affected child and one unaffected sibling) from the Simons Simplex Collection, enabled the

discovery of 120 new candidate genes with rare de novo SNV associated with ASD (Iossifov et al., 2014),(De Rubeis et al., 2014; Sanders et al., 2012) and the identification of a subclass of candidate genes (e.g. *RIMS1, CUL7*) where transmitted mutations may create a sensitized background but they are not completely penetrant (Krumm et al., 2015). DNM represent an important cause of NDDs, hence the term *de novo paradigm* for NDDs was coined. WES effectively detected DNM in patients presenting with ID (de Ligt et al., 2012; Vissers et al., 2010) and epilepsies (Lin et al., 2017; Nava et al., 2014). To complete the mutational characteristics of NDDs-relevant risk genes and to delineate genic and non-genic susceptibility variants, researchers have used WGS of quartet families (parents and two affected siblings). The results showed that affected siblings often carry different relevant mutations and they also demonstrated higher clinical variability than those that shared a risk variant (Yuen et al., 2015).

WES and WGS are already powerful when used individually but researchers have sought to cumulate their strengths and studied over 17000 DNM from 3500 trios across different NDDs (ASD, ID, epilepsy). The findings were of importance for they not only showed that the elevated DNM (a catalog of all the DNM identified among NDDs is freely available in the NPdenovo database) frequency is dominated by loss-of-function/deleterious SNV but it also identified 53 candidate genes that are associated with more than one disorder, suggesting a possible shared genetic etiology. This association of one or more independent phenotypes with the same gene or variation in the same gene is called phenotypic pleiotropy (Li et al., 2016). To better understand the pathophysiology of NDDs, it is then pertinent to ask whether such genes, that are associated with more than one disorder, are involved in common processes, or are active only in discrete brain areas at specific developmental time points (See chapter 1 – The genetic landscape of ASD).

Thus, the abovementioned technologies represent powerful tools for the molecular genetic dissection of patients affected by NDDs. Their venturing into clinical practice and association with the routine phenotype-driven diagnosis holds a promise for personalized diagnosis and therapy of NDDs.

2.3 The promise of genetics

The early occurrence of genetic glitches and the relatively late onset of symptoms that enable the diagnosis of NDDs, represent a major pitfall in identifying the cause and delivering the right kind of therapy. To complicate things further, for most of the NDDs therapies hinge largely on behavioral or educational interventions (Warren et al., 2011) and on treating associated rather than core symptoms of the disorder. Thus, for the majority of people with NDDs the outcomes are poor or very poor in adulthood (Fountain, Winter, & Bearman, 2012). Given such challenges, it is relevant to ask how could genetics contribute to their improvement.

First and foremost, genetic testing can lead to active monitoring and early intervention, even before the onset of the disorder. Furthermore, knowing the genetic cause of a disorder may implicate a specific biological pathway in its onset. Therefore, targeted pharmacological interventions could be made with already existing drugs. Studies reported that 55% of 187 genetic findings led to changes in clinical management (Henderson et al., 2014) and 10 out of 118 probands undergoing WES benefited from a revised diagnosis and clinical assessment (Dixon-Salazar et al., 2012). Lastly, since NDDs are associated with cognitive and behavioral profiles, genetic information can guide the choice of behavioral treatment (Bruining et al.,

2014). Nonetheless, despite these advantages, the multiple guidelines proposing the use of genetic testing for individuals with NDDs are not implemented constantly in clinical practice (Volkmar et al., 2014). This is either due to scarcity of resources, or due to a lack of medical staff prepared to analyze and interpret genetic results. To circumvent this, a proper dissemination of up to date findings about NDDs genetics to all clinical staff is desirable. On the other hand, there is genetic counseling, which would have an informative role among parents or families. Given that the recurrence rate with one previously affected sibling is around 15%, in case of ASD/ID, decisions regarding future pregnancies can be made with caution as long as the parents have access to specialized genetic counseling information (Wood et al., 2015).

2.4 Modeling NDDs: potentials and limitations

Along with the genetic advancements of the past decade came also the generation and characterization of numerous models for NDDs. An ideal model of a human disorder is characterized by construct validity (model mimics the genetic insult that causes the disease), face validity (the model's phenotype resembles the one of the human disease) and predictive validity (the model and the patients respond similarly to certain treatments) (Sztainberg & Zoghbi, 2016). Several systems (cells, rodents, primates) have been used to generate models of NDDs that can partially reproduce disease features and can be of interest for understanding underlying mechanisms as long as researchers acknowledge their limitations and do not overestimate their implications (Figure 5c).

The most favored model organism, the mouse, has been extensively employed for modeling neurological disorders with a known genetic cause, such as FXS (*Fmr1* KO) (FXS) (Bernardet & Crusio, 2006), Dravet syndrome (DS) (*Scn1a* KO) (Han et al., 2012), *Nrxn1a* KO (Grayton, Missler, Collier, & Fernandes, 2013), *Nlgn3* KO (Baudouin et al., 2012), Phelan-McDermid syndrome (PMDS-*Shank 3* KO) (Wang et al., 2011) or RS (*Mecp2* KO) (Hulbert & Jiang, 2016). Modeling NDDs in mice has many advantages since they share 95-98% genomic equivalence with humans, have a relatively rapid reproduction time, are cost-effective and allow scientists to precisely manipulate their genome in a temporal/spatial specific manner. However, mice also present with important limitations like evolutionary distance from humans, the impossibility to assess certain features as language and facial recognition. To overcome some of the limiting features, non-human primate models complement the mouse assays and due to their well-developed prefrontal cortex are expected to more closely model complex behavior and higher cortical functions (K. K. Watson & Platt, 2012), whereas zebrafish and invertebrates assure efficient, high-throughput genetic screens (McCammon & Sive, 2015).

Alongside animal models, *in vitro* use of stem cell biology enabled the generation and characterization of human neurons. Employing either human embryonic stem cells (hESCs) or human induced pluripotent stem cells (hiPSCs) differentiated into functional neurons, researchers managed to recapitulate several neuronal synaptic defects for monogenic forms of NDDs like RS (Marchetto et al., 2010), FXS (Elsabbagh et al., 2012; Urbach, Bar-Nur, Daley, & Benvenisty, 2010), Prader-Willi and Angelman syndromes (AS) (Chamberlain et al., 2010), PMDS (Shcheglovitov et al., 2013), DS (Jiao et al., 2013) and Timothy syndrome (Birey et al., 2017; S. P. Pasca et al., 2011). The genomic conservation, the high experimental tractability, the ability to model diseases with cells obtained directly from affected individuals and the unlimited source of cells to generate these models are just some of the advantages of stem

cell based technologies. Conversely, the high heterogeneity among iPSCs clones, the early postnatal developmental stages exhibited by neurons differentiated *in vitro*, the lack of high order connectivity or the difficulty to model neuronal migration and lamination in a 2D system are some of the obvious shortcomings of iPSC-derived disease models. Fortunately, recently several researchers developed protocols for the generation of 3D cortical organoids (mini-brains/spheroids) providing avenues to study features of cortical lamination and brain development *in vitro* (Hattori, 2014; A. M. Pasca et al., 2015) thus contributing additional tools for studying the mechanisms underlying NDDs (Birey et al., 2017; Quadrato, Brown, & Arlotta, 2016).

2.5 Bridging the gap between research and clinic – personalized therapeutic approaches for NDDs

Axiomatically the biggest advantage of genetic studies is to provide clues about the underlying neurobiology of NDDs and transition those clues into clinical practice (Figure 5d).
At present, the available treatment for NDDs consists of a combination of behavioral therapies (Zarafshan, Salmanian, Aghamohammadi, Mohammadi, & Mostafavi, 2017) and drugs approved for ameliorating comorbidities like irritability, anxiety and seizures, while in many cases the core symptoms of NDDs remain unsolved.
However, the combination of genetics and functional analysis led to the discovery of several molecular pathways involved in NDDs that were targeted to evaluate novel therapeutic strategies. Particularly, inhibiting the mechanistic target of rapamycin (mTOR) led to rescue of physiological, morphological and behavioral abnormalities in mice modeling diseases associated with protein translation defects like TS (Tsai et al., 2012), *PTEN*-associated macrocephaly (Zhou et al., 2009) or 15q11-13 duplication syndrome (Oguro-Ando et al., 2015). Multiple clinical trials, with pending results, are investigating the pharmacokinetics and pharmacodynamics of rapamaycin and its analogs (sirolimus, everolimus) for treating TS with associated ASD (Budde et al., 2016; Kohrman, 2012). Increasing levels of IGF1 and BDNF via transcriptional modulation through phosphatidylinositol 3-kinase (PI3K) signaling also rescued certain physiological and behavioral anomalies in RS mouse models (Castro et al., 2014; Kline, Ogier, Kunze, & Katz, 2010). Clinical studies investigating the use of human recombinant IGF1 in treating patients with RS (Pini et al., 2016) or with PMDS (Kolevzon et al., 2014) show some promising results. IGF1 administration leads to a higher endurance to social and cognitive testing in patients. Modulation of excitation/inhibition ratio has been completed with antagonists of mGluRs or agonists of GABA A and GABA B receptors, and has shown varying degrees of preclinical efficacy in mouse models of FXS displaying increased mGluR5 signaling (Darnell & Klann, 2013). However, several finished clinical trials with FXS patients did not report encouraging results. Contrary to what was predicted by a decade of studies in FXS animal models, administration of mavoglurant, an mGluR5 antagonist (Berry-Kravis et al., 2016) or arbaclofen, a GABA B receptor agonist (Lozano, Martinez-Cerdeno, & Hagerman, 2015; Veenstra-VanderWeele et al., 2017), to adolescents and adults showed no significant improvement of behavioral traits in a randomized, double-blind, placebo-controlled phase 2 trial. Conversely, in a mouse model of PMDS with complete deletion of *Shank3,* researchers reported a decreased mGluR5 signaling in the striatum and cortex. The administration of a benzamide derivative leads to an augmentation of mGluR5 activity and rescues the functional and behavioral defects in mice. Thus, pharmacological treatments aimed at increasing mGluR5 activity may represent an option

for patients with *SHANK3* mutations (Vicidomini et al., 2017; Wang et al., 2016). The contrasts between mGluR5 activity in FXS and PMDS suggest that the dysfunction leads to distinct phenotypes in different brain regions/genetic backgrounds highlighting the importance of genetically discriminating between different forms of NDDs and the convergence onto a common molecular pathway underlying NDDs pathophysiology (Figure 5d).

Recently, new approaches for the treatment of ASDs have been proposed using compounds for which the study rationale was based on genetic findings. For instance, AS is mostly caused by loss-of-function mutations in the maternal allele of the imprinted UB3A gene, while the paternal allele is silenced by a long noncoding RNA (*UBE3A* antisense transcript). Using antisense oligonucleotides (ASOs) (Figure 5d) the paternal allele was unsilenced restoring the UB3A protein levels and leading to improvement of cognitive deficits in an AS mouse model (Meng et al., 2015). Following a similar rationale, ASOs were used at restoring normal levels of MeCP2 and rescuing neurological deficits, both impaired social behavior and seizures, in a mouse carrying an extra copy of *Mecp2* (Sztainberg et al., 2015). Replacing a defective gene may as well be achieved by gene therapy using adeno-associated virus (AAV) vectors (Gadalla et al., 2017). However, making ASOs and AAV amenable to translation into clinical trials is challenging due to their safety, pharmacokinetics and distribution in the brain (Beaudet & Meng, 2016). In a similar vein, WES of consanguineous families with ASD, ID and epilepsy led to the identification of mutations in the gene *BCKDK* (Branched Chain Ketoacid Dehydrogenase Kinase), encoding an enzyme regulating the catabolism of the branched-chain amino acids (BCAAs). The *Bckdk* mouse model displayed abnormal brain amino acid profiles and dietary supplementation with the missing BCAAs reversed certain neurological phenotypes (Figure 5d). Furthermore, BCAAs dietary supplementation in patients led to a normalization of their plasma BCAA levels, pointing out the potential of BCAA supplementation as therapy in patients with *BCKDK* mutations (Garcia-Cazorla et al., 2014; Novarino et al., 2012a).

Besides identifying new targets for therapy, genetic findings are suitable for personalizing existing pharmacotherapy or behavioral interventions. In this sense, WES with targeted gene analysis (e.g. *SCN8A, KCNQ2*) is an effective diagnosis tool for patients with epilepsies influencing anti-epileptic drug selection, adverse effect minimization and consideration of epilepsy surgery based on each patient's genetic script (Balestrini et al., 2017). In the case of people with *SHANK3* deletions, they tend to have more advanced receptive communication skills than verbal language ability (Phelan & McDermid, 2012) thus they could rather benefit from assistive communication strategies that may not have been in focus unless the genetic cause of their ASD was known.

Newly, a very common trend uses genetic findings for the application of targeted drug repurposing based on single gene defects (Figure 5d). Such an approach already appears promising for personalizing therapies for epilepsy cases arising from gain-of-function mutations in ion-channel subunit genes (e.g. *GRIN2A, GRIN2B, SCN8A*). Nonetheless, important barriers remain in order to translate these approaches to non-ion channel epilepsy genes and loss-of-function mutations (Hu, Chen, Myers, Yuan, & Traynelis, 2016; Symonds, Zuberi, & Johnson, 2017). Likewise, recent observations indicate that metformin, a worldwide first-line therapy for type 2 diabetes, rescues core phenotypes in adult FXS mice due to a normalization of ERK signaling, of eIF4E phosphorylation and of matrix metalloproteinase 9 expression (MMP-9) (Gantois et al., 2017). Given that the previously mentioned clinical trials with mGluR5 antagonists have failed, metformin represents a new

therapeutic avenue for clinical studies involving FXS patients. Administration of oxytocin, a peptide usually administered to initiate uterine contractions that also appears to be involved in modulating social behavior, improved ASD-like social deficits in several mouse models (Insel, 2010) and in a *Shank3*-deficient rat (Harony-Nicolas et al., 2017), but the clinical effectiveness of oxytocin on ASD should still be considered tentative due to mixed findings (Ooi, Weng, Kossowsky, Gerger, & Sung, 2017).

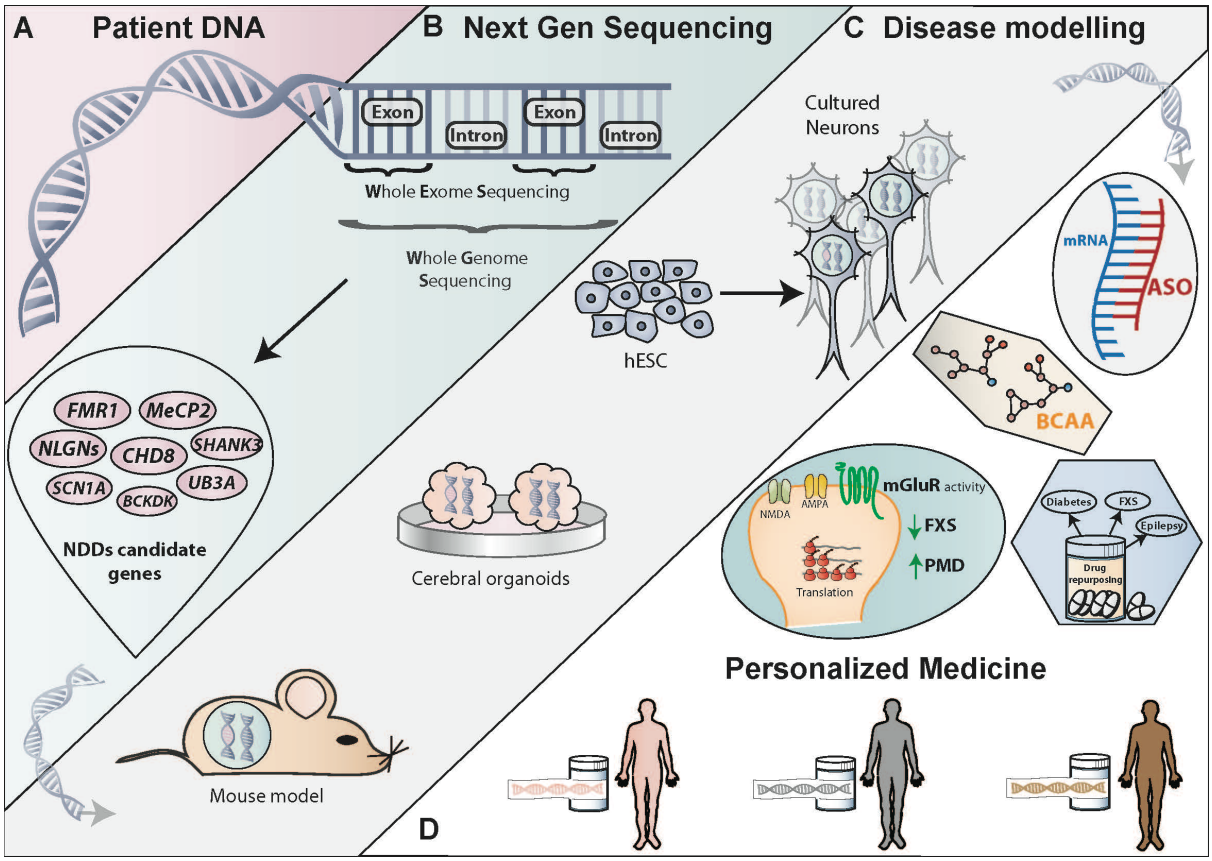

Figure 5. Genomic sequencing guides the way from patient DNA to personalized medicine.

(A). Patient DNA used for sequencing. (B). Next generation sequencing helps deciphering the genetic code within exons (dark blue section - whole exon sequencing) or throughout the entire genome (dark and light blue section - whole genome sequencing). Mutations are identified in a series of genes that are NDDs predisposing (pink ovals). (C). The mutations are regenerated in models (mice, organoids or hESC derived neurons) in order to understand their underlying mechanism. (D). Disease modeling reveals targets that enable the implementation of personalized medicine. ASO (antisense oligonucleotides - gray panel) and BCAA (branched chain amino acids - beige panel) are two examples of personalized therapies probed in mouse models. mGLUR (metabotropic glutamate receptor) activity (green panel) needs to be decreased in FXS and increased in PMDS. Drug repurposing (blue panel) enables the usage of the same drug for different diseases due to novel mechanisms identified.

2.6 Discussion

Genetic findings provide a solid causal foundation for understanding the relationship between molecular pathways, cellular and circuit dysfunction and eventually behavior.
The clinical impact of genetic knowledge is already relevant in daily practice, where for one third of the individuals with a NDD the genetic etiology can be established thus guiding the

identification of treatable somatic comorbidities and the implementation of genetic counseling.

Research done with animal models and in human cell lines helped putting into context the observations from post-mortem human brains and the genetic glitches identified in patients suffering from NDDs. However, for every question answered there is at least another one arising due to the very complex genetic nature of NDDs acknowledging the evermore need for an interdisciplinary approach combining genetics, functional genomics and experimental design and their integration into a robust biological model. Disease modeling is indeed a lengthy process that requires years of research but in the end it's a requisite that allows a safe knowledge transition from the bench to the clinic.

Based on considerations derived from experimental modeling, potential treatments for certain NDDs made it to the clinical trial avenue and most of them have simply failed. Such endeavors robustly point out the current obstacles in the translatability process: finding the critical time window for treatment, given the developmental roles of many NDDs genes and the right outcome measurement, choosing the right target, designing correctly the clinical trials, placebo effects or the mere lack of overlap between preclinical models and humans. In this sense, one of the most pertinent examples is the one of the FXS trials where one plausible explanation of the negative results could be the fact that the mGluR5 theory is either not valid, either the cohort was not properly stratified (e.g. per age) or it manifests differently in humans compared to rodents. Furthermore, identifying objective measures of response, such as biomarkers (Loth et al., 2016) that are robust and ideally have a parallel in animal models, will add to the current efforts of shifting from the one-size-fits-all model to personalized treatment models. In chapter 3 a potential personalized treatment model will be described based on preclinical data that could set the road for a possible transition into a future clinical trial.

3 Chapter 3 - Impaired amino acid transport at the blood brain barrier is a cause of autism spectrum disorder

3.1 Summary

In a previous article, abnormalities in the branched chain amino acid (BCAA) catabolic pathway were described as a cause of ASD. Here we show that the *solute carrier transporter 7a5* (*SLC7A5*), a large neutral amino acid transporter localized at the blood brain barrier (BBB), has an essential role in maintaining normal levels of brain BCAAs. In mice, deletion of *Slc7a5* from the endothelial cells of the BBB leads to atypical brain amino acid profile, abnormal mRNA translation and severe neurological abnormalities. Furthermore, we identified several patients with autistic traits and motor delay carrying deleterious homozygous mutations in the *SLC7A5* gene. Finally, we demonstrate that BCAA intracerebroventricular administration ameliorates abnormal behaviors in adult mutant mice. Our data elucidate a neurological syndrome defined by *SLC7A5* mutations and support an essential role for the BCAA in human brain function.

3.2 Introduction

Autism spectrum disorders (ASD) is a group of syndromes of heterogeneous etiologies. The genetic architecture of ASD is very complex and mutations in a single gene rarely account for a significant proportion of ASD patients. Despite their genetic heterogeneity, ASD may be less diverse functionally. Indeed, in many instances the great number of genes implicated in neurological disorders converges on a smaller number of biological pathways (See chapter 1) (De Rubeis et al., 2014).

We recently identified mutations in the gene *branched chain keto-acid dehydrogenase kinase* (*BCKDK*) in several patients with ASD, ID and epilepsy (Novarino et al., 2012a, 2012b). *BCKDK* is the enzyme responsible for the rate-limiting step in the catabolic pathway of the Branched Chain Amino Acids (BCAAs), a group of essential amino acids comprising valine, leucine and isoleucine. The most direct consequence of *BCKDK* mutations is a hyper-catabolism of the BCAAs, resulting in abnormally low levels of serum and brain BCAAs (Novarino et al., 2012a, 2012b).

The brain is dependent on a constant supply of BCAAs from the periphery. Should BCAAs be substantially important for the brain, factors facilitating BCAA uptake might be critical for the proper function of the central nervous system. The Large Neutral Amino Acid Transporter 1 (LAT1) is encoded by the *SLC7A5* gene (Verrey, 2003). The transporter is localized at the blood brain barrier (BBB) and forms a heterodimer with the glycoprotein CD98, encoded by the *SLC3A2* gene.

Here we studied a mouse model in which *Slc7a5* was deleted from the BBB and found that *Slc7a5* is particularly important to set brain BCAA levels within a normal range. Mice with defective BCAA transport at the BBB show abnormal activation of the amino acid response (AAR) pathway and a corresponding reduction in mRNA translation along with neuronal activity imbalance and behavioral problems. To probe whether *SLC7A5* is essential also in humans, we performed genetic analysis of a cohort of neurological pediatric patients. We identified and functionally validated, mutations in *SLC7A5* in several patients with ASD and

motor coordination problems. Notably, neurological abnormalities can be treated in adult mice by 3-week long intracerebroventricular (i.c.v.) BCAA delivery.

3.3 Methods

Experimental model and subject details

*Unless otherwise specified, experiments were performed by Dora Clara Tărlungeanu.

Mice

Experiments were performed in accordance with protocols approved by the Institutional Animal Care and Use Committee at IST Austria. Generation of the *Tie2*-Cre and *Slc7a5* floxed lines has been described previously (Kisanuki et al., 2001; Sinclair et al., 2013). For all experiments we made use of littermates derived from crossing Cre negative *Slc7a5*$^{fl/fl}$ females with Cre positive *Slc7a5*$^{fl/+}$ males. Mice were backcrossed to the N10 generation in C57BL/6J mice. Overall, *Tie2*^{Cre};*Slc7a5*$^{fl/fl}$ transgenic animals were viable and fertile. Mice were housed together with their littermates in groups of 3-4 animals per cage and kept on a regular 12 h light/dark cycle (7:00-19:00 light period). Food and water were available ad libitum. Experiments were carried out under pathogen-free conditions and health status of the mouse line was routinely checked by a veterinary. Experiments were carried out with randomly chosen littermates of the same sex. Both males and females were used with exception of the three-chamber test for which only males were employed. The genotype, age and developmental stage of the employed animals are specified separately for each experiment. For all the experiments the animals were drug and test naïve but when possible mice were employed for different tests starting with the less aversive test (see behavioral study description).

Human subjects and sample collection

Patients were identified from a cohort of over 2500 families, with at least one member of the family displaying a childhood onset neurological condition of likely genetic origin, from several world-wide recruitment efforts targeting patients with intellectual disability, structural brain diseases or neurodevelopmental disorders. Recruitment was focused in the major population centers of the Middle East including Morocco, Libya, Egypt, Saudi Arabia, Kuwait, UAE, Oman, Jordan, Pakistan, Turkey and Iran, with consanguinity rates (i.e. rate of marriage between first or second cousins) of approximately 50% compared with <1% is US and Western Europe. Among the recruited cohort, consanguinity was present in 63% of parents, suggesting some bias in sampling towards those with affected children due to recessive disease. Sampling was performed on both parents and all available genetically informative siblings to include affected and unaffected members, as well as extended family members if appropriate, consistent with IRB guidelines. All patients were evaluated directly by one of the co-authors with specialty training in neurology, child neurology and/or clinical genetics, and in accordance with local medical practices. All patients/families enrolled in IRB approved protocols based at referral institutions, and each family provided consent for study. Sequencing was performed on at least one but sometimes two affected or the father-mother-affected trio per family. Families 1426 and 1465 were identified and employed in this study because of comprising patients with homozygous disruptive mutations in the

SLC7A5 gene. Diagnosis of autism was set prior to whole exome sequencing and according to internationally accepted guidelines (DSM-V and CARS interview). Videos documenting the neurological examination and clinical features documentation were obtained in most of the cases.

Patient 1426-5 (female) was born at full term by normal delivery to a healthy mother after an uneventful pregnancy. There was no history of intellectual disability or epilepsy in the family. No chromosomal abnormalities were identified. Occipito-frontal head circumference (OFC) was -2 SD at birth and -5 SD in late childhood. The girl never learned to walk; she shows increased tone, clonus and dystonia since 5 years of age. She can bear some weight on the legs with support. She shows impaired social interaction, eye-to-eye gaze, and restrictive behaviors but has a social smile. She can understand simple commands but does not have speech. CARS (childhood autism rating scale) score at the age of 33 was 31 (autism cutoff 30). She has no seizures and she does not take any medication. She has no other health problems. There are no progressive features.

Patient 1426-6 (male), 1426-8 (female), 1426-16 (male) and 1426-19 (male) presentation and history are essentially similar to patient 1426-5. In late childhood all the patients present with various degrees of microcephaly (see Figure 10B). CARS score for patients 1426-6 and 1426-8 were 31 and 34 at the age of 17 and 12 years, respectively. Patient 1426-16 died of an unrelated cause during the preparation of this manuscript; therefore there is not updated information for this patient.
Importantly, all the affected individuals of family 1426 have normal plasma amino acid concentrations (Table S5).

Patient 1465-3 (male) was the second child, born to consanguineous parents (who were first cousins) at full term, after an uneventful pregnancy. He presented with intractable epilepsy and neurodevelopmental delay during his infancy period. The medical history of the family is notable for a previous case of microcephaly. The patient began walking at 48 months. Upon examination, his weight, height and head circumference measurements were under 3rd percent, he was hypotonic and microcephalic with slightly dysmorphic face. He was unable to speak. He had joint laxity in his lower extremities and pes planus in both feet.
Patient 1465-4 (male) has also been born at full term after a normal pregnancy, but displayed similar symptoms of abnormal development. Like his brother, he was brought to medical attention due to intractable seizures, which started when he was six months old. When he was 24-months-old he was able to sit without support. He never developed speech. At the time of examination, he was found to have microcephaly, hypotonia, slightly dysmorphic face, scoliosis, decreased subcutaneous fatty tissue and joint laxity in his hands and lower extremities. He was unable to speak or write, and was able to walk with support.

*Patient recruitment and characterization was done by Majdi Kara - Libya, Fatma Mujgan Sonmez - Turkey, Kaya Bilguvar - USA, Anide Johansen - USA, Seham Esharif - Libya, Tawfeg Ben-Omran - Qatar, Meral Topcu - Turkey, Murat Gunel - USA and Joseph Gleeson - USA.

Cell lines
Mutant and control fibroblasts were generated from explants of dermal biopsies following informed consent under protocols approved by the University of California San Diego or Yale

University. Primary skin fibroblasts from affected and unaffected passage-matched controls were cultured in Dulbecco's Modified Eagle Medium supplemented with 10% fetal bovine serum and 1X Penicillin-Streptomycin. Cell lines were maintained in a 5% CO_2 incubator at 37^{o}C. Cell lines were routinely tested to exclude *Mycoplasma* contaminations.

Protein model

The SLC7A5 homology model was built based on the X-ray structure of the agmatine/arginine AdiC transporter from *E. Coli* in the outward-occluded arginine-bound conformation (PDB identifier 3L1L (Gao et al., 2010)). SLC7A5 and AdiC are members of the amino acid-polyamine-organocation (APC) transporter superfamily and exhibit sequence identity of about 22% (Geier et al., 2013; Saier, Yen, Noto, Tamang, & Elkan, 2009). We used PyMOL to visualize the model and predict possible mutation effect on the protein structure (DeLano, 2002).

**In silico* design was done by Avner Schlessinger – USA.

Amino acid analysis

Plasma amino acid analysis in mice

Adult mice were euthanized by cervical dislocation, decapitated and blood was collected (200 µL) from their trunks into commercially available anticoagulant treated tubes (e.g. heparin tubes Vacuette, Greiner Bio One). Cells were removed from plasma by centrifugation for 10 min at 2000 X g at 4°C. Following centrifugation the plasma supernatant was transferred into clean polypropylene tubes and kept at -70°C until assayed for amino acid concentrations by High Performance Liquid Chromatography (HPLC). Mouse plasma amino acid values reported in Table S1 represent mean ± SEM obtained from n=4 mice per genotype. HPLC measurements were done at Archimed Life Gmbh, Austria.

Plasma amino acid analysis in humans

Patient blood samples were collected under fasting conditions. Blood samples were collected on Guthrie cards and analyzed by LC-MS/MS and flow injection analysis-tandem mass spectrometry (FIA-MS/MS) (Novarino et al. 2012). Plasma amino acid values reported in Table S5 are the result of a single blood amino acid test. Similarly, previous investigation didn't reveal serum amino acid levels abnormalities.

*Patient recruitment and characterization was done by Majdi Kara - Libya, Fatma Mujgan Sonmez - Turkey, Kaya Bilguvar - USA, Anide Johansen - USA, Seham Esharif - Libya, Tawfeg Ben-Omran - Qatar, Meral Topcu - Turkey, Murat Gunel - USA and Joseph Gleeson - USA.

Brain amino acid analysis in mice

Adult mice were euthanized by cervical dislocation, decapitated and the left hemisphere of the brain was collected, weighed and immediately homogenized in 1 ml of ice-cold radio immunoprecipitation assay (RIPA) buffer (50 mM Tris-HCl, pH=7.4, 1% NP-40, 0.5% Na-deoxycholate, 0.1% SDS, 150 mM NaCl, 2 mM EDTA – all from Sigma-Aldrich) in the presence of cOmplete Protease Inhibitor Cocktail (Complete, Roche). The tissue was disrupted using a glass homogenizer, transferred into a collecting tube, and left on ice for 1

hour. The homogenate was centrifuged for 40 minutes at 100,000 X g at 4°C in a SW41Ti rotor in a Beckman Optima XPN-80 ultracentrifuge (Beckman Coulter), the supernatant was collected and deproteinized by the addition of an equal volume of a solution of 8% (wt/vol) 5-sulfosalicylic acid (Sigma-Aldrich) and stored at -70°C until assayed for amino acid concentrations. At the time of the assay, the samples were thawed, mixed, centrifuged for 30 min at 5,000 X g at 4°C to remove the precipitated protein and assessed by HPLC (performed at Archimedlife GmbH). Four to eight animals per genotype/per time point (E14.5, P2 and P40) were employed for determination of brain amino acid levels. HPLC analysis was performed blinded to genotype. Brain amino acid samples were tested in duplicate in 2 to 3 independent experiments except for the E14.5 for which all the samples were measured in duplicate but collected and measured at the same day. HPLC measurements were done at Archimed Life Gmbh, Austria.

RNA-sequencing

Adult mice were euthanized under anesthesia and the brains were quickly dissected on ice. The cerebellum was used for RNA extraction by using 700 µL Trizol (Thermo Fisher Scientific) for homogenization and 140 µL chloroform (Sigma-Aldrich), followed by centrifugation at 12000g for 15 minutes at 4°C. The upper aqueous phase was transferred to a new tube and 1.5 volumes of 100% ethanol were added. Total RNA was extracted by using the RNA Clean&Concentrator-5 prep Kit (Zymo Research). RQ1 RNase-Free DNase (Promega) treatment was also applied as described in the kit instructions manual. RNA sample quality was checked by using the NanoDrop spectrophotometer (Thermo Fisher Scientific) and the Bioanalyzer 2100 with the RNA 6000 Nano kit (Agilent). Then 1.5 µg total RNA was used to generate cDNA libraries by following the manufacturer's instructions in the SENSE mRNA-Seq Library Prep Kit V2 (Lexogen). Quality check of the generated libraries was assessed by using the Bioanalyzer 2100 with the High Sensitivity DNA Analysis Kit (Agilent). Libraries were sequenced on Illumina HiSeq 2500 instrument.

Western blot

Adult mice were euthanized under anesthesia, the brain was dissected and homogenized in ice-cold RIPA buffer (50 mM Tris-HCl, pH=7.4, 1% NP-40, 0.5% Na-deoxycholate, 0.1% SDS, 150 mM NaCl, 2 mM EDTA – all from Sigma-Aldrich) supplemented with cOmplete Protease Inhibitor Cocktail (Complete, Roche) and/or with phosphatase inhibitor cocktail 3 (Sigma Aldrich). After 1 hour of incubation on ice, the lysates were centrifuged at 4°C at 14.000g for 15 minutes. The protein concentration of the supernatant was measured using the BioRad protein assay method (BioRad). For the Western blot, 30-50 µg proteins were mixed with Laemmli buffer 6x (375 mM Tris pH=6.8, 12%SDS, 60% glycerol, 600 mM DTT, 0.06% bromphenol blue – all fro Sigma-Aldrich), heated to 95°C and then separated on 6-15% SDS-PAGE gels in running buffer (3.03 g Tris base, 14.1 g glycine, 1 g SDS –Sigma-Aldrich, 1 L MilliQ water). Proteins were transferred to a nitrocellulose membrane using a transfer buffer (3.03 g Tris base, 14.1 g glycine, 1 L MilliQ water) for 2 hours at 4°C in a Bio-Rad Micro Cell Western blotting apparatus (300 mA constant intensity). The membranes were blocked for 1 hour with 5% milk in 1x TBS with 1% Tween (TBST) and incubated with primary antibody overnight at 4°C. After 4x10 min washes with TBST, the membranes were incubated with the secondary antibody for 1 hour at room temperature. Horseradish peroxidase coupled anti-IgG antibody was detected using an enhanced chemiluminescence substrate: Pierce ECL kit/Super Signal West Pico kit/Super Signal West Femto Maximum

Sensitivity Substrate (Thermo Fisher Scientific). The following primary antibodies were used: rabbit anti-4E-BP1 (1:1000, Cell Signaling, 9644); rabbit anti-phospho-4E-BP1(1:1000, Cell Signaling, 2855); rabbit anti-eIF4E (1:1000, Cell Signaling, 2067); rabbit anti-phospho-eIF4E (1:1000, Cell Signaling, 9741); rabbit anti-eIF2 alpha (1:1000, Cell Signaling, 9722); rabbit anti-phospho-eIF2 alpha (1:1000, Cell Signaling, 3398); rabbit anti-S6K (1:1000, Cell Signaling, 2708); rabbit anti-phspho-S6K (1:1000, Cell Signaling, 9234); rabbit anti-VGAT (1:200, Millipore, AB5062P); mouse anti-Tubulin beta 3 (1:1000, BioLegend, MMS-435P). Secondary antibodies: donkey anti-rabbit HRP (1:1000, Thermo Scientific, A16035); goat anti-mouse HRP (1:1000, Thermo Scientific, 31432). Each western blot was repeated at least in 2 independent experiments.

Polysome profiling

Adult mice were euthanized by cortical dislocation, dissected and the brains were removed. Cortices were separated and lysed in Lysis Buffer (20 mM HEPES pH 7.4, 150 mM KCl, 5 mM MgCl2, 0,5 mM DTT, 100 µg/mL cycloheximide- Sigma-Aldrich, Roche Complete Protease Inhibitors (EDTA-free), 40 U/mL RNAsin - Promega, 20 U/mL Superasin – Thermo Fischer Scientific) using a dounce. Lysates were centrifuged for 10 min at 2000 x g at 4°C and the resulting supernatants were supplemented with NP-40 and Triton X-100 (both to 1%) and incubated on ice for 5 min. After centrifugation for 10 min at 20000 x g at 4°C the debris-free supernatants were flash-frozen and stored at -80°C until further use. Thawed supernatants were loaded onto 14 × 95mm Polyclear centrifuge tubes (Seton) containing 17.5–50% sucrose gradients (in Gradient Buffer containing 20 mM Tris-HCl pH 7.4, 5 mM MgCl2, 150 mM NaCl, 1 mM DTT, 100 µg/mL cycloheximide); the sucrose gradients were generated using the Gradient Master 108 programmable gradient pourer (Biocomp) and were centrifuged for 2.5 h at 35,000 r.p.m. in a SW40Ti rotor in a Beckman L7 ultracentrifuge (Beckman Coulter). After centrifugation gradients were fractionated and measured for RNA content using a Piston Gradient Fractionator (Biocomp) attached to a UV monitor (BioRad). Data represents mean ± SEM obtained from n=9 KO and 10 WT mice from N=2 independent experiments.

*Polysome profiling was done by Dora Clara Tărlungeanu in collaboration with Christoph Janiesch and Kent Duncan – ZMN Hamburg, Germany.

Immunohistochemistry

Adult mice were anesthetized by intraperitoneal injection (i.p.) of Ketamin 100mg/kg, Xylazine 10mg/kg and Acepromazin 3mg/kg as a mixture in one syringe. Unconscious state of the mouse was verified by pinching the hind limb (interdigital reflex). The diaphragm was opened from the abdominal side to expose the heart. A small incision was made in the right atrium and a butterfly needle was placed in the left ventricle to infuse phosphate buffered saline (PBS – Sigma-Aldrich) solution (25 mM Phosphate Buffer (PB), 0.9% NaCl) at 7 ml/min for 2 minutes using a perfusion pump. Afterwards the PBS was exchanged with a fixative solution consisting of 4% Paraformaldehyde (PFA- Sigma-Aldrich) + 0.05% Glutaraldehyde (Sigma-Aldrich) solution in 0.1M PB (5-10 minutes). The brains were removed and post-fixed overnight in 4% PFA at 4°C. Next, brains were cryoprotected in 30% sucrose solution at 4°C for one day and embedded in Optimum Cutting Temperature (O.C.T., Tissue Tek) or removed from the sucrose and kept on dry ice and sliced. Free-floating 20 µm sections were cut using either a Microm HM560 cryostat (Thermo Fisher Scientific) or a sliding VT 1200S

vibratome (Leica Microsystems). Cryostat sliced sections were used for stainings that required antigen retrieval (e.g. SLC7A5 staining) whereas the vibratome sliced sections were used for non-antigen retrieval staining and were collected in PBS. Slices were washed twice with PBS (10 min) at room temperature and then antigen retrieval was performed for 20 min at 98°C in Target Retrieval Solution (Dako) pH=6 in an electric pot. Samples were cooled to room temperature and then washed again twice with PBS (10 min). The sections were permeabilized in 0.5% Triton-X 100 in PBS for 30 minutes and then blocked for 40 min in 5% normal goat serum (Sigma-Aldrich) in 0.5% Triton-X 100 in PBS at room temperature. Sections were then incubated overnight with primary antibody at 4°C. The sections were washed (3x10 min) with 0.01% Triton-X 100 in PBS and incubated with secondary antibody for 1 hour at room temperature in a dark place. Sections were incubated with DAPI (10 min) and then washed (3x10 min) with 0.01% Triton-X 100 in PBS and mounted onto glass slides with Mowiol (Sigma-Aldrich). Fluorescent signal was detected using a LSM 700 inverted confocal microscope (Zeiss). The following primary antibodies were used: rabbit anti-SLC7A5 (1:200, received from Prof. Kanai (Matsuo et al., 2000)); rat anti-MECA32 (1:600, Novus Biologicals, NB100-77668); rabbit anti-Parvalbumin (1:500, Abcam, ab11427); rat anti-Ctip2 (1:400, Abcam, ab18465); rabbit anti-Cux1 (1:400, Santa Cruz, sc13024); rabbit anti-Somatostatin (1:1000, Penlabs, T-4103); rabbit anti-Calretinin (1:4500, Swant, 7697); rabbit anti-VGAT (1:200, Millipore, AB5062P); rabbit anti-Neuroligin 2 (1:500, Synaptic System, 129203). The secondary antibodies used were: donkey anti-rabbit (1:1000, Alexa Fluor 488, Life Technologies, A-21206); goat anti-rat (1:1000, Alexa Fluor 647, Life Technologies, A-21247). Immunohistochemistry experiments were repeated in at least 3 independent experiments.

Nissl staining

Adult mice were anesthetized and perfused with PFA 4% as described in the immunohistochemistry section. The brains were removed and post-fixed for 2 hours in 4% PFA at 4°C. Next, brains were transferred to 70% ethanol overnight at 4°C. The next day the ethanol was replaced with fresh 70% ethanol for another hour at room temperature, followed by 90% ethanol for 3 hours at room temperature and eventually 100% ethanol overnight at room temperature. On the following day brains were placed in a 1:1 mix of 100% ethanol : paraffin solution (ethanol is added from time to time to avoid complete evaporation) for 12 hours at 65°C and then moved to paraffin overnight at 65°C in an incubator. After this step brains were left to solidify in paraffin blocks and then 10 µm sections were cut on a HM 355S Microtome (Thermo Fisher Scientific). Paraffin slices were cleared with warm Roti-Histol (Carl Roth) for 10 min and passed through absolute ethanol to water (96%, 90%, 70%, 50%, 30%, water) each step for 5 min. Slices were then kept in 1% Cresyl Violet acetate (Thermo Fisher Scientific) solution for 4 min, followed by destaining solution (100 ml ethanol with 2 ml 100% acetic acid) for 5-10 sec, absolute ethanol for 30 sec and final absolute ethanol for 1 min. At the end slices were cleared with Roti-Histol (10 min) and mounted with DPX (Sigma-Aldrich). Images were acquired using the BX53 upright light microscope with an attached DP70 digital camera (Olympus) and processed with Photoshop CS5.1 (Adobe Systems). Nissl staining observation was repeated with 3 mice per genotype at two different developmental stages.

Electrophysiology

Littermates of the same sex but different genotypes were randomly used to prepare brain slices. Acute sagittal slices (300 µm) were prepared from the cortex and from the cerebellum of 19 to 22 days old mice (here referred as P21). Animals were anesthetized by an i.p. injection of a mixture of ketamin (100 mg/kg), xylazin (10 mg/kg) and acepromazin (3 mg/kg), then transcardially perfused with ice-cold carbogenated solution containing (mM): 64 NaCl, 25 NaHCO3, 2.5 KCl, 1.25 NaH2PO4, 10 glucose, 120 sucrose, 7 MgCl2 and 0.5 CaCl2 (all from Sigma-Aldrich, unless otherwise stated). After decapitation, brains were removed for sectioning in the same ice-cold cutting solution using a VT 1200S vibratome (Leica Microsystems). Slices were recovered in room-temperature carbogenated regular artificial cerebrospinal fluid (mM): 125 NaCl, 2.5 KCl, 1.25 NaH2PO4, 25 NaHCO3, 25 glucose, 1 MgCl2 and 2 CaCl2 (~320 mOsm, 7.2–7.4 pH) for 30 min and transferred to a recording chamber (RC-41LP, Warner Instruments) for experiments typically between 1 and 7 h after slicing. Slices were visualized under infrared-differential interference contrast (IR-DIC) using a BX-51WI microscope (Olympus) with a QIClickTM charge-coupled device camera (Q Imaging Inc, Surrey). Cerebellar Purkinje cells and cortical layer 2-3 pyramidal cells with a prominent apical dendrite were visually identified with a microscope equipped with IR-DIC optics mainly by location, shape and Clampex online membrane test parameters.
Borosilicate glass recording microelectrodes (World Precision Instruments) were pulled on a P-1000 horizontal puller (Sutter Instruments) and backfilled with an internal solution containing (mM): 115 cessium methanesulphonate, 8 NaCl, 10 HEPES, 0.3 EGTA, 10 Cs4BAPTA, 5 lidocaine N-ethyl chloride, 4 MgATP, 0.3 NaGTP, and 0.2% biocytin. Internal pH was adjusted to ~7.3 with CsOH and osmolarity adjusted to ~295 mOsm with sucrose. Typical internal resistance was around 1.7–3.5 MΩ. After seal rupture and internal equilibrium (5 min to allow proper dialysis of Cs+ internally), cells were recorded with series-resistance values <10 MΩ (recording traces were excluded for data analysis if series resistance changed by >25%). Slices were perfused with room temperature carbogenated regular aCSF at a rate of approximately 2 ml/min−1. Miniature excitatory postsynaptic currents (mEPSCs) were recorded at a holding potential of –70 mV and miniature inhibitory postsynaptic currents (mIPSC) at the reversal potential for mEPSC (+ 10 mV). All voltage clamp traces were recorded in the presence of 1 µM tetrodotoxin (Bio Trend) with theoretical liquid junction potential not corrected for. Signals were filtered at 0.1 kHz, digitized at 10 kHz and data acquired using a MultiClamp 700B amplifier and a Digidata 1550A.

*Electrophysiology experiments for *Slc7a5* mouse line were done by Elena Deliu – IST Austria, for *Bckdk* mouse line were done by Emanuela Morelli – IST Austria.

Electron microscopy
21 days old mice were anesthetized by i.p. injection of Ketamin 100mg/kg, Xylazine 10mg/kg and Acepromazin 3mg/kg as a mixture in one syringe. Unconscious state of the mouse was verified by pinching the hind limb (interdigital reflex). The diaphragm was opened from the abdominal side to expose the heart. A small incision was made in the right atrium and a butterfly needle was placed in the left ventricle to infuse PBS at 7 ml/min for 2 minutes using a perfusion pump. Afterwards the PBS was exchanged with a fixative solution containing 4% PFA + 5% Glutaraldehyde in 0.1M PB (5-10 minutes). The brains were removed and post-fixed overnight in a 0.4% PFA in 0.1M PB at 4°C. 70 µm sections were cut using a Vibroslicer (Leica Microsystems), collected in PB and stored in PB+0.02% NaN_3.

Sections were washed in PB and osmified with 2% osmium (Agar Scientific Ltd) in 0.1M PB for 45 min at room temperature. They were then washed in 0.1M PB (10 min) and distilled water (3x10 min), and contrasted with 0.1% uranylacetate (Agar Scientific) in 50% ethanol solution for 30 min at room temperature in the dark. Samples were washed in distilled water (3x10 min) and dehydrated in ascending ethanol solutions (50%, 70%, 90%, 96% and 100% for 10 min each), infiltrated in propylene oxide (2x10 min) and embedded in Durcupan ACM (Sigma-Aldrich): propylene oxide mix 1/2 for 1h at room temperature, 2/1 for 1h at room temperature and mere Durcupan overnight at room temperature. Samples were mounted on siliconized coverslips, placed on a heating plate for 30 min at 37°C and put in an oven for 2 days at 60°C to polymerize resin. The region of interest (layer 2/3 somatosensory cortex) was cut and re-embedded in a resin block for further slicing. 70 nm ultrathin serial sections were cut using an UC7 ultramicrotom (Leica Microsytems), collected on formvar-coated copper-slot grids and examined in FE-SEM Merlin VP Compact with STEM detector (Zeiss).

*Sample preparation was done by Dora Clara Tărlungeanu in collaboration with the Electron Microscopy facility – IST Austria.

Behavioral studies

All behavioral studies were carried out during the light period. Mice were habituated to the test room for at least 1 h before each test. In order to recover, mice were given one day between tests. All behavior apparatuses were cleaned between each trial with 70% ethanol. All behavioral tests were performed starting with the least aversive task first and ending with the most aversive. Behavioral tests were performed with P55 to P65 mice except for the juvenile social interaction test for which P25 to P35 animals were employed and the ultrasonic vocalization test for which P2 to P10 pups were used. Data are presented as mean ± SEM.

Open field test

Exploratory behavior in a novel environment was assessed by a 20 min session in an open field chamber (45cmL x 45cmW x30cmH) made out of grey Plexiglas. The animal was placed in the center of the arena and then recording was started. Locomotor activity (distance traveled and velocity) in the center/periphery of the arena as well as rearing were recorded by using a video camera and analyzed using the EthoVision XT 11.5 software (Noldus).

Three chamber test

Mice were tested for sociability as described previously (Moy et al., 2007). Specifically, the testing apparatus was a rectangular clear Plexiglas three chambers box (60cm (L) x 40cm (W) x 20 cm (H)). The dividing walls had doorways allowing access to each chamber. Age and sex matched animals were used for all tests. C57BL/6J mice were used as stranger mice and were habituated to placement inside the wire cage. Each test animal was first placed into the center chamber with open access to both left and right chamber, each chamber containing an empty round wire cage. The wire cage (12cmH, 11cm diameter) allows nose contact between mice but prevents fighting. After 10 min of habituation, during the social phase, an age-matched stranger was placed in the left chamber while a novel object was placed into the right chamber. The test animal was allowed to freely explore the social apparatus for 10 min and show whether it prefers to interact with the novel object or with the stranger mouse. At the end of the first 10 min, each mouse was tested in a second 10 min session to evaluate the preference for a novel stranger, which was placed inside the

right wire cage. Number of nose contacts (<5cm proximity) with the caged mouse was calculated.

Juvenile social interaction

Juvenile social interactions were assessed in 25-35 days old mice in the Noldus PhenoTyper 3000 Observer chamber (30cm (L) x 30cm (W) x 35 cm (H)) as previously described (Silverman et al., 2011). Prior to the interaction session mice were individually housed for 1 hour. Two animals were placed simultaneously in the chamber and then recording started. Three types of interactions were assessed: wild-type/knockout; wild-type/wild-type and knockout/knockout, between age and sex matched subjects. Interactions were tracked for 10 min using a digital camera incorporated in the PhenoTyper chamber. Ineractions were scored using the EthoVision XT 11.5 software (Noldus) and included number of nose-nose sniffing and distance between subjects.

Walking beam test

Fine motor coordination and balance was assessed by the beam walking assay (Carter, Morton, & Dunnett, 2001). This test essentially examines the ability of the animals to remain upright and to walk on an elevated and relatively narrow beam. The beam apparatus consists of several 1 meter-long beams with diameters of 5 cm, 3 cm and 1 cm, resting 50 cm above the floor on two poles. During the test a mouse is placed on one extremity of the beam and a black box was placed at the end of the beam as finish point. The test took place over 3 consecutive days, 2 days training and 1 day testing (3 trials per day). In between trials mice were allowed to rest in their cages for 10 min. On the training days mice were allowed to cross the 5 and 3 cm beams while on the test day mice walked on the 1 cm beam. A nylon hammock was stretched below the beam to cushion any falls. A video camera was set on a tripod to record the performance. Performance on the beam was quantified by measuring the latency to cross the beam.

Isolation-induced ultrasonic vocalizations (USVs) in mouse pups

Whistle like sounds (between 30-90 kHz) were recorded from newborn pups as previously described (Scattoni, Crawley, & Ricceri, 2009). A microphone (part of the Noldus UltraVox XT system) was placed inside a dark, soundproof polycarbonate box (37cm (L) x 37cm (W) x 57cm (H)). Neonatal pups (postnatal days 2, 4, 6, 8, 10) were separated from their mother and placed inside the recording chamber. USVs were recorded for 3 minutes and afterwards the pup was placed back with its mother until weaning time.

Gait measurement test

Gait was analyzed by performing the footprint test as previously described (Carter et al., 2001). Specifically, the fore and hind paws were painted with nontoxic dyes of different colors and then the mouse was allowed to walk in a straight line (in a narrow corridor using as bait a cage at the end of the walkway) over absorbent paper. The footprint patterns were then analyzed for stride length, sway length and stance length.

Marble burying test

Stereotyped behavior was assessed by placing adult mice (60 days old) into an usual animal cage (30cm (L) x 20cm (W) x 20cm (H), Tecniplast) filled with 5cm deep chip bedding, as previously described (Deacon, 2006). Bedding was reused between sex matched animals. A regular pattern of glass marbles (5 rows of 4 marbles) was placed on the bedding and the subject was allowed to explore for 25 min. The number of buried (to 2/3 of their depth in bedding) marbles was counted.

Hind limb clasping test

As previously described (Guyenet et al., 2010), mice were grasped by their tail and suspended. Hind limb position was observed for 10 seconds. If the hind limbs were retracted towards the abdomen then the mouse was marked as positive for clasping. The test was repeated three times. At the end of the test the mouse was placed back into its cage. The test was repeated three times for each animal.

Kyphosis test

Kyphosis is a characteristic curvature of the spine that is common in mouse models of certain neurological disorders (Guyenet et al., 2010). The mouse was removed form its cage and placed on a flat surface. While it was walking, we observed whether it was able to easily straighten its spine completely. If it was not the case, the mouse was marked as positive for kyphosis. At the end of the test the mouse was placed back into its cage. The test was repeated three times for each animal.

Intracerebroventricular dye injection

40 days old mice were injected s.c. with meloxicam 5 mg/kg one hour prior surgery in order to achieve analgesia and then anesthetized initially with isoflurane 4% and O2 0.5-1L/min in a gas chamber. Once anesthetized (checked by toe pinching), the mouse was placed in a Kopf stereotaxic frame and a nose cone was placed over the nose with isoflurane volume turned down to 2% to maintain the anesthesia. After sterilizing the surgical site with betadine, a midline incision was made over the skull and a small hole was drilled above the left lateral ventricle. Using a Hamilton syringe, connected to the Kopf stereotactic frame, 10 µL of dye was delivered into the ventricle in order to check later on the injection site accuracy. The coordinates used relative to bregma were: anterioposterior (AP) = -0.5 mm, medial lateral (ML) = -1.1 mm, dorsal ventral (DV) = -3 mm. To allow diffusion of the dye into the brain, the needle was left for 5 min at the site of injection. The incision was manually closed using a topical tissue adhesive (GLUture, World Precision Instruments). Two hours later the mouse was euthanized and the brain was kept overnight in 4% PFA. The next day the brain was embedded in 3% agarose blocks and then sliced (100 µm) using a VT 1200S vibratome (Leica Microsystems) in order to assess the diffusion of the dye in the entire ventricular system and to confirm the correct positioning of the needle in the left ventricle.

Serial surgical implantation of cannula and osmotic pumps

One day before the surgery, a micro-osmotic pump (ALZET model 1007D) was filled with 100 µL of a saline amino acid solution (isoleucine 100 mM, leucine 100 mM). The pump was then connected through a plastic catheter to a cannula with a 0.5 mm spacer attached to it (ALZET Brain Infusion Kit 3). The pump was designed to deliver the solution at a rate of 0.5 µL/hour for 7 days. The pump and cannula assembly was kept in saline overnight at 37^{o}C. Adult mice were injected s.c. with meloxicam 5 mg/kg one hour prior surgery in order to achieve analgesia and then anesthetized initially with isoflurane 4% and O_2 0.5-1L/min in a gas chamber. Once anesthetized (checked by toe pinching), the mouse was placed in a Kopf stereotaxic frame and a nose cone was placed over the nose with isoflurane volume turned down to 2% to maintain the anesthesia. Eyes were covered with ointment in order to prevent drying out. During surgery metamizol 200mg/kg was administered subcutaneously (s.c.) to ensure maintenance of analgesia. After sterilizing the surgical site with betadine, a midline incision was made over the skull and a subcutaneous pocket was created on the back of the animal. The pump was then inserted inside the pocket and a small hole was drilled above the left lateral ventricle following the coordinates identified during the

calibration study performed with dye injections and as previously described (DeVos & Miller, 2013), AP = -0.5 mm, ML = -1.1 mm, DV = -2.5 mm. The incision was manually closed using a topical tissue adhesive (GLUture, World Precision Instruments). The incision site was sterilized with betadine and an ointment was applied to keep the spot moisturized. One week later the pump was replaced with a 200 µL micro-osmotic pump (ALZET model 2002) filled with the same amino acid solution as mentioned above. The replacement procedure was done following the same steps as described for the 100 µL pump. The mice were singly caged until the time for behavioral testing (e.g. walking beam test, gait measurement, open field test). Behavioral tests were performed with P55 to P65 mice. At the end of the three-week administration, mice were euthanized and their brains were dissected for HPLC protein analysis. Data represent means ± SEM; *n*=10 (untreated) control, *n*=4 (treated) control, *n*=11 (untreated) mutant and *n*=8 (treated) mutant mice.

Whole exome sequencing, homozygosity profile and variant prioritization

DNA was extracted from peripheral blood leukocytes using salt extraction. For family 1426 blocks of homozygosity were determined by HomozygosityMapper. Whole-Exome Sequencing and variant analysis was performed using solution hybrid SureSelect reagents (Agilent, Mountain View, CA) and sequenced on an Illumina GAIIx or HiSeq2000 instrument (Gnirke et al., 2009). The sequence reads were aligned to the human genome (hg19), genetic variants were delineated using the Genome Analysis ToolKit (GATK 1.1) software and SAMTools (v1.4-r985) algorithms, for both single nucleotide polymorphisms (SNPs) and Indels.

Variants were prioritized using the following criteria:

1. The variant was predicted to perturb protein function. All synonymous and intronic variants were excluded unless the variant was within a predicted splice site (+ or -2 bp from splice junction). Any variation that was predicted to alter gene expression or protein function was included. These included nonsynonymous variations in coding regions (i.e. missense) or alterations resulting in frameshifts, premature stop codons, loss of stop codons, coding INDELS, and splice sites (i.e. ± 2 nucleotides from an exon junction).
2. The variant was rare as defined by allele frequency of less than 0.2%. Allele frequencies were determined by an in-house database of over 1500 Middle Eastern exomes, and public databases provided by The Exome Variant Server from NHLBI GO Exome Sequencing Project (ESP) and dbSNP135.
3. The variant was present in a region of homozygosity as defined by HomozygosityMapper
4. The variant was highly conserved throughout evolution as determined by a number of conservation scores including GERP, PhastCons, and PolyPhen2. Variations with negative GERP scores or vertebrate PhastCons scores less than .8 were excluded. Typical conservation criteria for the candidate genes provided in this study were GERP > 4 and vertebrate PhastCons > .9.
5. The variant segregated with the disease in the family pedigree. All variants following the above criteria were considered for each family independent of its predicted severity (i.e. no variants were excluded based upon type of mutation).

The remaining variants were ranked by type of mutation (indels > nonsense > missense), amino acid conservation across species and protein damage prediction based upon location of the mutation in a specialized protein domain. The variants were annotated for novelty and compared with dbSNP (build 132) and control samples analyzed by whole-exome

sequencing experiments performed by our human genomics groups. Variants were analyzed against the RefSeq gene definitions, a list that includes 18,933 specific genes. Where multiple isoforms gave varying results the one most likely to lead to protein disruption was chosen.

*WES analysis was done by Ahmet Okay Caglayan – Turkey/USA and Gaia Novarino - IST Austria.

Sanger sequencing

Primers were designed using the Primer3 program and tested for specificity using ENSEMBL's BLAST software. PCR products were treated using Exonuclease I (Thermo Fisher Scientific) and Shrimp Alkaline Phosphatase (Affymetrix) and sequenced using the Big Dye terminator cycle sequencing Kit v.3.1 (Applied Biosystems) on an ABI 3100 DNA analyzer (Applied Biosystems). The sequence data were analyzed using Sequencher 4.9 (Gene Codes).

Leucine uptake assay

Leucine uptake was performed as previously described (Sinclair et al., 2013). Briefly, 300.000 cells were plated in a single well of 6 well plates two days before the assay. The day of the experiment the cells were washed twice with HBSS and incubated in HBSS containing [^{3}H] leucine (Perkin Elmer) 0.5 uCi/ml alone or in the presence of 10 mM leucine or 3 mM BCH (Wang et al., 2011). Cells were incubated at 37°C for 1 hour. At the end of the incubation each well was washed twice with cold PBS and lysed with 1 mM NaOH for 2 hours at 37°C. Total leucine uptake was measured by liquid scintillation counting (Packard Tri-Carb 2100TR).

Cloning, mutagenesis and expression of the human SLC7A5 wild-type and mutants

The construct pH6EX3-wt SLC7A5 obtained as previously described (Galluccio, Pingitore, Scalise, & Indiveri, 2013) and containing the SLC7A5 cDNA was used for site-directed mutagenesis. Specific mutants of the SLC7A5 cDNA were obtained by PCR overlap extension methods, as previously done for other proteins (Galluccio et al., 2015), using the primers in Table S4.

To supply tRNA for rare codons, Rosetta(DE3)pLysS E. coli strain was transformed either with SLC7A5 wild type or mutant proteins (Galluccio et al., 2013) and selected on agar plates supplemented with ampicillin and chloramphenicol. A colony was picked and cultured overnight at 37 °C under rotary shaking (about 200 rpm) in selective LB broth and the day after was diluted 1:10 in same medium. When the culture reached the mid logarithmic phase of growth, 0.4 mM IPTG was added and temperature was lowered at 28°C for 4 hours as previously described (Galluccio et al., 2013).

Purification of human SLC7A5 wild-type and mutants

Pellets from induced cell lysates were used for protein purification as previously described (Napolitano et al., 2015). In brief, after washing (0.1 M Tris HCl pH 8.0), pellets were solubilized using a 20 mM Tris/HCl pH 8.0 buffer containing 10 mM DTE, 0.8 % sarkosyl, 3.5 M urea, 10 % glycerol, 200 mM NaCl. Solubilized cell lysates were centrifuged (12,000 g, 10 min, 4 °C) and the supernatants were applied on a His Trap HP column (5 ml Ni Sepharose), connected to fast protein liquid chromatography (FPLC) ÄKTA start and equilibrated with 10

mL buffer (20 mM Tris HCl pH 8.0, 10 % glycerol, 200 mM NaCl, 0.1 % sarkosyl, and DTE 2 mM). During purification procedure, column was washed with 10 mL of washing buffer (20 mM Tris HCl pH 8, 10 % glycerol, 200 mM NaCl, 0.1 % n-Dodecyl β-D-maltoside and 3 mM DTE – all from Sigma-Aldrich). Then, proteins were eluted by an isocratic step of 400 mM imidazole in the above described buffer. Fractions 6-8 (2.5 mL) were pooled and desalted on a PD-10 column using a desalting buffer (20 mM Tris HCl pH 8.0, 10% glycerol, 0.05% n-Dodecyl β-D-maltoside and 10 mM DTE).

Reconstitution of human SLC7A5 wild type and mutants in proteoliposomes

The purified SLC7A5 wild type and mutants were reconstituted by removing the detergent using the batch-wise method as previously described (Napolitano et al., 2015). In brief, 4 µg of protein (in 200 µL) were mixed to 100 µL of 10% C12E8, 100 µL of 10% egg yolk phospholipids (w/v) in the form of sonicated liposomes prepared as previously described (Scalise et al., 2014), 20 mM Tris HCl pH 7.5, 10 mM DTE, 100 mM K-gluconate and 10 mM l-His, except where differently indicated, in a final volume of 700 µL. The mixture was incubated with 0.5 g Amberlite XAD-4 resin under rotatory stirring (1200 rev/min) at room temperature (25 °C) for 90 min (Napolitano et al., 2015).

Transport measurements

After reconstitution uptake and efflux experiments were conducted at 25°C. For uptake experiments, 600 µL of proteoliposomes were passed through a Sephadex G-75 column (0.7 cm diameter × 15 cm height) pre-equilibrated with 20 mM Tris HCl pH 7.5 and sucrose at appropriate concentrations to balance the internal osmolarity. Transport was started by adding 5 µM [^{3}H]His to the proteoliposomes. For efflux experiments, proteoliposomes containing 2 mM His, were preloaded with 5 µM [^{3}H]His at high specific radioactivity (1µCi/ml) for 30 min by transporter-mediated exchange equilibration. Proteoliposomes were then passed through Sephadex G-75, as above described, to remove external compounds. Efflux was started by adding, or not, 1 mM of unradiolabelled His. In both uptake and efflux assays, transport was stopped by adding a mix of 10 µM 2-amino-2-norbornanecarboxylic acid (BCH) and 1 µM HgC_{l2} at the desired time interval. In control samples, the inhibitor was added at time zero. At the end of the transport assay, each sample of proteoliposomes (100 µL) was passed through a Sephadex G-75 column (0.6 cm diameter × 8 cm height) to separate the external from the internal radioactivity. Proteoliposomes were eluted with 1 mL 50 mM NaCl and collected in 4 mL of scintillation mixture, vortexed and counted. The experimental values were corrected by subtracting each sample inhibited at time zero. For kinetic measurements, the initial rate of transport was measured by stopping the reaction after 10 min, i.e., within the initial linear range of [^{3}H]His uptake.

Ultracentrifugation of proteoliposomes

SLC7A5 WT and SLC7A5-A246V reconstituted proteoliposomes were passed through Sephadex G-75 column and 500 µl were ultracentrifuged (110,000 g, 1 h 30 min, 4°C). Pellets were washed with 20 mM Tris HCl pH 8.0 and ultracentrifuged again. Pellets were solubilized with 3% SDS and subjected to SDS-PAGE 12% run and western blot analysis. SLC7A5 WT and mutants were immuno-detected using anti-SLC7A5 antibody 1:2000, upon overnight incubation at 4°C. The reaction was detected by Electro Chemi Luminescence (ECL) assay after incubation with secondary antibody anti-rabbit 1:5000.

*Proteoliposome experiments were done by Michele Galluccio, Mariafrancesca Scalise and Cesare Indiveri – University of Calabria, Italy.

Quantification and statistical analysis

* Unless otherwise specified, data was analyzed by Dora Clara Tărlungeanu.

Statistical values including the exact *n,* statistical significance, definition of center, and dispersion and precision measures are reported in the Figure Legends. Student's *t*-test was mostly used and one-way ANOVA was used where appropriate (i.e., multiple comparisons). Data are shown as means ± SEM and were judged to be statistically significant when $p < 0.05$. In each graph circles/dots represent individual values. All data sets were analyzed using Shapiro–Wilk test for normality.

Amino acid data
Amino acid levels were normalized on the initial protein concentration and are displayed as fold change (log2 transformed) to levels in controls. Data analysis was done in GraphPad Prism 7 and student's *t*-test was used to test for significance. Mouse plasma amino acid values reported in Table S1 represent mean ± SEM obtained from n=4 mice per genotype. Brain amino acid values represent mean ± SEM obtained from 4 to 8 mice per genotype per time point from at least 2 independent experiments.

RNA-sequencing
Demultiplexed raw reads were trimmed before alignment as suggested by the library preparation kit, i.e. the first 9 bases of each read were removed using the FASTX toolkit. Trimmed reads were aligned to the mouse genome using STAR version 2.5.4 (genome: GrCm38, gene annotation: Gencode release M8). Reads that didn't align uniquely were discarded. Read counts per gene were also calculated using STAR (option -quantMode GeneCounts). Differential expression analysis was performed in R 3.2.4 employing the Bioconductor package DESeq2 version 1.10.1 using an FDR threshold of 0.05, a local fit for the dispersion estimation and default parameters otherwise. Gene Ontology enrichment analysis was done using the Bioconductor package GOstats version 2.36.0 with a p-value cutoff of 0.001 and conditional testing enabled. GO enrichment results were visualized using a custom script. RNA sequencing was performed employing n=3 mice per genotype.

*RNA-seq analysis was done by Christoph P. Dotter – IST Austria.

Protein data

Western blot
Western blot images were acquired by Peqlab Fusion SL Advance Multi Imaging system (VWR) and quantified using ImageJ software. Protein levels are displayed as fold change. Student's *t*-test was used to test for significance (GraphPad Prism 7). Data represent mean ± SEM obtained from two to five mice per genotype typically from at least 2 independent experiments.

Polysome profiling

Analysis was performed blinded to genotype. For quantitative analysis of individual elements (e.g. 80S monosomes, polysomes, etc) from the polysome profiles, all traces were first exported to Microsoft Excel and adjusted as necessary to ensure matching x/y-axis scales. Traces were then exported to Photoshop CS5.1 and ImageJ for processing, baseline setting, cropping and pixel counting. The pixel counts were used for determining polysome/monosome values and for plot generation. Student's *t*-test was used for the statistical analysis (GraphPad Prism 7). Data represents mean ± SEM obtained from n=9 KO and 10 WT mice from two independent experiments. All data sets were analyzed using Shapiro–Wilk test for normality.

*Polysome profiles were analyzed by Christoph Janiesch and Kent Duncan – ZMN Hamburg, Germany.

Immunohistochemistry

Fluorescent signal was detected using a LSM 700 inverted confocal microscope (Zeiss) and images were processed with Photoshop CS5.1 (Adobe Systems). Control and mutant samples were always treated equally and in parallel (e.g. if brightness or contrast were adjusted identical changes were applied for all the samples). For each antibody, immunostainings were repeated in multiple animals (typically 3 per genotype) obtaining comparable results. We counted all parvalbumin, somatostatin and calretinin interneurons as well as VGAT and NLGN2 puncta intensity on coronal sections at different positions. Neurons/puncta quantified in a given animal were added together. Means and SEM were calculated across animals, and student's *t*-test was done across animals (*n*=3 animals per genotype).

Neuronal data

Analysis was performed blinded to genotype using pCLAMP 10.4 software (Axon Instruments/Molecular Devices). Statistical analyses were performed using Origin Software (Origin Inc), Clampfit and R. All data sets were analyzed using Shapiro–Wilk test for normality. Data sets with normal distributions were analyzed for significance using one-way ANOVA measures with Bonferroni post-hoc test, using *P < 0.05, **P < 0.005. Data sets with non-normal distributions were analyzed using the 2-tailed Mann-Whitney U test using *P < 0.05. Exact P values are presented in each figure. Cumulative distributions were analyzed using the Kolmogorov-Smirnov test. Data represent means ± SEM, $n_{cells}/n_{animals}$/genotype: 14/7/*Tie2*^{Cre};*Slc7a5*$^{fl/+}$ and 13/5/*Tie2*^{Cre};*Slc7a5*$^{fl/fl}$ (mEPSC); 16/7/*Tie2*^{Cre};*Slc7a5*$^{fl/+}$ and 18/5/*Tie2*^{Cre};*Slc7a5*$^{fl/fl}$ (mIPSC).

*Electrophysiologal data for *Slc7a5* mouse line was analyzed by Elena Deliu – IST Austria, for *Bckdk* mouse line was analyzed by Emanuela Morelli – IST Austria.

Electron microscopy

Analysis was performed blinded to the genotype. ATLAS 5 array tomography (Zeiss) was used for image acquisition and 3D reconstruction of sample data. Image J software was used for quantification of the symmetric synapse vesicular pool and measurement of the presynaptic terminal area. All data sets were analyzed using Shapiro–Wilk test for normality and met the criteria for normality. GraphPad Prism 7 was used for statistical analysis

applying student's *t*-test. Data represent means ± SEM; $n_{synapses}$/genotype: 27/control and 22/mutant.

*Data analysis was done by Dora Clara Tărlungeanu in collaboration with Ryuichi Shigemoto – IST Austria.

Behavior

Quantification of the different behavioral parameters was done using the EthoVison XT 11.5 (Noldus) and UltraVox XT software (Noldus). Data met the criteria for normal distribution (Shapiro–Wilk test), thus student's *t* test was used for statistical analysis for most of the behavioral data. For the three chamber test one-way ANOVA with Fisher's post-hoc test was applied and for the juvenile social interaction test one-way ANOVA with Bonferroni's post-hoc test was used (GraphPad Prism 7). Number of animals employed for each test is reported in the figure legend describing each experiments and range from n=6 to n= 13 animal per genotype. At least two independent cohorts were examined for each test.

Transport measurement data

For the efflux experiments, the [^{3}H]His efflux was calculated by subtracting radioactivity values at each time point from that present in the proteoliposomes at time zero.

Uptake data were fitted in a first-order rate equation to obtain rate constants and in Michaelis–Menten or Linewever-Burk equations. Efflux data were fitted in a single exponential decay equation. The Grafit software (version 5.0.13) was used for data fitting.

To measure the specific activity of SLC7A5 WT and mutants, protein quantity was estimated from Coomassie blue stained SDS-PAGE gels by using the Chemidoc imaging system equipped with Quantity One software (Bio-Rad) as previously described (Galluccio et al., 2012). Data represent mean ± SD obtained from n= 4 to 5 independent experiments.

For the fibroblast leucine uptake assay the results of were obtained from at least 3 independent experiments (5 for family 1426 and 3 for family 1465) each one employing fibroblasts from at least 1 unaffected and 1 affected individual of the same family. For family 1426, given the very invasive procedure, we obtained skin biopsies only from 2 affected (patient 1426-6 and 1426-19) and 2 unaffected individuals (1426-1 and 1426-2). The graph in Figure 11E represents the average of the transport values obtained for either both the affected or the unaffected subjects in all the performed experiments. As deducible from the small error bar we didn't notice strong variability among individuals of the same family.

*Proteoliposome experiments data was analyzed by Michele Galluccio, Mariafrancesca Scalise and Cesare Indiveri – University of Calabria, Italy.

Data and software availability

Data resources

The data reported here is deposited into GEO under the accession numbers: GSE87808 (RNA-seq *Slc7a5*) and GSE39447 (microarrays *Bckdk*), and into NCBI Sequence Read Archive: SRS351252 (whole exome sequencing).

Additional resources

The URLs for data presented herein are as follows:
Online Mendelian Inheritance in Man (OMIM): http://www.omim.org
SeattleSeq Annotation: http://gvs.gs.washington.edu/
Genome browser: http://www.genome.ucsc.edu/
HPLC analysis: http://www.archimedlife.com/de/

3.4 Results

3.4.1 *SLC7A5* mediates BCAA flux at the BBB

Earlier *in vitro* studies described the sodium independent LAT1 as a large neutral amino acid (LNAA) transporter, including the BCAAs (Mastroberardino et al., 1998). The light subunit of the carrier, encoded by *SLC7A5,* is sufficient to transport LNAAs (Napolitano et al., 2015). The contribution of *SLC7A5* to brain LNAA/BCAA homeostasis *in vivo*, however, remains completely unknown.

To understand the physiological role of *Slc7a5 in vivo*, we employed a conditional (floxed) *Slc7a5* knock out mouse line (*Slc7a5*^{fl}) (Sinclair et al., 2013). In wild type animals, *Slc7a5* is considerably expressed in the plasma membrane of the endothelial cells of the BBB during development and in adulthood but it is mostly undetectable in other tissues (Figure 6A and Figure S1A-C). Thus, we crossed the *Slc7a5*$^{fl/fl}$ mouse with the *Tie2Cre* mouse line, expressing the Cre recombinase starting from embryonic day (E) 11.5 in the endothelial cells of blood vessels and BBB (Figure S1D) (Kisanuki et al., 2001). As expected, endothelial cells of the BBB of *Tie2*^{Cre}*;Slc7a5*$^{fl/fl}$ mice show complete lack of expression of *Slc7a5* (Figure 6A).

The exchange between blood and cerebrospinal fluid of a wide range of metabolically important molecules, including amino acids, is known to be constrained already early during development, arising with the BBB formation. However, some studies reported that many amino acids, including the BCAAs, are transported into the developing brain at much higher rate than in adulthood (Braun, Cornford, & Oldendorf, 1980; Lefauconnier & Trouve, 1983). Whether this reflects a greater metabolic demand of the developing brain or the immaturity of the BBB is unknown (R. E. Watson, Desesso, Hurtt, & Cappon, 2006). Hence, we asked how removal of *Slc7a5* from the BBB affects brain amino acid levels at different developmental stages.

We found that E14.5 *Tie2*^{Cre}*;Slc7a5*$^{fl/fl}$ mice don't show major changes in brain LNAA and BCAA levels (Figure 6B), suggesting either that at E14.5 the BBB is still immature, with amino acids leaking into the brain, or that another transporter may regulate LNAA and BCAA fluxes across the BBB during early development. In contrast, after birth and in adult stages brain BCAA, especially leucine and isoleucine, levels are abnormally low in *Tie2*^{Cre}*;Slc7a5*$^{fl/fl}$ animals (Figure 6C-D), indicating that *Slc7a5* expression is essential to regulate BCAA uptake by the brain. Surprisingly, the brain levels of several other LNAAs (e.g. tyrosine and tryptophan) in *Slc7a5* mutants are comparable to the ranges observed in control (*Tie2*^{Cre}*;Slc7a5*$^{fl/+}$) animals, while a few other amino acids (e.g. histidine, serine and phenylalanine) show an elevated level in mutants compared to controls. In particular, brain histidine concentration is several fold higher in the *Tie2*^{Cre}*;Slc7a5*$^{fl/fl}$ mice than in control animals (Figure 6B-D). This result supports the idea that SLC7A5 works as an antiporter and that histidine is the main counter amino acid (Figure S2) (Napolitano et al., 2015).

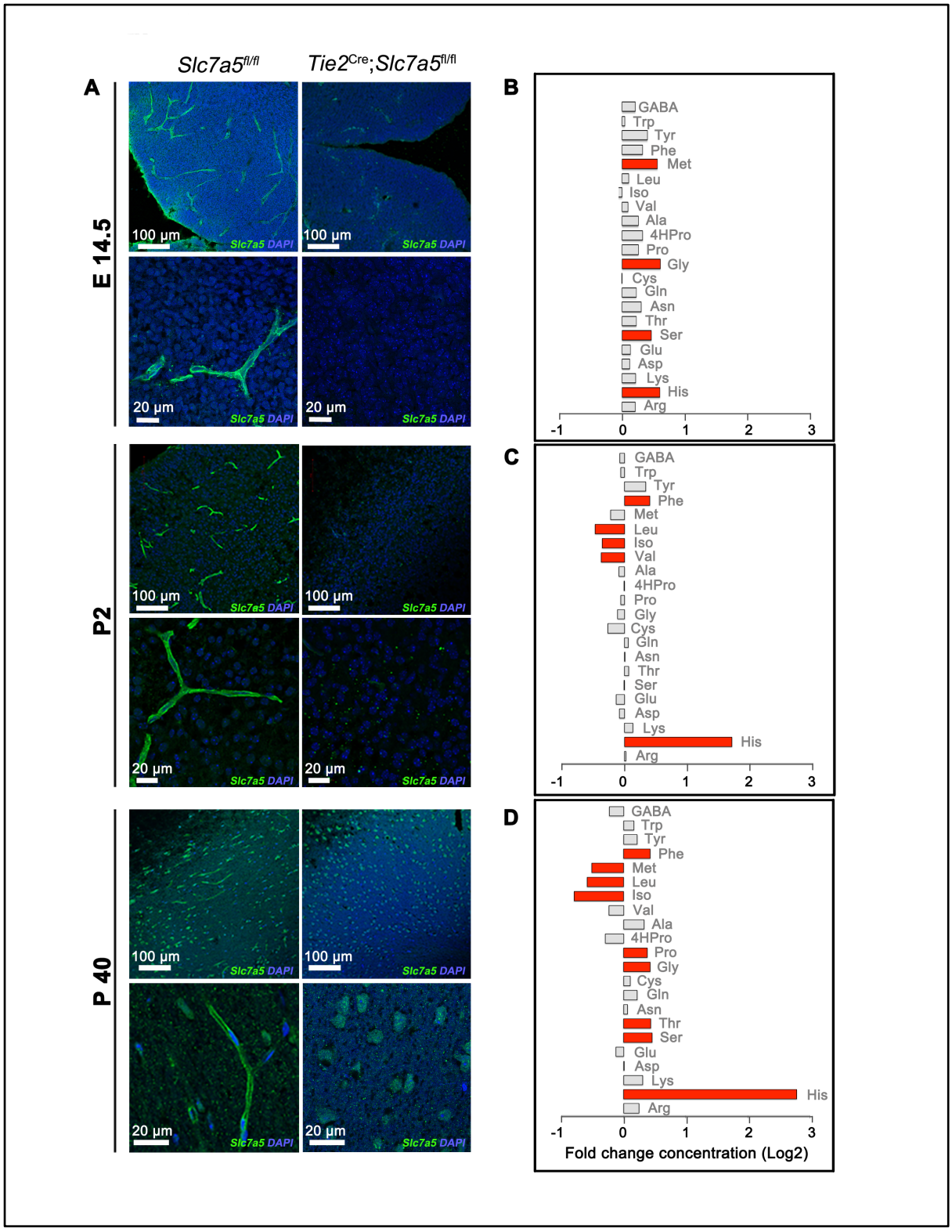

Figure 6. Slc7a5 mediates BCAA flux at the BBB.

(A) Representative images showing Slc7a5 (green) localization at the BBB in control animals (*Slc7a5*$^{fl/fl}$, left*)* and its complete deletion in endothelial cells of the BBB in Cre positive mice (*Tie2*^{Cre}*;Slc7a5*$^{fl/fl}$, right). Immunostainings were performed in cortical slices at embryonic day 14.5 (E14.5 top), postnatal day 2 (P2, middle) and adulthood (>P40, bottom). Nuclei were stained with DAPI (blue). (B-D) Brain amino acid levels in *Tie2*^{Cre}*;Slc7a5*$^{fl/fl}$ mice at E14.5 (B), P2-14 (C) and >P40 (D). Levels of amino acids were normalized on protein

concentration and shown as fold change (log2 transformed) to levels in age-matched controls. In red are represented the amino acids with a fold change >1.3 and P value <0.05 (n>4 mice/genotype/time point).
See also Figure S1, S2 and Table S1.

Thus, in the absence of *Slc7a5* expression at the BBB, the mammalian brain accumulates histidine while failing to gather normal amounts of BCAAs. Importantly, neither the serum amino acid profile nor the level of brain neurotransmitters are affected in the *Tie2*^{Cre}*;Slc7a5*$^{fl/fl}$ animals (Figure S2C and Table S1). While this last result contradicts previous hypotheses (del Amo, Urtti, & Yliperttula, 2008), it is in agreement with our *in vitro* experiments showing that SLC7A5 does not facilitate the movement of neurotransmitters (Figure S2A-B).

3.4.2 Deletion of *Slc7a5* from the BBB activates the AAR signal transduction pathway in the brain

In vitro, SLC7A5 transports not only the BCAAs but also other LNAAs, including phenylalanine, tyrosine and tryptophan (Napolitano et al., 2015). However, brain levels of these amino acids were not reduced in *Tie2*^{Cre}*;Slc7a5*$^{fl/fl}$ mice but rather slightly increased (Figure 6D). This suggests that additional BBB-located transporters might efficiently compensate for *Slc7a5* loss by mediating the passage of several LNAAs, but not of BCAAs. Indeed, RNA sequencing of mouse brain revealed a significant up-regulation of *Slc7a1* and *Slc7a3* genes (Figure 7A-B) encoding for the amino acid transporters Cat1 and Cat3 (Fotiadis, Kanai, & Palacin, 2013). This finding suggests that *in vivo* Cat1 and Cat3 may contribute to preserve brain levels of LNAAs, other than BCAAs, in the *Tie2*^{Cre}*;Slc7a5*$^{fl/fl}$ mice.
Furthermore, differential gene expression analysis revealed the up-regulation of genes implicated in serine biosynthesis in *Tie2*^{Cre}*;Slc7a5*$^{fl/fl}$ mice (Figure 7B), explaining the modest but significant increase in brain serine level observed in the mutant animals (Figure 2D). An increase in the expression of genes encoding for amino acid transporters and serine biosynthetic enzymes has been previously linked to the activation of the AAR, a process implemented by individual cells to respond to amino acid deprivation (Kilberg, Shan, & Su, 2009). Consistently, RNAseq analysis of *Tie2*^{Cre}*;Slc7a5*$^{fl/fl}$ mouse brain, revealed the up-regulation of a number of other amino acid-related genes (e.g. aminoacyl-tRNA synthetases) (Figure 7A-B). Among them we noticed a significant up-regulation of mRNAs encoding for the amino acid responsive transcription factors *Atf4* and *Atf5* and the eukaryotic initiation factor 4E binding protein *4ebp1* (Figure 7A), all part of the AAR pathway. *Atf4* and *Atf5* have been implicated in the regulation of the central nervous system development and function. Specifically, *Atf4* modulates synaptic plasticity and long-term memory formation (Chen et al., 2003), while *Atf5* has been implicated in cell growth and development, especially in the nervous system (Angelastro et al., 2003). Aberrant expression of *Atf4* and/or *Atf5* has been implicated in cognitive dysfunctions and neuropsychiatric abnormalities, including altered emotional behavior (Green et al., 2008) and behavioral inflexibility (Trinh et al., 2012).
Importantly, our gene expression analysis didn't reveal any abnormality ascribable to increased histidine levels, suggesting that, despite histidine being the most affected amino acid by *Slc7a5* deletion, changes in its level do not lead to severe molecular defects. Similarly, we didn't detect changes attributable to alterations of other amino acids such as phenylalanine.

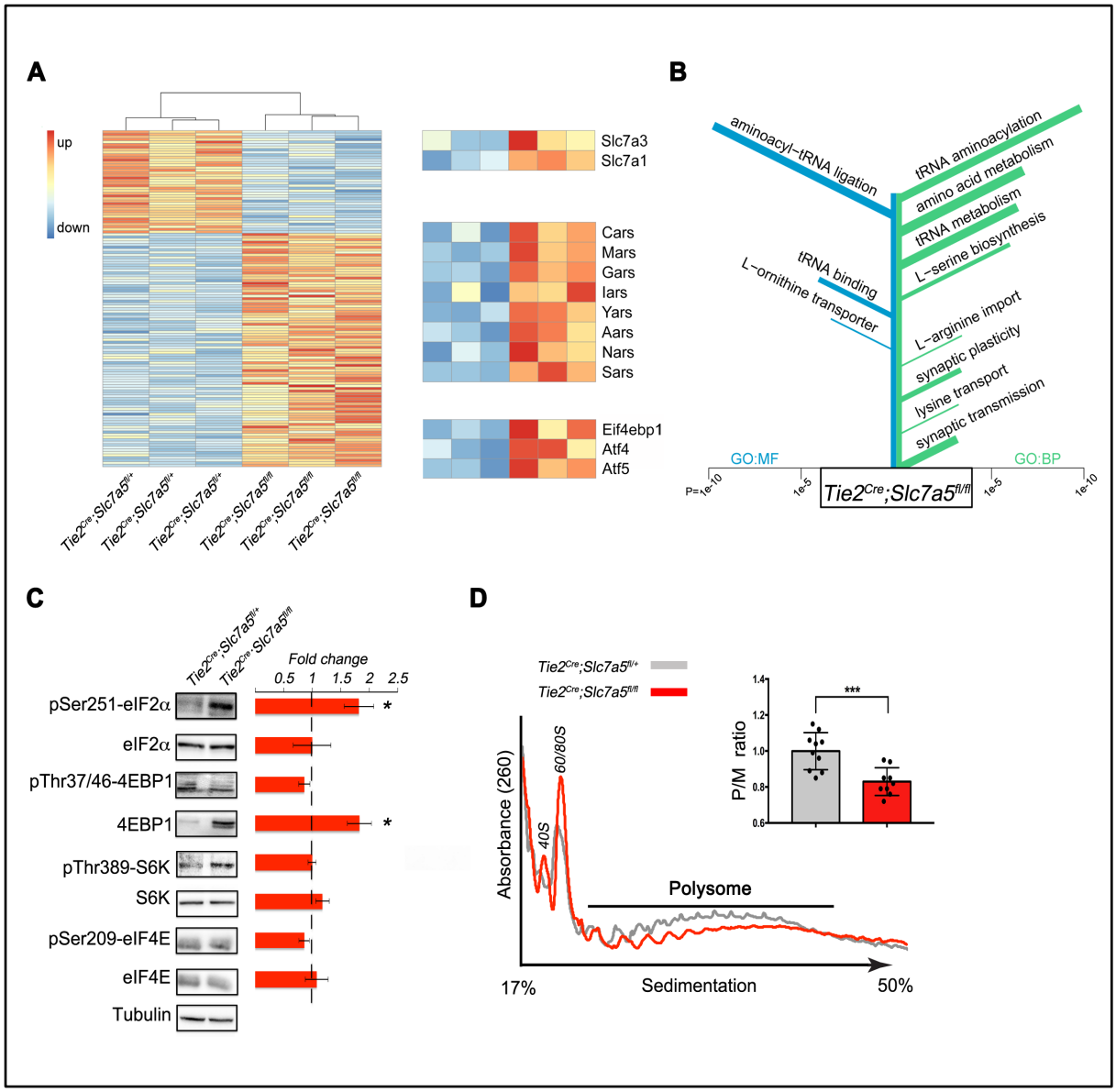

Figure 7. Activation of the amino acid response pathway in the brain of Slc7a5 *mutant mice.*

(A) RNA sequencing of adult brain in *Tie2^{Cre};Slc7a5$^{fl/+}$* and *Tie2^{Cre};Slc7a5$^{fl/fl}$* mice revealed 131 differentially expressed genes (FDR-adjusted P-value ≤ 0.05). The heat map displays log transformed count data normalized to library size. Genes expressed at lower levels in *Tie2^{Cre};Slc7a5$^{fl/fl}$* (40 genes) are displayed at the top and genes up-regulated in *Tie2^{Cre};Slc7a5$^{fl/fl}$* (91 genes) are shown at the bottom. Zoomed rows on the right emphasize differentially expressed genes associated with amino acid import (GO:0089718), tRNA aminoacylation (GO:0006418) and amino acid response, respectively (*n*=3 mice/genotype).
(B) Results of GO Enrichment analysis on the set of 131 differentially expressed genes. Terms are sorted according to P-value with the most significantly enriched terms at the top: GO terms for molecular functions (GO:MF, left, blue); GO terms for biological processes (GO:BP, right, green). The length of each bar indicates the P-value while the width indicates the amount of genes in the set associated with the term. RNA-seq was done at Vienna Biocenter, RNA-seq analysis was done by Christoph Dotter –IST Austria.
(C) Western blot analysis from cortical lysates of *Tie2^{Cre};Slc7a5$^{fl/+}$* (control) and *Tie2^{Cre};Slc7a5$^{fl/fl}$* mice, indicating that mutants exhibit increased phospho-eIF2α and total 4EBP1 protein levels but normal levels of total eIF2α, phospho-4EBP1, phospho-S6K, S6K, phospho-eIF4E and eIF4E. Tubulin was used as internal control. Representative blots (left) and fold change ratio (right); *P<0.05 (means ± SEM; *n*≥4 mice/genotype).
(D) Polysome profile from cortical lysates of control and *Tie2^{Cre};Slc7a5$^{fl/fl}$* mice. Typical tracings indicating positions of 40S, 60S and 80S ribosome peaks and polysome (P)/monosome (M) ratio quantifications;

***P<0.001 (right inset: means ± SEM; *n*=10 control and *n*=9 mutant mice). Polysome profile analysis was done by Christoph Janiesch and Kent Duncan – ZMN Hamburg, Germany.

3.4.3 Altered mRNA translation in *Slc7a5* mutant mice

Amino acid deprivation and activated AAR signaling pathway are associated with suppression of protein synthesis via phosphorylation of the translation initiation factor eIF2α. In the past few years several genes regulating mRNA translation have been implicated in cognitive deficits (Costa-Mattioli et al., 2005; Gkogkas et al., 2013; Santini et al., 2013). We therefore examined the effect of *Slc7a5* knock out at the BBB on translation and associated pathways in the brain.

To assess the impact of leucine and isoleucine deficiency on mRNA translation in the brain of *Tie2*^{Cre}*;Slc7a5*$^{fl/fl}$ mice, we first performed western blot analysis of neocortical lysates obtained from wild-type and mutant animals. Specifically, we evaluated the expression and activity status of a number of proteins involved in the regulation of protein synthesis (Figure 7C). We observed a significant increase in the total levels of 4EBP1 protein (Figure 7C), consistent with increased 4EBP1 mRNA levels seen in our RNAseq data (Figure 7A), and of phosphorylated eukaryotic initiation factor 2 alpha (eIF2α) (Figure 7C), indicating that removal of *Slc7a5* from the BBB and the consequent decrease in brain BCAA concentration may lead to the suppression of cap-dependent translation initiation. In contrast, in none of our experiments did we detect abnormal activation of the mammalian target of rapamacyin (mTOR) pathway (Figure 7C), whose activity was shown to be regulated by leucine levels *in vitro* (Wolfson et al., 2016). This may suggest that *in vivo*, under chronic leucine deficiency, the mTOR complex is alternatively regulated.

To test whether abnormal regulation of 4EBP1 and eIF2α in mice lacking *Slc7a5* leads to changes in translation efficiency in the brain, we performed polysome profiling of wild type and *Tie2*^{Cre}*;Slc7a5*$^{fl/fl}$ cortices. Importantly, in *Tie2*^{Cre}*;Slc7a5*$^{fl/fl}$ mouse cortical lysates we observed a significant shift of ribosomes from actively translating polysomes toward the monosomal fraction (Figure 7D), the hallmark of decreased translation initiation. We conclude that BCAA shortage and associated effects of 4EBP1 levels and increased eIF2α phosphorylation elicit deficient translation initiation in the brain.

3.4.4 *Slc7a5* conditional knock out animals show motor delay and autism-related phenotypes

Behavioral impairments resulting from abnormal regulation of cap-dependent translation have been previously described (Banko & Klann, 2008; Santini et al., 2013; Trinh et al., 2012). Thus, we tested *Tie2*^{Cre}*;Slc7a5*$^{fl/fl}$ mice for global behavioral changes. *Tie2*^{Cre}*;Slc7a5*$^{fl/fl}$ mice are born at Mendelian ratio and appear normal in size but display kyphosis (44% of mutant mice) and hind limb clasping (89% of mutant mice). In an open field *Tie2*^{Cre}*;Slc7a5*$^{fl/fl}$ mice show reduced explorative behavior and lower velocity (Figure 8A). Rearing, a form of vertical exploration, was significantly reduced in the *Tie2*^{Cre}*;Slc7a5*$^{fl/fl}$ mice (Figure 8B). Nonetheless, *Slc7a5* mutant mice and wild type littermates have similar habituation time course (Figure S3A), suggesting that the diminished activity results from locomotion defects rather than a faster habituation to the field. Therefore we tested the *Tie2*^{Cre}*;Slc7a5*$^{fl/fl}$ mice for fine motor coordination and locomotion problems. Indeed, *Tie2*^{Cre}*;Slc7a5*$^{fl/fl}$ animals

presented significant difficulties in the walking beam test (Figure 8C) and gait abnormalities (Figure 8D-E).

Since in our previous work we implicated BCAA deficiency in ASD (Novarino et al., 2012a), we tested *Tie2*^{Cre}*;Slc7a5*$^{fl/fl}$ for autism-like phenotypes. *Tie2*^{Cre}*;Slc7a5*$^{fl/fl}$ do not show excessive grooming or perseverative behaviors (Figure S3B), activities which can be, however, severely complicated by the presence of motor deficits in the mutants. Thus, we tested *Tie2*^{Cre}*;Slc7a5*$^{fl/fl}$ mice for social interaction abnormalities. We first employed a three-chamber social arena to probe the mutant animals for self-initiated interactions with a wild-type unfamiliar mouse. This analysis revealed that while wild-type mice have more close interactions with an unfamiliar mouse than an object, the *Tie2*^{Cre}*;Slc7a5*$^{fl/fl}$ mice show no preference between these two (Figure 8F). We then tested juvenile animals for social play and found that *Tie2*^{Cre}*;Slc7a5*$^{fl/fl}$ mice tend to stay farther apart from their cage-mate and display a decreased number of nose-to-nose contacts (Figure 8G). Finally, we measured isolation-induced ultrasonic vocalizations (USV) emitted by mouse pups separated from the mother. *Tie2*^{Cre}*;Slc7a5*$^{fl/fl}$ pups display increased number of USV starting from P8 when compared with their wild-type littermates (Figure 8H), a behavior observed in other autism models (Gkogkas et al., 2013). Interestingly, the excessive number of USVs emitted by the mutant pups may be due to an increased repetition of a specific repertoire of vocalization patterns (Romano, Michetti, Caruso, Laviola, & Scattoni, 2013).

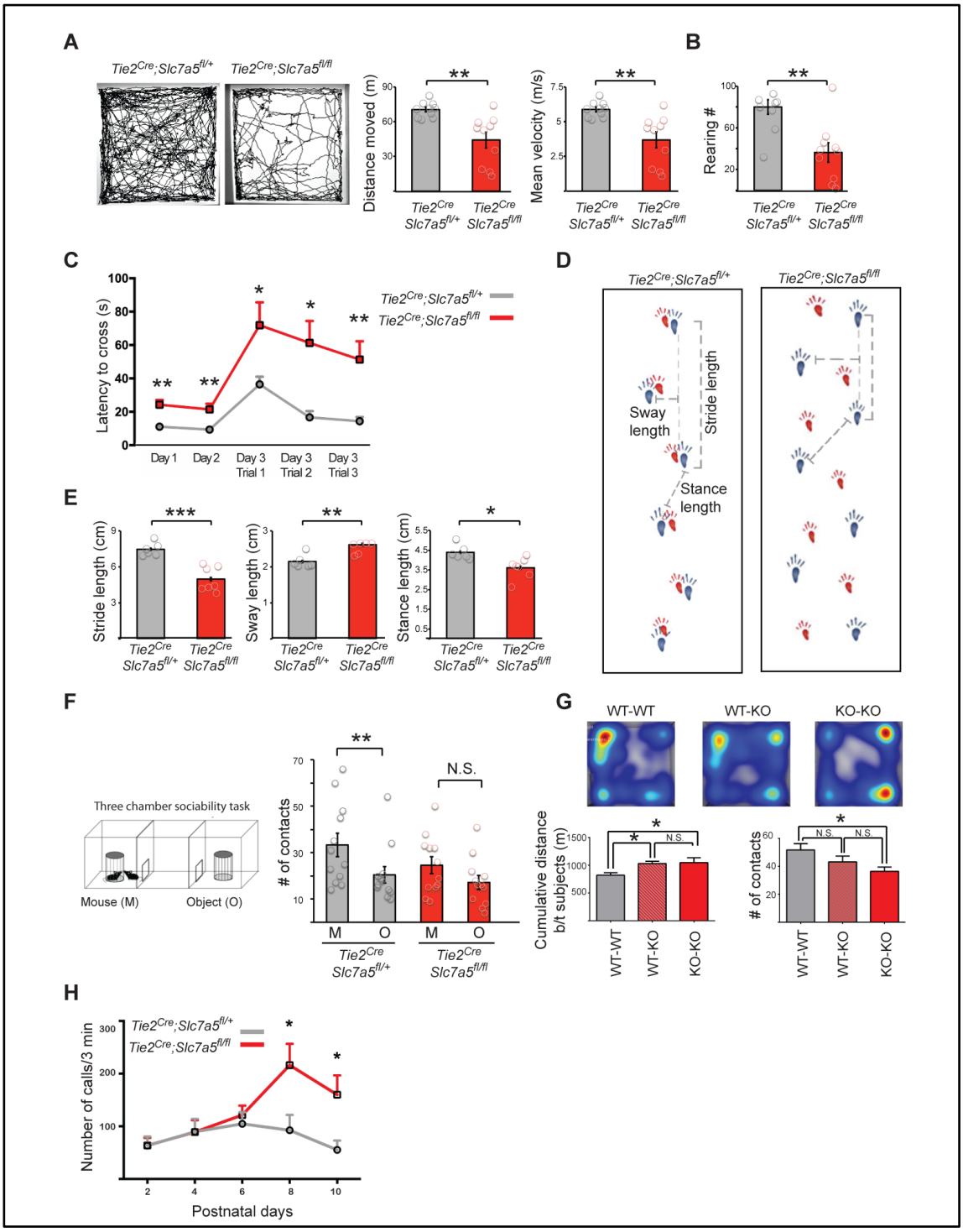

Figure 8. Neurobehavioral abnormalities in the Tie2^{Cre};Slc7a5$^{fl/fl}$ *mice.*

(A-D) Decreased exploratory behavior and locomotion abnormalities in the *Tie2^{Cre};Slc7a5$^{fl/fl}$* mice. (A) Open field test. Representative trajectories (left) and quantification of the total distance moved (middle) and the velocity (right) indicating that *Tie2^{Cre};Slc7a5$^{fl/fl}$* mice are outperformed by controls; **P<0.01 (means ± SEM; *n*=10 mice/genotype). (B) Comparison of the number of rearings pointing out deficiencies in the mutants; **P<0.01 (means ± SEM; *n*=10 mice/genotype) (C) Walking beam performance on training days (Day 1, Day 2) and on the three trials of the test day (Day 3), showing elevated latency to cross the beam in the mutants; *P<0.05, **P<0.01 (means ± SEM; *n*=7 mice/genotype). (D) Representative images of control (left) and *Tie2^{Cre};Slc7a5$^{fl/fl}$* strides (right) in the gait test. Forepaw (red) and hindpaw (blue). (E) Altered gait of the

Tie2^{Cre}*;Slc7a5*$^{fl/fl}$ mice is evidenced by inter-genotype comparison of stride, sway and stance length quantifications; *P<0.05, **P<0.01, ***P<0.001 (means ± SEM; *n*=7 mice/genotype).
(F) Three chamber social interaction test (left) and quantifications (right) of the number of contacts with the caged mouse (M) or with the caged object (O) revealing abnormal social interaction pattern in the mutant mice (mutants show no preference for the M over the O, as opposed to controls); **P<0.01, N.S. not significant (means ± SEM; *n*=12 mice/genotype).
(G) Juvenile *Tie2*^{Cre}*;Slc7a5*$^{fl/fl}$ mice display fewer reciprocal social interactions. *Slc7a5* mutant mice tend to stay farther apart from their cage mate (heat-map and bottom left graph) and exhibit fewer nose-to-nose contacts (bottom right graph). WT= *Slc7a5*$^{fl/+}$; KO= *Tie2*^{Cre}*;Slc7a5*$^{fl/fl}$. *P<0.05 (means ± SEM; *n*=8 mice/genotype).
(H) Isolation induced USV at various postnatal days show that *Tie2*^{Cre}*;Slc7a5*$^{fl/fl}$ mice emit an increased number of calls starting at P8. *P<0.05 (means ± SEM; *n*=10 mice/genotype).
See also Figure S3.

3.4.5 Inhibitory activity defects in *Tie2*^{Cre}*;Slc7a5*$^{fl/fl}$ mice

Social interaction abnormalities have been suggested to arise from cortical excitation/inhibition imbalance (Yizhar et al., 2011), a correlation also observed in animals with abnormal regulation of translation (Gkogkas et al., 2013; Santini et al., 2013). We evaluated synaptic function in 21 days old *Tie2*^{Cre}*;Slc7a5*$^{fl/fl}$ mice using whole-cell recordings of pyramidal neurons in layer 2/3 of the somatosensory cortex. Examination of synaptic transmission revealed a slight increase in the amplitude of miniature excitatory postsynaptic currents (mEPSCs) and a marked reduction in the frequency of miniature inhibitory synaptic currents (mIPSCs) (Figure 9A-B), indicating a significant excitation/inhibition imbalance.
To determine whether the synaptic alterations in *Tie2*^{Cre}*;Slc7a5*$^{fl/fl}$ mice are selective to the somatosensory cortex, we performed the same experiment in other brain regions. Given the locomotion abnormalities observed in *Tie2*^{Cre}*;Slc7a5*$^{fl/fl}$ mice, we tested inputs received by the Purkinje cells. Similarly to the neocortex, *Tie2*^{Cre}*;Slc7a5*$^{fl/fl}$ mouse cerebellar Purkinje cells display a significant reduction in mIPSC frequency (Figure S3C-D).
Changes in mIPSC frequency are generally due to differences in the number of functional synaptic sites and/or in the presynaptic release probability at existing sites (changes in the GABA vesicular pool or vesicular turnover rate). Therefore, we examined overall brain morphology (Figure S4A), cortical layering (Figure S4B) and inhibitory neuron distribution (Figure S4C) and found that for these parameters somatosensory cortices of mutant animals were undistinguishable from the control. We further looked for differences in pre- and postsynaptic markers of inhibitory synapses. Importantly, we observed that the intensity of the vesicular GABA transporter (VGAT) staining, a marker for GABAergic presynaptic terminals, was lower in the somatosensory cortices of *Tie2*^{Cre}*;Slc7a5*$^{fl/fl}$ mice (Figure 9C and Figure S4D). However, the GABAergic postsynaptic marker neuroligin 2 (Varoqueaux, Jamain, & Brose, 2004) appeared qualitatively and quantitatively similar in the somatosensory cortex of the mutant and control mice (Figure 9D and Figure S4E). The marked reduction of VGAT and normal neuroligin 2 protein levels in *Tie2*^{Cre}*;Slc7a5*$^{fl/fl}$ mice were also confirmed by western blot analysis of cortical lysates (Figure 9E). To determine whether the reduction in VGAT staining intensity was due to a specific lessening of VGAT or a decline in the number of VGAT-containing vesicles we analyzed inhibitory synapses by electron microscopy. In agreement with the electrophysiology results, we detected a significant reduction of vesicle number in symmetric synapses in the somatosensory cortices of *Tie2*^{Cre}*;Slc7a5*$^{fl/fl}$ mice compared with control animals (Figure 9F).

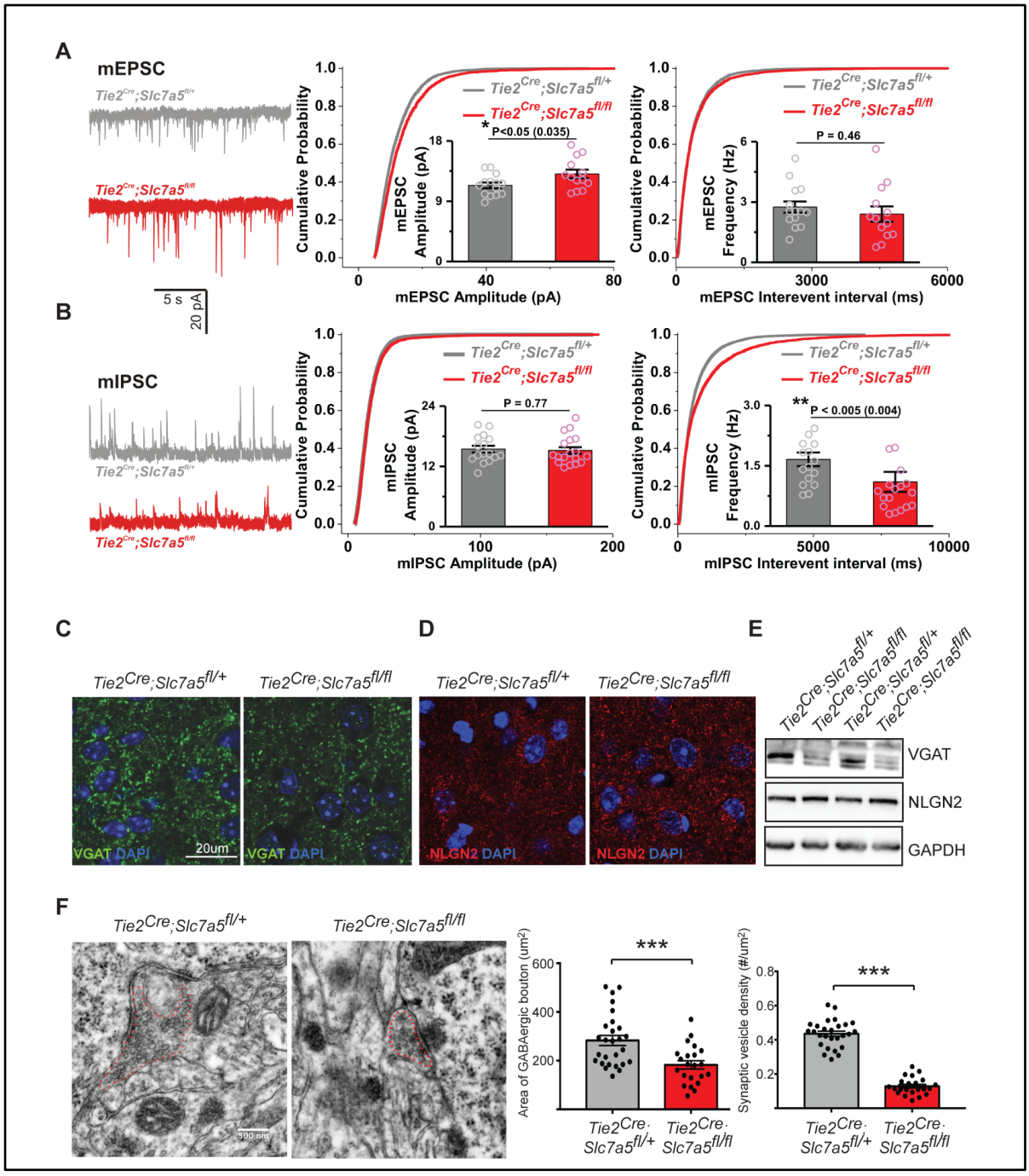

Figure 9. Excitation/inhibition imbalance in Tie2^{Cre};Slc7a5$^{fl/fl}$ *somatosensory cortex.*

(A-B) Left: Representative mEPSC (A) and mIPSC (B) recordings from *Tie2^{Cre};Slc7a5$^{fl/+}$* and *Tie2^{Cre};Slc7a5$^{fl/fl}$* somatosensory cortex (SCX) layers 2-3 pyramidal neurons; Right: Cumulative probability distributions of peak amplitudes and inter-event intervals of mEPSC (A) and mIPSC (B) in the two genotypes. Insets: quantifications of mean amplitudes and mean frequencies of the corresponding currents, with significant differences in mutants versus controls. D=0.093, P<10^{-11} (mEPSC amplitudes) and D=0.099, P<10^{-15} (mIPSC interevent intervals); (means ± SEM, $n_{cells}/n_{animals}$/genotype: 14/7/*Tie2^{Cre};Slc7a5$^{fl/+}$* and 13/5/*Tie2^{Cre};Slc7a5$^{fl/fl}$* (mEPSC); 16/7/*Tie2^{Cre};Slc7a5$^{fl/+}$* and 18/5/*Tie2^{Cre};Slc7a5$^{fl/fl}$* (mIPSC). Electrophysiological experiments were done by Elena Deliu – IST Austria.

(C) Representative confocal images of VGAT-positive synaptic puncta (green) in control (left) and *Tie2^{Cre};Slc7a5$^{fl/fl}$* (right) cortical sections displaying decreased staining intensity in the mutants. Nuclei were stained with DAPI (blue).

(D) Confocal imaging of cortical sections labeled for Neuroligin 2 (NLGN2, red) of control (left) and *Tie2^{Cre};Slc7a5$^{fl/fl}$* (right) animals revealing no difference between genotypes. Nuclei were stained with DAPI (blue). Scale bar as in (C).
(E) Western blot analysis from cortical lysates indicating decreased VGAT (top) and similar NLGN2 protein levels (middle) in *Tie2^{Cre};Slc7a5$^{fl/fl}$* mice compared with controls. GAPDH (bottom) was used as internal control.
(F) Electron microscopy imaging of the SCX layers 2-3 showing that *Tie2^{Cre};Slc7a5$^{fl/fl}$* mice have a decreased area of GABAergic boutons and decreased density of vesicles per bouton. Typical micrograph images (left), summary graphs of presynaptic area (middle) and vesicle density (right); ***P<0.001 (means ± SEM; $n_{synapses}$/genotype: 27/control and 22/mutant). Electron microscopy experiments were done together with the EM facility and Ryuichi Shigemoto - IST Austria.
See also Figure S4 and S5.

3.4.6 *Tie2^{Cre};Slc7a5$^{fl/fl}$* mutant mice resemble *Bckdk* knock out animals

The reduction in brain BCAA levels observed in *Tie2^{Cre};Slc7a5$^{fl/fl}$* adult mice is comparable to what we measured in *Bckdk$^{-/-}$* animals (Novarino et al., 2012a). *Bckdk$^{-/-}$* mice, in addition, display reduced serum BCAA levels and a marked increase in brain levels of several other LNAAs (Novarino et al., 2012a) but normal neurotransmitter concentrations (Figure S5G). Thus, it remained unclear whether neurological abnormalities in *BCKDK* mutant patients and mice are due to alterations in serum or brain BCAA. Alternatively, the pathological conditions observed in patients carrying mutations in *BCKDK* could be due to increased brain LNAA levels.
We compared *Bckdk$^{-/-}$* and *Tie2^{Cre};Slc7a5$^{fl/fl}$* mouse lines and observed a great phenotypic overlap. Similarly to *Tie2^{Cre};Slc7a5$^{fl/fl}$* mice, *Bckdk* mutants show motor coordination abnormalities, autism-related behaviors, decreased mIPSC frequency (Figure S5A-F) and activation of the AAR pathway (Novarino et al., 2012a, 2012b) implying that *Bckdk$^{-/-}$* and *Tie2^{Cre};Slc7a5$^{fl/fl}$* mice share pathophysiological mechanisms.

3.4.7 *SLC7A5* mutations in patients with ASD and motor delay

Given the essential role of *SLC7A5* in regulating brain BCAA homeostasis and the phenotypic overlap between *Bckdk* and *Slc7a5* mutant mice, we reasoned that mutations in *SLC7A5,* could lead to ASD and motor abnormalities in humans. Thus, we collaboratively screened whole exome sequencing (WES) data from more than 2000 families with documented parental consanguinity, presenting with children with various neurological diseases. We identified two independent families with multiple children affected by ASD, microcephaly and motor problems all harboring homozygous missense mutations in the gene *SLC7A5*.
Family 1426 is a consanguineous family with two branches and 5 affected individuals (Figure 10A-C). WES analysis of patients 1426-5 and 1426-19 (Figure 10A) identified a unique shared homozygous missense variant in the *SLC7A5* gene (Table S2). The homozygous mutation falls in a linkage pick with LOD score >4 (Figure S6A) and segregates with the disorder in the rest of the family (confirmed by Sanger sequencing). The A246V mutation changes a highly conserved alanine situated in a stretch of preserved amino acids predicted to be important for amino acid transport (Figure 10A-B). In an additional cohort of 1000 neurodevelopmental disorder patients analyzed by WES we identified Family 1465 including two patients with identical ASD, microcephaly and motor delay (Figure 10A-C) sharing a predicted deleterious homozygous mutation (Figure S6B) in *SLC7A5* leading to the change of the conserved proline in position 375 to a leucine (P375L) (Figure 10A). Both genetic variants were not present in more than 200 ethnically-matched, healthy control

chromosomes, nor in our data set of over 2000 chromosomes or in publicly available databases (Table S2).

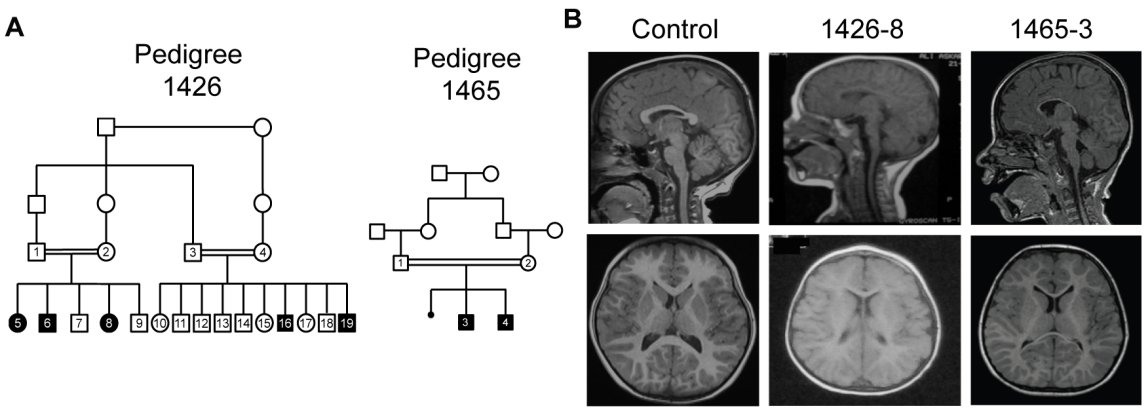

C

Patient	1426-5	1426-6	1426-8	1426-19	1465-3	1465-4
Gender	F	M	F	M	M	M
Origin	Libya	Libya	Libya	Libya	Turkish	Turkish
Age at diagnosis	N/A	N/A	5 months	N/A	2 weeks	5-6 months
HC at birth (SD)	N/A	-2/-3	N/A	N/A	- 3	- 3
HC at latest examination (SD)	-5	-2,3	-5,5	-5	N/A	N/A
Developmental milestones						
Gross motor (normal/delayed/absent)	Delayed	Delayed	Delayed	Delayed	Delayed	Delayed
Fine motor (normal/delayed/absent)	Delayed	Delayed	Delayed	Delayed	Delayed	Delayed
Language (normal/delayed/absent)	Delayed	Delayed	Delayed	Delayed	Absent	Absent
Social (normal/delayed/absent)	Delayed	Delayed	Delayed	Delayed	Delayed	Delayed
Seizure						
Type	-	-	-	N/A	GTC	GTC
Onset	-	-	-	N/A	1year	6 months
Autism associated disorder						
Impaired social interactions	+	+	+	N/A	+	+
Impaired eye-to-eye gaze, facial expression	+	+	+	N/A	+	+
Impaired ability to form peer relationships	+	+	+	N/A	+	+
Lack of spontaneous play	+	+	+	N/A	+	+
Restrictive behavior, interests and activities	+	+	+	N/A	+	+
Stereotyped, repetitive behavior	-	-	-	N/A	+	+
Inflexible adherence to routines or rituals	+	+	+	N/A	+	+
Additional CNS investigations						
MRI	N/A	Cortical atrophy	Normal	N/A	Thin CC	Thin CC

Figure 10. Mutations in the human SLC7A5 *lead to ASD and motor deficits.*

(A) *SLC7A5* mutations identified in families 1426 and 1465 in individuals with ASD, motor deficits and microcephaly. Pedigrees 1426 and 1465 display first-cousin consanguinity, five and two affected patients (solid symbols) respectively and unaffected members (open symbols)
(B) MRI from one patient for each family showing microcephaly and thin corpus callosum but normal axial T1 sequence of the brain. Control child brain MRIs were obtained from unrelated individuals.
(C) Clinical presentation of patients from family 1426 and 1465. HC, head circumference; SD, standard deviation; GTC, generalized tonic clonic; N/A not available; CC, corpus callosum.
Patient recruitment was done by Majdi Kara, Fatma Mujgan Sonmez, Kaya Bilguvar, Anide Johansen, Seham Esharif, Tawfeg Ben-Omran, Meral Topcu, Murat Gunel and Joseph Gleeson. WES analysis was done by Ahmet Okay Caglayan and Gaia Novarino.
See also Table S2.

3.4.8 Functional assessment of *SLC7A5* A246V and P375L mutations

We mapped the two genetic variants onto a homology model of SLC7A5 (Geier et al., 2013). A246 is located in transmembrane helix 6 in close proximity to the extracellular side and to the channel (Figure 11B). Mutation of this residue to the larger valine is therefore likely to impact the transporter's structure by disrupting helix–helix packing and ligand transport. P375 is located in transmembrane helix 9 in close proximity to the cytoplasmic side (Figure 11B). Proline often plays a key role in introducing kinks in helices and allowing conformational changes important for transporter function. Thus, mutation of this residue to leucine is likely to disrupt the flexibility required for transport by SLC7A5.

To validate the functional impact of the A246V and P375L substitution we performed transport assays. Therefore, the recombinant A246V and P375L mutant proteins were successfully expressed (Figure S7A), reconstituted in proteoliposomes (Figure 11C-D) and tested with a series of transport assays (Napolitano et al., 2015).

From transport time course analysis it was evident that the mutant A246V was virtually inactive (Figure 11C). As predicted by the homology model (Figure 11B) the functional defect may be ascribed to a higher steric hindrance of the valine side chain with respect to that of alanine. To verify this hypothesis and that the functional change was specifically ascribed to the pathological variant we analyzed an artificial mutant, A246G, (Figure S7A) in which the 246 side chain had been abolished. In contrast to the patient-specific A246V mutation, the A246G variant didn't show any transport defect (Figure 11C and Figure S7B). To exclude that the loss of activity observed in the A246V mutant could be due to reconstitution failing, we assessed the efficiency of protein reconstitution. We found no differences in the reconstitution of the A246V mutant compared to the WT protein (Figure S7A). Taken together, all the data confirmed that the substitution of A246V was functionally disruptive.

In contrast, the P375L mutant showed no significant variations in time dependent activity and external Km with respect to WT (Figure S7C-D). Owing to the location of P375 in an intracellular moiety of the protein (Figure 11B), we determined also the internal Km for this mutant (about 25 mM; 27 ± 9.9) (Figure S7E). Interestingly, the Km value was roughly five times that of the WT (about 5 mM; 5.2 ± 2.3), suggesting that some variations in the substrate binding/translocation pathway may occur upon mutation. We further performed efflux experiments for evaluating possible differences in the antiport reaction catalyzed by SLC7A5. The measurements were performed using intraliposomal histidine concentration (2 mM), to create conditions similar to the intracellular environment. Surprisingly, the mutant P375L was mostly uncoupled. Indeed, while WT showed a very slow efflux in absence of external substrate, according to its antiport mode, the mutant unidirectional efflux was much faster with a nearly complete proteoliposome emptying (Figure 11D). The anomaly observed in the P375L mutant indicates that, *in vivo*, loss of intracellular SLC7A5 substrate(s) impairs the driving force for taking up SLC7A5 substrates.

To further validate the functional impact of *SLC7A5* mutation in the patient-specific genetic background, we obtained human dermal fibroblasts from two affected and a few unaffected members of Family 1426 and Family 1465 and performed [^{3}H]-leucine uptake assay (Sinclair et al., 2013). *SLC7A5* transcript is expressed in human dermal fibroblasts and its level is not affected by the missense mutations (Figure S7F). Cells carrying the homozygous A246V or P375L variant, however, show a significant reduction in [^{3}H]-leucine uptake when compared

with control cells (Figure 11E). Thus, the substitution of the SLC7A5 alanine 246 into a valine, or of the proline 375 into a leucine, is sufficient to significantly reduce the SLC7A5-mediated BCAA uptake.

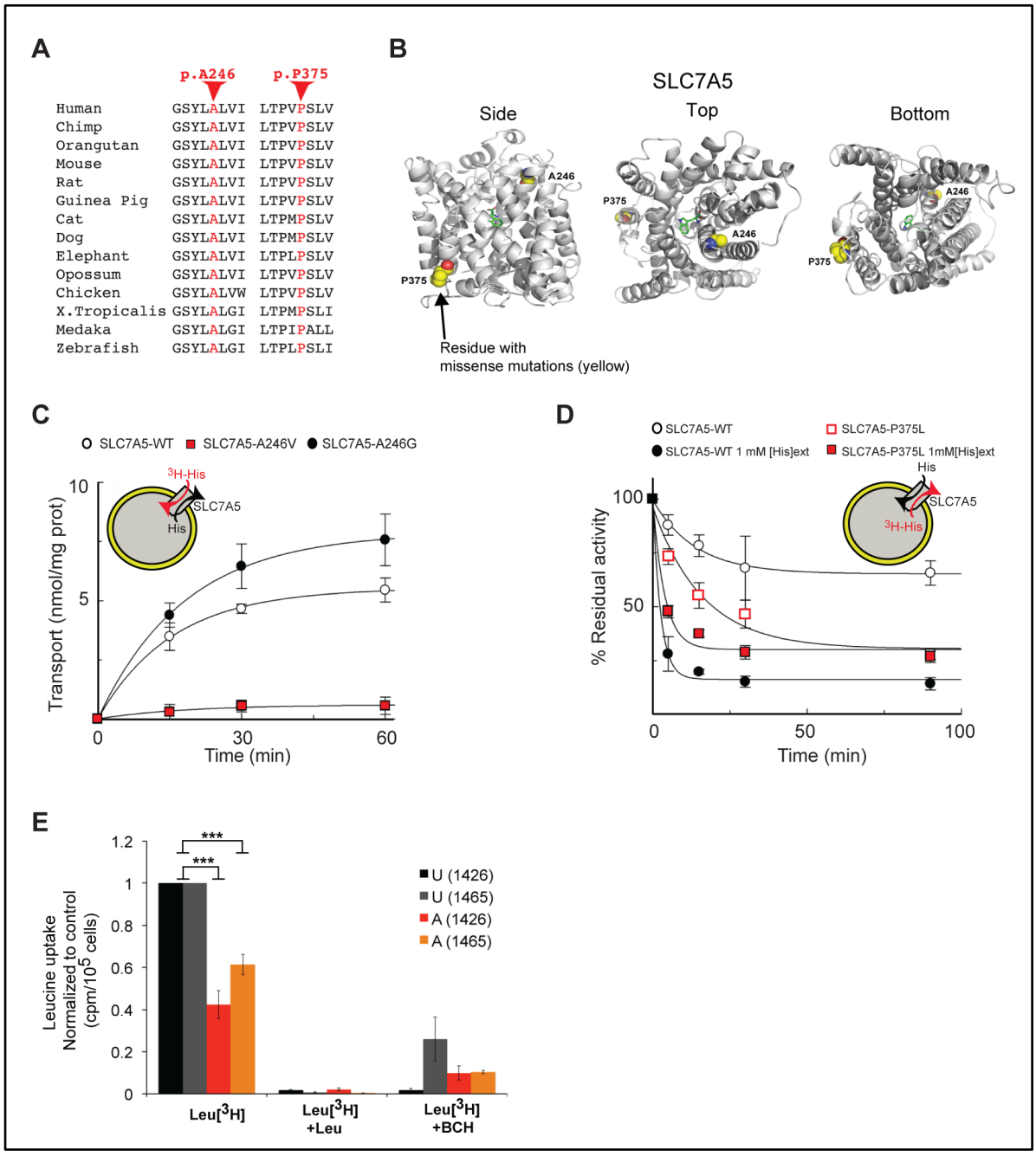

Figure 11. A246V and P375L mutations compromise SLC7A5 function.

(A) Conservation of the SLC7A5 A246 and P375 in several species.
(B) Side, top and bottom views of the predicted structure of SLC7A5 in complex with tryptophan showing SLC7A5 backbone atoms (gray ribbon), atoms of the residues constituting the missense mutations (yellow spheres) and the ligand tryptophan (green sticks); oxygen atoms (red) and nitrogen atoms (blue). *In silico* analysis done by Avner Schlessinger.
(C) SLC7A5 wild-type, A246V and A246G mutants over-expressed and purified by fast protein liquid chromatography were reconstituted in proteoliposomes. Transport is followed as uptake (red arrow) of external [^{3}H]His in exchange with internal His. Transport was started by adding external 5 µM [^{3}H]His at time

zero to proteoliposomes containing 10 mM His reconstituted with SLC7A5-WT (○), SLC7A5-A246V (■) or SLC7A5-A246G (●) and stopped at the indicated times (means ± SD; *n*=5 experiments).
(D) Time dependence of [^{3}H]His efflux from proteoliposomes reconstituted with SLC7A5-WT or SLC7A5-P375L was measured. Proteoliposomes reconstituted with SLC7A5-WT (○, ●) or SLC7A5-P375L (□,■), containing 2 mM His were radioactivity-preloaded. Efflux was measured in absence (○,□; uniport) or presence of external 1 mM His (●,■; antiport). Percentage of His efflux was calculated with respect to time 0 (means ± SD; *n*=4 experiments). Proteoliposome experiments were done by Michele Galluccio, Mariafrancesca Scalise and Cesare Indiveri – University of Calabria, Italy.
(E) Radio-labeled leucine ([^{3}H]Leu) transport analysis in human fibroblasts from affected (A) and unaffected (U) members of families 1426 and 1465 illustrating a significant reduction in leucine uptake by the cells of affected patients. Specificity of leucine uptake was assessed by competition with 10 mM cold leucine (Leu) or 10 mM 2 BCH; ***P<0.001 (means ± SEM; *N*≥3 experiments performed with fibroblasts from two patients and one healthy control/family).
See also Figure S7.

3.4.9 BCAA intracerebroventricular injections rescue neurological abnormalities in adult *Slc7a5* mutant mice

The identification of ASD patients carrying mutations in the *SLC7A5* gene prompted the question whether this condition is potentially treatable. Therefore, we injected leucine and isoleucine stereotaxically into the brain of adult *Tie2*^{Cre}*;Slc7a5*$^{fl/fl}$ mice for 3 weeks (Figure 12A). Injected mice were then tested for some of the behavioral phenotypes described in Figure 3 and brain amino acid levels. Notably, after 3 weeks of i.c.v. leucine and isoleucine delivery (Figure 12A) their brain level was normalized (Figure 12B and Table S3) and the mutant mice showed a significant improvement in neurobehavioral abnormalities. Specifically, we observed a decreased number of *Tie2*^{Cre}*;Slc7a5*$^{fl/fl}$ mice showing the clasping (50% of injected vs 89% of non injected mutant mice) and the kyphosis phenotype (25% of injected vs 44% of non injected mutant mice). Most importantly, we could not detect any difference between treated *Tie2*^{Cre}*;Slc7a5*$^{fl/fl}$ and wild type mice in the open field test neither in velocity and distance moved nor in the number of rearings (Figure 12C). The gait of the injected *Tie2*^{Cre}*;Slc7a5*$^{fl/fl}$ mice was improved with a complete normalization of the sway length (Figure 12D). Importantly, wild type animals injected with the leucine/isoleucine mixture were indistinguishable from the non-injected animals of the corresponding genotype (Figure 12C-D), indicating that leucine and isoleucine specifically improve behavior of *Slc7a5* mutants. Worth mentioning is the fact that the rescue of the social and vocalization abnormalities could not be tested given technical issues presented by the presence of the implanted pump and the size of the animals (see methods).
Although further tests are required to determine the extent and efficacy of the treatment, our data suggest that certain neurobehavioral abnormalities observed in *Slc7a5* mutants can be rescued by i.c.v. administration of leucine and isoleucine in adulthood. Even if we cannot entirely disregard a role of the increased level of other amino acids, these results support the idea that the reduction in brain leucine and isoleucine levels is the determinant factor in the appearance of the neurological phenotypes observed in humans and mice lacking *SLC7A5* expression.

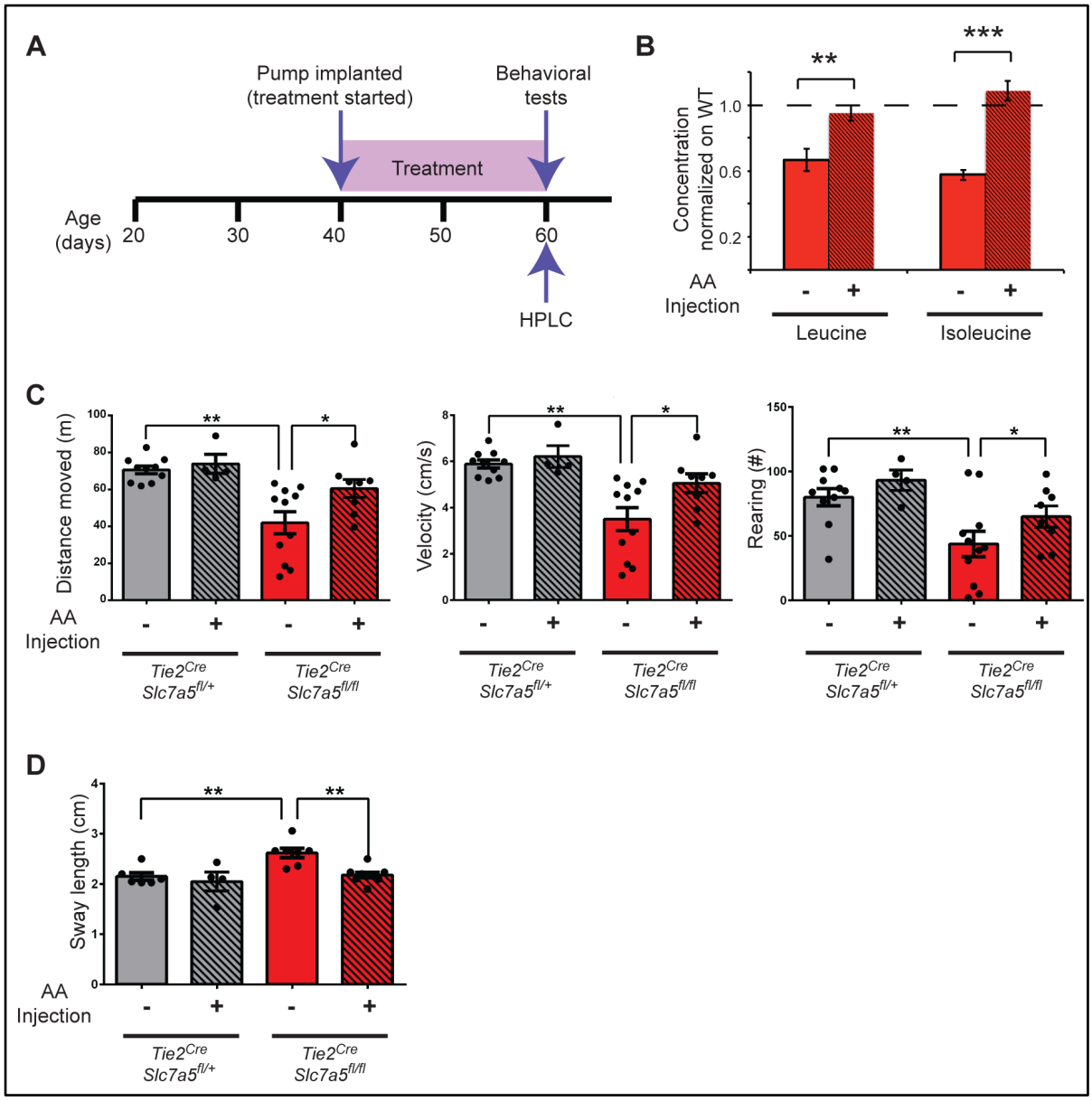

Figure 12. Normalization of Tie2^{Cre};Slc7a5$^{fl/fl}$ *mouse behavior after leucine and isoleucine i.c.v. administration.*

(A) Timeline of treatment and HPLC and behavioral tests.
(B) Brain levels of leucine (left) and isoleucine (right) in age-matched animals receiving (+) or not receiving (-) the i.c.v. treatment. Amino acid levels were normalized to protein concentration and to wild-type levels. **P<0.01, ***P<0.001 (means ± SEM; *n*=8 mice/genotype).
(C) Quantification of the total distance moved (left), velocity (middle) and number of rearings (right) in the open field revealing similar behavior in treated (+) *Tie2^{Cre};Slc7a5$^{fl/fl}$* mice and non-treated (-) or treated (+) controls (*Tie2^{Cre};Slc7a5$^{fl/+}$*) but significant differences with non-treated (-) *Tie2^{Cre};Slc7a5$^{fl/fl}$* mice; *P<0.05, **P<0.01 (means ± SEM; *n*=10 (-) control, *n*=4 (+) control, *n*=11 (-) mutant and *n*=8 (+) mutant).
(D) Similar sway length in treated (+) mutant mice and non-treated (-) or treated (+) control (*Tie2^{Cre};Slc7a5$^{fl/+}$*) animals but significant difference with non-treated (-) *Tie2^{Cre};Slc7a5$^{fl/fl}$* mice; **P<0.01 (means ± SEM; *n*=10 (-) control, *n*=4 (+) control, *n*=11 (-) mutant and *n*=8 (+) mutant).
See also Table S3.

3.4.10 Conditional deletion of *Slc7a5* in the neuroprogenitor cells leads to microcephaly

The patients identified with homozygous *SLC7A5* missense mutations presented not only with ASD and motor abnormalities but also with microcephaly (see Figure 10B). However, the *Tie2^{Cre};Slc7a5$^{fl/fl}$* mouse model employed here did not recapitulate the microcephalic phenotype described in patients. Intrigued by this observation we wanted to understand whether this could be due to a human *vs.* mouse species difference or due to the expression of *Slc7a5* in other tissues than the endothelial cells of the BBB. We have shown already that at E14.5 *Tie2^{Cre};Slc7a5$^{fl/fl}$* mice don't show major changes in brain LNAAs and BCAAs levels (Figure 6B), suggesting that at E14.5 the BBB might be immature, with amino acids leaking promiscuously into the brain. Thus, specific brain cell types developing at this time point receive all the amino acids necessary for growth and proliferation. These amino acids are employed either directly as building blocks for protein synthesis or as signaling molecules for important pathways involved in cell proliferation like mTOR (See chapter 1). Given our observations and making use of the Cre lines we had available at our institute, we addressed the role of *Slc7a5* in brain development by conditionally deleting it in neural progenitors using the *Slc7a5* floxed mice and the well described Nestin-Cre mice (Dubois, Hofmann, Kaloulis, Bishop, & Trumpp, 2006). By day E14.5/E15 full recombination occurred in all progenitor cell types present in the neuroectoderm, the developing mesonephros and in the somites (Dubois et al., 2006). The Nestin^{Cre};Slc7a5$^{fl/fl}$ knockout mice were born at the expected Mendelian ratio and their body weight was decreased compared to the controls (Figure 13A,B) - we used Slc7a5$^{fl/fl}$ or Slc7a5$^{fl/+}$ as controls. Furthermore, the Nestin^{Cre};Slc7a5$^{fl/fl}$ mice had a decreased milk content in their stomachs, were weak (data not shown) and died within one or two days from birth. The Nestin^{Cre};Slc7a5$^{fl/fl}$ brains appeared smaller (Figure 13C) and their weight was significantly decreased compared to controls (Figure 13D) with a decreased brain to body size ratio observable at E19.5/P0 (Figure 13E), suggesting developmental defects. The difference in brain size could be either due to a decrease in cell number or cell size or to an increase in cell death. To investigate the cause of the observed microcephaly we analyzed the gross morphology of the knockout brains at P0, by means of Nissl staining, and found a decrease in cortical thickness compared to control animals (Figure 13F). Preliminary immunolabelings of the projection neurons sitting in lower layers (Ctip2^{+}) or upper layers (Cux1^{+}) suggested a slight but significant reduction in the density of the upper layer Cux1^{+} neurons in P0 mice, as compared to controls (Figure 13G). To exclude a possible effect of the Nestin-Cre line itself on the observed reduction in upper layer neurons, which develop around E14.5 the same time when the Nestin-Cre line is fully active, we also compared the cortical layers of *Nestin^{Cre};Slc7a5$^{+/+}$* mice to control animals and observed no significant differences (Figure 13G). Since a decrease in cell proliferation can be attributable to defects in mTOR signaling, we performed western blot analysis on whole brain lysates at different developmental time points and identified a significant increase in the levels of 4EBP1 protein in the brains of *Nestin^{Cre};Slc7a5$^{fl/fl}$* mice at P0 (Figure 13H) supporting thus the idea that increased blockade of protein elongation affects overall protein synthesis and leads to a defective cell proliferation. However, given that the Nestin-Cre mediated recombination occurs also in several other tissues (Dubois et al., 2006) it is important to bear in mind the risk of potential complex phenotypes due to multi-organ defects. Further experiments will be performed to elucidate the exact cause of the microcephaly, like neurogenesis control (BrdU & Ki67 labeling); cell death quantification or the implications of peripheral organs on the

microcephaly onset due to the recombination pattern of the Nestin-cre line. So far these preliminary data indicate that the microcephaly of Nestin^{Cre};*Slc7a5*$^{fl/fl}$ mice at P0 is the result of a decrease in cortical cell numbers.

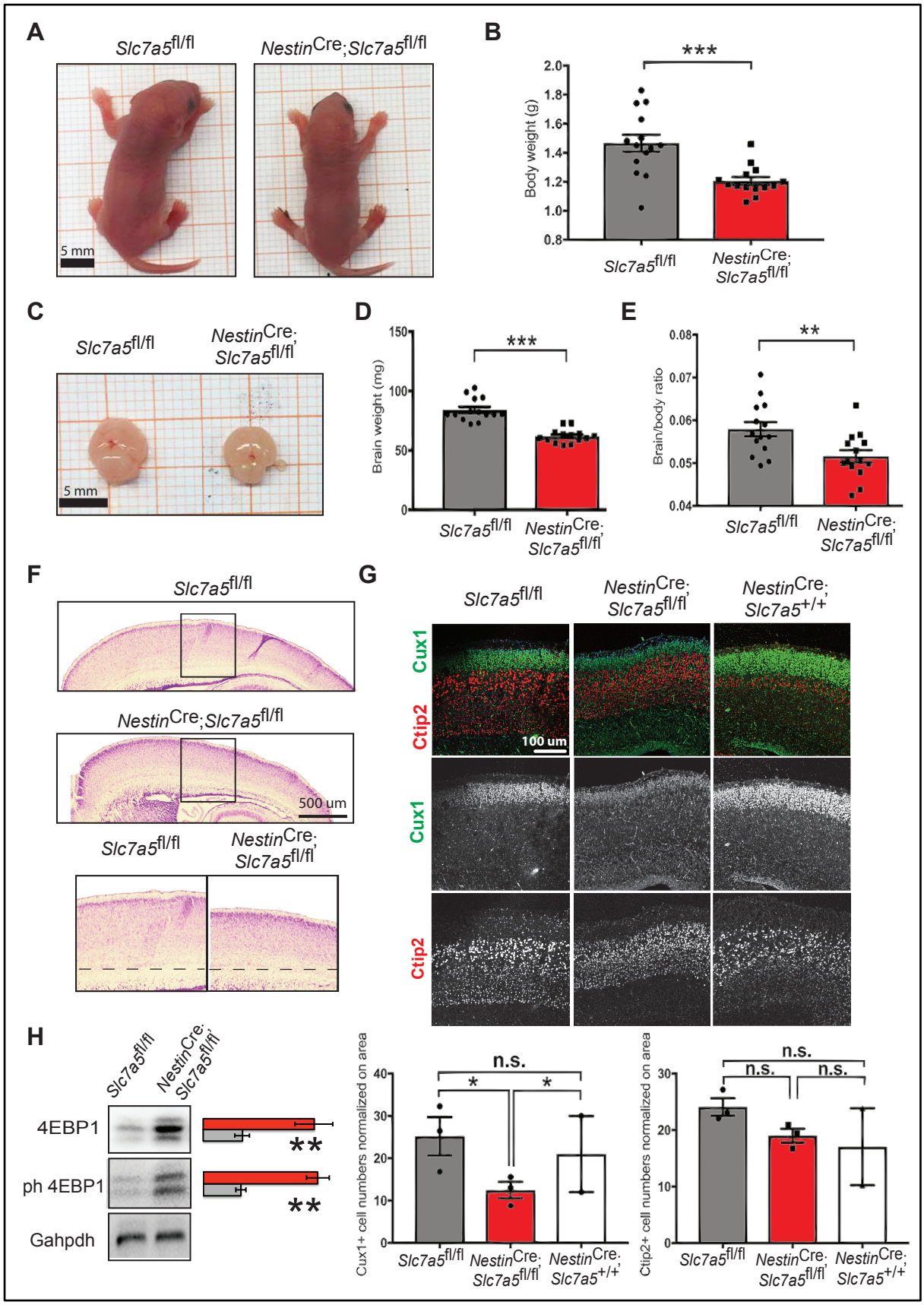

Figure 13. Slc7a5 deletion from neural progenitor cells leads to microcephaly.

(A). Body size of control *Slc7a5*$^{fl/fl}$ animals (left) and mutant *Nestin*^{Cre}*;Slc7a5*$^{fl/fl}$ (right) animals at P0. Scale bar = 5 mm.
(B). Body weight of mutant *Nestin*^{Cre}*;Slc7a5*$^{fl/fl}$ animals (right, red bar) is significantly decreased compared to control animals (left, grey bar) at P0. ***P <0.001 (means ± SEM; *n*=14 animals/genotype).
(C). Brain size of control *Slc7a5*$^{fl/fl}$ animals (left) and mutant *Nestin*^{Cre}*;Slc7a5*$^{fl/fl}$ (right) animals at P0. Scale bar = 5 mm.
(D). Brain weight of mutant *Nestin*^{Cre}*;Slc7a5*$^{fl/fl}$ animals (right, red bar) is significantly decreased compared to control animals (left, grey bar) at P0. ***P <0.001 (means ± SEM; *n*=14 animals/genotype).
(E). Decreased brain/body ratio in mutant *Nestin*^{Cre}*;Slc7a5*$^{fl/fl}$ animals (right, red bar) compared to control animals (left, grey bar) at P0. **P <0.01 (means ± SEM; *n*=14 animals/genotype).
(F). Nissl staining of control *Slc7a5*$^{fl/fl}$ animals (upper panel) and mutant *Nestin*^{Cre}*;Slc7a5*$^{fl/fl}$ (middle panel) animals at P0. Decreased cortical thickness in mutants (lower panel, right) compared to controls (lower panel, left). Scale bar = 500 um.
(G). Immunolabeling of upper cortical layer neurons (Cux1+, green) and lower cortical layer neurons (Ctip2+, red) at P0. Decreased cell number and staining intensity in mutant *Nestin*^{Cre}*;Slc7a5*$^{fl/fl}$ animals (middle column) compared to controls (left column) or to *Nestin*^{Cre}*;Slc7a5*$^{+/+}$ animals carrying only the Nestin- Cre recombinase (right column). Cux1+ cell numbers (lower left graph) are decreased in mutant *Nestin*^{Cre}*;Slc7a5*$^{fl/fl}$ animals (red bar) compared to controls (grey bar) or to *Nestin*^{Cre}*;Slc7a5*$^{+/+}$ animals (white bar). Ctip2+ cell numbers (lower right graph) are similar in all three genotypes. *P<0.05; n.s. = not significant (means ± SEM; *n*=5 animals for control and mutants, *n*=2 for *Nestin*^{Cre}*;Slc7a5*$^{+/+}$). Scale bar = 100um.
(H). Western blot analysis from whole brain lysates of control *Slc7a5*$^{fl/fl}$ and *Nestin*^{Cre}*;Slc7a5*$^{fl/fl}$ mice, indicating that mutants exhibit increased total 4EBP1 and phospho-4EBP1 protein levels at P0. Gapdh was used as internal control. Representative blots (left) and quantification (right); **P<0.01 (means ± SEM; *n*=6 animals/genotype).

3.5 Discussion

Although SLC7A5 has been described as a BBB amino acid transporter, studies accurately verifying its expression or examining its function at the BBB are completely missing in the literature. Moreover, transport studies were performed using only *in vitro* systems thus lacking the expression of other carriers with possibly overlapping substrates and its physiological importance remained almost completely undetermined.

Our study shows that *SLC7A5* loss of function leads to ASD and motor dysfunctions in humans and mice. This fits with our previous work in which we have shown that mutations implicated in abnormal BCAA catabolism lead to ASD and fine motor coordination problems (Novarino et al., 2012a). Along the same line, an increase in the brain levels of these same amino acids leads to the maple syrup urine disorder, characterized by cognitive dysfunctions, seizures and hypotonia (Menkes, Hurst, & Craig, 1954; Snyderman, Norton, Roitman, & Holt, 1964; Zinnanti et al., 2009). Although we acknowledge that ASD due to *SLC7A5* mutations may be an extremely rare condition, the present study indicates that fine-tuning of brain BCAA and LNAA concentrations is key for normal brain function and that mutations affecting genes contributing to BCAA homeostasis and the downstream signaling cascade may underlie a larger subgroup of ASD. In addition, this work has several important pathophysiological implications.

We show that *Slc7a5* expression at the BBB is particularly important to set a correct brain BCAA concentration. In fact, a lack of *Slc7a5* expression at the BBB leads to a significant reduction in brain BCAA levels, particularly leucine and isoleucine. Surprisingly, we didn't detect significant reductions in the brain levels of the other LNAAs, which in the mutant mice are rather slightly increased, indicating that additional carriers are involved in their transport. Among the most altered amino acids, beside leucine and isoleucine, we detected histidine, suggesting that this amino acid may have a special role in the function of the transporter. Noteworthy, the normal brain histamine levels (Figure S2C) as well as the RNA-seq data obtained from mutant mice exclude an alteration of histaminergic transmission. Moreover, abnormally high serum and cerebrospinal fluid histidine levels have been reported in healthy individuals implying that increased histidine concentration is non-pathological (Lam, Cleary, Wraith, & Walter, 1996).

Furthermore, we show that deletion of *Slc7a5* from the BBB leads to activation of the AAR pathway and reduced cap-dependent translation. How exactly abnormal regulation of translation leads to the observed phenotypes in *SLC7A5* mutant humans and mice remains to be investigated. However, we observed that inhibitory neurons may be more sensitive to altered amino acid levels as Atf5, a key molecule in the AAR pathway, has been reported to be preferentially expressed in GABA-synthetizing neurons (Zeisel et al., 2015). Accordingly, we found that deletion of *Slc7a5* from the BBB is sufficient to reduce cortical inhibitory activity, resulting in cortical excitation/inhibition imbalance and probably causing the observed neurological complications. In addition, we also found that the deletion of *Slc7a5* from the neural progenitor cells (i.e. $Nestin^{Cre};Slc7a5^{fl/fl}$ line) recapitulates the microcephaly observed in patients carrying *SLC7A5* missense mutations. Based on our preliminary findings, the microcephaly is the result of a decrease in cortical upper layer cell numbers but the exact mechanism of onset requires further investigation.

Notably, besides representing a new subgroup of ASD, BCAA-related ASD may also represent a group of treatable conditions. Indeed, BCAA dietary administration in *BCKDK* null mice and humans (Novarino et al., 2012a) as well as leucine and isoleucine i.c.v.

injection in adult *Tie2*^{Cre}*;Slc7a5*$^{fl/fl}$ mice lead to a significant improvement of the neurobehavioral abnormalities.

4 Chapter 4 - Conclusions and future directions

Science is always in a constant evolution, and research into complex disorders such as autism makes no exception. Many advances have been made not only in the technologies being used, but also in the way autism is defined. The transition from autism to ASD brought along not only a widening in the phenotypes that characterize this disorder but also the recognition of a complex gene-environment susceptibility landscape. Unequivocally, the recent progress in genomic technologies has revolutionized our knowledge about the genetics of ASD and NDDs in general. Furthermore, the increasing numbers of international, large study cohorts that combine ASD patients data and scientific knowledge from research groups all over the world have led to a series of reproducible scientific findings. Taken together all these efforts help understand the susceptibility landscape and set the stage for preventive and personalized therapeutic research.

ASD may be viewed as one of the more complex of the complex diseases. Starting with the complex phenotypic spectrum, which includes known genetic disorders (i.e. FXS, RS), to the male bias observed within numerous cases, to the abundant genetic findings, and finally to the increased potential for gene-gene interactions, gene-environment interactions, and epigenetic effects there are ample proofs for complexity.

To tackle these complexities, the aim set forth in this study was to navigate from autistic phenotype to genetic disentangling of risk factors, from risk gene to animal models and eventually to preclinical evidence for a potential personalized therapy approach. We initialized this study by pondering on the role of the BCAAs in brain function and development based on the results obtained in a previous publication where patients presenting with ASD, ID and epilepsy were carriers of homozygous mutations in the gene *BCKDK* - involved in BCAA metabolism – and displayed abnormally low levels of serum and brain BCAAs. Given that BCAAs appeared to be essential for the brain, factors facilitating their uptake would have also been critical for the proper function of the CNS. Thus, we showed that the solute carrier transporter 7a5 (Slc7a5), a large amino acid transporter located mainly at the BBB, has an essential role in maintaining normal levels of brain BCAAs. Furthermore, we continued the quest of understanding the role of this transporter and identified several patients with ASD, microcephaly and motor delay carrying deleterious homozygous mutations in the *SLC7A5*. In mice, deletion of *Slc7a5* from the endothelial cells of the BBB led to decreased levels of brain BCAAs, altered cap-dependent translation and severe neurological phenotype. However, BCAA i.c.v. administration ameliorated certain abnormal behaviors in the adult mutant mice.

Disrupted protein translation has been described in multiple models of syndromic ASD (See Chapter 1) and the connection between uncontrolled translation and ASD has become strong enough to initiate a series of studies using pharmacological inhibitors for multiple forms of ASD (See 2.5). In our findings, due to a BCAA deficiency further downstream amino acid starvation cascades become active leading to a stall in protein production opposed to the uncontrolled over-translation of proteins seen in other ASD models where the mTOR pathway is affected. Thus, even if by different means, the numerous disruptions are inhibiting normal cellular responses that guard the integrity of protein translation pointing out that too much or too little synthesis leads in the end to similar phenotypes.

Worth reiterating, in light of the pathophysiological hypothesis underlying ASD (See 1.7.1), is the fact that the deletion of Slc7a5 from the BBB was sufficient to reduce cortical inhibitory activity, altering the excitation/inhibition balance and probably causing the neurological

phenotype. Similarly, most of the functionally characterized ASD-mutations lead to an imbalance in the excitation/inhibition ratio (See 1.7.1). Thus, drugs acting on GABA transmission are considered an opportunity for the treatment of ASD and epilepsy (Braat & Kooy, 2015). It is therefore tempting to reason that identifying the rules by which simple molecules such as the BCAAs may regulate GABAergic transmission might have a crucial impact on the development of novel individualized therapeutic strategies for ASD.
In conclusion, the results provided in this work - even though in their infancy - represent a good foundation for further studies investigating how amino acids contribute to normal and diseased brain states.

5 References

Amir, R. E., Van den Veyver, I. B., Wan, M., Tran, C. Q., Francke, U., & Zoghbi, H. Y. (1999). Rett syndrome is caused by mutations in X-linked MECP2, encoding methyl-CpG-binding protein 2. *Nat Genet, 23*(2), 185-188. doi:10.1038/13810

Angelastro, J. M., Ignatova, T. N., Kukekov, V. G., Steindler, D. A., Stengren, G. B., Mendelsohn, C., & Greene, L. A. (2003). Regulated expression of ATF5 is required for the progression of neural progenitor cells to neurons. *J Neurosci, 23*(11), 4590-4600.

Atmaca, M., Yildirim, H., Ozdemir, H., Tezcan, E., & Poyraz, A. K. (2007). Volumetric MRI study of key brain regions implicated in obsessive-compulsive disorder. *Prog Neuropsychopharmacol Biol Psychiatry, 31*(1), 46-52. doi:10.1016/j.pnpbp.2006.06.008

Autism, Developmental Disabilities Monitoring Network Surveillance Year Principal, I., Centers for Disease, C., & Prevention. (2012). Prevalence of autism spectrum disorders--Autism and Developmental Disabilities Monitoring Network, 14 sites, United States, 2008. *MMWR Surveill Summ, 61*(3), 1-19.

Bagni, C., Tassone, F., Neri, G., & Hagerman, R. (2012). Fragile X syndrome: causes, diagnosis, mechanisms, and therapeutics. *J Clin Invest, 122*(12), 4314-4322. doi:10.1172/JCI63141

Banko, J. L., & Klann, E. (2008). Cap-dependent translation initiation and memory. *Prog Brain Res, 169*, 59-80. doi:10.1016/S0079-6123(07)00004-0

Bateup, H. S., Johnson, C. A., Denefrio, C. L., Saulnier, J. L., Kornacker, K., & Sabatini, B. L. (2013). Excitatory/inhibitory synaptic imbalance leads to hippocampal hyperexcitability in mouse models of tuberous sclerosis. *Neuron, 78*(3), 510-522. doi:10.1016/j.neuron.2013.03.017

Baudouin, S. J., Gaudias, J., Gerharz, S., Hatstatt, L., Zhou, K., Punnakkal, P., . . . Scheiffele, P. (2012). Shared synaptic pathophysiology in syndromic and nonsyndromic rodent models of autism. *Science, 338*(6103), 128-132. doi:10.1126/science.1224159

Bauminger, N., Shulman, C., & Agam, G. (2003). Peer interaction and loneliness in high-functioning children with autism. *J Autism Dev Disord, 33*(5), 489-507.

Beaudet, A. L., & Meng, L. (2016). Gene-targeting pharmaceuticals for single-gene disorders. *Hum Mol Genet, 25*(R1), R18-26. doi:10.1093/hmg/ddv476

Bernardet, M., & Crusio, W. E. (2006). Fmr1 KO mice as a possible model of autistic features. *ScientificWorldJournal, 6*, 1164-1176. doi:10.1100/tsw.2006.220

Berry-Kravis, E., Des Portes, V., Hagerman, R., Jacquemont, S., Charles, P., Visootsak, J., . . . von Raison, F. (2016). Mavoglurant in fragile X syndrome: Results of two randomized, double-blind, placebo-controlled trials. *Sci Transl Med, 8*(321), 321ra325. doi:10.1126/scitranslmed.aab4109

Birey, F., Andersen, J., Makinson, C. D., Islam, S., Wei, W., Huber, N., . . . Pasca, S. P. (2017). Assembly of functionally integrated human forebrain spheroids. *Nature, 545*(7652), 54-59. doi:10.1038/nature22330

Bourgeron, T. (2009). A synaptic trek to autism. *Curr Opin Neurobiol, 19*(2), 231-234. doi:10.1016/j.conb.2009.06.003

Braat, S., & Kooy, R. F. (2015). The GABAA Receptor as a Therapeutic Target for Neurodevelopmental Disorders. *Neuron, 86*(5), 1119-1130. doi:10.1016/j.neuron.2015.03.042

Braun, L. D., Cornford, E. M., & Oldendorf, W. H. (1980). Newborn rabbit blood-brain barrier is selectively permeable and differs substantially from the adult. *J Neurochem, 34*(1), 147-152.

Brown, V., Jin, P., Ceman, S., Darnell, J. C., O'Donnell, W. T., Tenenbaum, S. A., . . . Warren, S. T. (2001). Microarray identification of FMRP-associated brain mRNAs and altered mRNA translational profiles in fragile X syndrome. *Cell, 107*(4), 477-487.

Bruining, H., Eijkemans, M. J., Kas, M. J., Curran, S. R., Vorstman, J. A., & Bolton, P. F. (2014). Behavioral signatures related to genetic disorders in autism. *Mol Autism, 5*(1), 11. doi:10.1186/2040-2392-5-11

Budde, K., Zonnenberg, B. A., Frost, M., Cheung, W., Urva, S., Brechenmacher, T., . . . Bissler, J. J. (2016). Pharmacokinetics and pharmacodynamics of everolimus in patients with renal angiomyolipoma and tuberous sclerosis complex or lymphangioleiomyomatosis. *Br J Clin Pharmacol, 81*(5), 958-970. doi:10.1111/bcp.12834

Cameron, A., Bansal, A., Dua, T., Hill, S. R., Moshe, S. L., Mantel-Teeuwisse, A. K., & Saxena, S. (2012). Mapping the availability, price, and affordability of antiepileptic drugs in 46 countries. *Epilepsia, 53*(6), 962-969. doi:10.1111/j.1528-1167.2012.03446.x

Canitano, R. (2007). Epilepsy in autism spectrum disorders. *Eur Child Adolesc Psychiatry, 16*(1), 61-66. doi:10.1007/s00787-006-0563-2

Carson, R. P., Van Nielen, D. L., Winzenburger, P. A., & Ess, K. C. (2012). Neuronal and glia abnormalities in Tsc1-deficient forebrain and partial rescue by rapamycin. *Neurobiol Dis, 45*(1), 369-380. doi:10.1016/j.nbd.2011.08.024

Carter, R. J., Morton, J., & Dunnett, S. B. (2001). Motor coordination and balance in rodents. *Curr Protoc Neurosci, Chapter 8*, Unit 8 12. doi:10.1002/0471142301.ns0812s15

Castro, J., Garcia, R. I., Kwok, S., Banerjee, A., Petravicz, J., Woodson, J., . . . Sur, M. (2014). Functional recovery with recombinant human IGF1 treatment in a mouse model of Rett Syndrome. *Proc Natl Acad Sci U S A, 111*(27), 9941-9946. doi:10.1073/pnas.1311685111

Chamberlain, S. J., Chen, P. F., Ng, K. Y., Bourgois-Rocha, F., Lemtiri-Chlieh, F., Levine, E. S., & Lalande, M. (2010). Induced pluripotent stem cell models of the genomic imprinting disorders Angelman and Prader-Willi syndromes. *Proc Natl Acad Sci U S A, 107*(41), 17668-17673. doi:10.1073/pnas.1004487107

Chen, A., Muzzio, I. A., Malleret, G., Bartsch, D., Verbitsky, M., Pavlidis, P., . . . Kandel, E. R. (2003). Inducible enhancement of memory storage and synaptic plasticity in transgenic mice expressing an inhibitor of ATF4 (CREB-2) and C/EBP proteins. *Neuron, 39*(4), 655-669.

Costa-Mattioli, M., Gobert, D., Harding, H., Herdy, B., Azzi, M., Bruno, M., . . . Sonenberg, N. (2005). Translational control of hippocampal synaptic plasticity and memory by the eIF2alpha kinase GCN2. *Nature, 436*(7054), 1166-1173. doi:10.1038/nature03897

Courchesne, E., Campbell, K., & Solso, S. (2011). Brain growth across the life span in autism: age-specific changes in anatomical pathology. *Brain Res, 1380*, 138-145. doi:10.1016/j.brainres.2010.09.101

Dani, V. S., & Nelson, S. B. (2009). Intact long-term potentiation but reduced connectivity between neocortical layer 5 pyramidal neurons in a mouse model of Rett syndrome. *J Neurosci, 29*(36), 11263-11270. doi:10.1523/JNEUROSCI.1019-09.2009

Daniels, A. M., & Mandell, D. S. (2014). Explaining differences in age at autism spectrum disorder diagnosis: a critical review. *Autism, 18*(5), 583-597. doi:10.1177/1362361313480277

Darnell, J. C., & Klann, E. (2013). The translation of translational control by FMRP: therapeutic targets for FXS. *Nat Neurosci, 16*(11), 1530-1536. doi:10.1038/nn.3379

de la Torre-Ubieta, L., Won, H., Stein, J. L., & Geschwind, D. H. (2016). Advancing the understanding of autism disease mechanisms through genetics. *Nat Med, 22*(4), 345-361. doi:10.1038/nm.4071

de Ligt, J., Willemsen, M. H., van Bon, B. W., Kleefstra, T., Yntema, H. G., Kroes, T., . . . Vissers, L. E. (2012). Diagnostic exome sequencing in persons with severe intellectual disability. *N Engl J Med, 367*(20), 1921-1929. doi:10.1056/NEJMoa1206524

De Rubeis, S., He, X., Goldberg, A. P., Poultney, C. S., Samocha, K., Cicek, A. E., . . . Buxbaum, J. D. (2014). Synaptic, transcriptional and chromatin genes disrupted in autism. *Nature, 515*(7526), 209-215. doi:10.1038/nature13772

Deacon, R. M. (2006). Digging and marble burying in mice: simple methods for in vivo identification of biological impacts. *Nat Protoc, 1*(1), 122-124. doi:10.1038/nprot.2006.20

Deciphering Developmental Disorders, S. (2015). Large-scale discovery of novel genetic causes of developmental disorders. *Nature, 519*(7542), 223-228. doi:10.1038/nature14135

del Amo, E. M., Urtti, A., & Yliperttula, M. (2008). Pharmacokinetic role of L-type amino acid transporters LAT1 and LAT2. *Eur J Pharm Sci, 35*(3), 161-174. doi:10.1016/j.ejps.2008.06.015

DeLano, W. L. (2002). Unraveling hot spots in binding interfaces: progress and challenges. *Curr Opin Struct Biol, 12*(1), 14-20.

DeVos, S. L., & Miller, T. M. (2013). Direct intraventricular delivery of drugs to the rodent central nervous system. *J Vis Exp*(75), e50326. doi:10.3791/50326

Dixon-Salazar, T. J., Silhavy, J. L., Udpa, N., Schroth, J., Bielas, S., Schaffer, A. E., . . . Gleeson, J. G. (2012). Exome sequencing can improve diagnosis and alter patient management. *Sci Transl Med, 4*(138), 138ra178. doi:10.1126/scitranslmed.3003544

Dubois, N. C., Hofmann, D., Kaloulis, K., Bishop, J. M., & Trumpp, A. (2006). Nestin-Cre transgenic mouse line Nes-Cre1 mediates highly efficient Cre/loxP mediated recombination in the nervous system, kidney, and somite-derived tissues. *Genesis, 44*(8), 355-360. doi:10.1002/dvg.20226

Edmonson, C. A., Ziats, M. N., & Rennert, O. M. (2016). A Non-inflammatory Role for Microglia in Autism Spectrum Disorders. *Front Neurol, 7*, 9. doi:10.3389/fneur.2016.00009

Elsabbagh, M., Divan, G., Koh, Y. J., Kim, Y. S., Kauchali, S., Marcin, C., . . . Fombonne, E. (2012). Global prevalence of autism and other pervasive developmental disorders. *Autism Res, 5*(3), 160-179. doi:10.1002/aur.239

Espinosa, J. S., & Stryker, M. P. (2012). Development and plasticity of the primary visual cortex. *Neuron, 75*(2), 230-249. doi:10.1016/j.neuron.2012.06.009

Fombonne, E. (2009). Epidemiology of pervasive developmental disorders. *Pediatr Res, 65*(6), 591-598. doi:10.1203/PDR.0b013e31819e7203

Fombonne, E., Roge, B., Claverie, J., Courty, S., & Fremolle, J. (1999). Microcephaly and macrocephaly in autism. *J Autism Dev Disord, 29*(2), 113-119.

Fotiadis, D., Kanai, Y., & Palacin, M. (2013). The SLC3 and SLC7 families of amino acid transporters. *Mol Aspects Med, 34*(2-3), 139-158. doi:10.1016/j.mam.2012.10.007

Fountain, C., Winter, A. S., & Bearman, P. S. (2012). Six developmental trajectories characterize children with autism. *Pediatrics, 129*(5), e1112-1120. doi:10.1542/peds.2011-1601

Fournier, K. A., Hass, C. J., Naik, S. K., Lodha, N., & Cauraugh, J. H. (2010). Motor coordination in autism spectrum disorders: a synthesis and meta-analysis. *J Autism Dev Disord, 40*(10), 1227-1240. doi:10.1007/s10803-010-0981-3

Frith, C. D. (2007). The social brain? *Philos Trans R Soc Lond B Biol Sci, 362*(1480), 671-678. doi:10.1098/rstb.2006.2003

Gadalla, K. K. E., Vudhironarit, T., Hector, R. D., Sinnett, S., Bahey, N. G., Bailey, M. E. S., . . . Cobb, S. R. (2017). Development of a Novel AAV Gene Therapy Cassette with Improved Safety Features and Efficacy in a Mouse Model of Rett Syndrome. *Mol Ther Methods Clin Dev, 5*, 180-190. doi:10.1016/j.omtm.2017.04.007

Galluccio, M., Amelio, L., Scalise, M., Pochini, L., Boles, E., & Indiveri, C. (2012). Over-expression in E. coli and purification of the human OCTN2 transport protein. *Mol Biotechnol, 50*(1), 1-7. doi:10.1007/s12033-011-9406-6

Galluccio, M., Pingitore, P., Scalise, M., & Indiveri, C. (2013). Cloning, large scale over-expression in E. coli and purification of the components of the human LAT 1 (SLC7A5) amino acid transporter. *Protein J, 32*(6), 442-448. doi:10.1007/s10930-013-9503-4

Galluccio, M., Pochini, L., Peta, V., Ianni, M., Scalise, M., & Indiveri, C. (2015). Functional and molecular effects of mercury compounds on the human OCTN1 cation transporter: C50 and C136 are the targets for potent inhibition. *Toxicol Sci, 144*(1), 105-113. doi:10.1093/toxsci/kfu259

Gantois, I., Khoutorsky, A., Popic, J., Aguilar-Valles, A., Freemantle, E., Cao, R., . . . Sonenberg, N. (2017). Metformin ameliorates core deficits in a mouse model of fragile X syndrome. *Nat Med, 23*(6), 674-677. doi:10.1038/nm.4335

Gao, X., Zhou, L., Jiao, X., Lu, F., Yan, C., Zeng, X., . . . Shi, Y. (2010). Mechanism of substrate recognition and transport by an amino acid antiporter. *Nature, 463*(7282), 828-832. doi:10.1038/nature08741

Garcia-Cazorla, A., Oyarzabal, A., Fort, J., Robles, C., Castejon, E., Ruiz-Sala, P., . . . Agullo, S. B. (2014). Two novel mutations in the BCKDK (branched-chain keto-acid dehydrogenase kinase) gene are responsible for a neurobehavioral deficit in two pediatric unrelated patients. *Hum Mutat, 35*(4), 470-477. doi:10.1002/humu.22513

Gaugler, T., Klei, L., Sanders, S. J., Bodea, C. A., Goldberg, A. P., Lee, A. B., . . . Buxbaum, J. D. (2014). Most genetic risk for autism resides with common variation. *Nat Genet, 46*(8), 881-885. doi:10.1038/ng.3039

Geier, E. G., Schlessinger, A., Fan, H., Gable, J. E., Irwin, J. J., Sali, A., & Giacomini, K. M. (2013). Structure-based ligand discovery for the Large-neutral Amino Acid Transporter 1, LAT-1. *Proc Natl Acad Sci U S A, 110*(14), 5480-5485. doi:10.1073/pnas.1218165110

Geisheker, M. R., Heymann, G., Wang, T., Coe, B. P., Turner, T. N., Stessman, H. A. F., . . . Eichler, E. E. (2017). Hotspots of missense mutation identify neurodevelopmental disorder genes and functional domains. *Nat Neurosci, 20*(8), 1043-1051. doi:10.1038/nn.4589

Gkogkas, C. G., Khoutorsky, A., Ran, I., Rampakakis, E., Nevarko, T., Weatherill, D. B., . . . Sonenberg, N. (2013). Autism-related deficits via dysregulated eIF4E-dependent translational control. *Nature, 493*(7432), 371-377. doi:10.1038/nature11628

Gnirke, A., Melnikov, A., Maguire, J., Rogov, P., LeProust, E. M., Brockman, W., . . . Nusbaum, C. (2009). Solution hybrid selection with ultra-long oligonucleotides for massively parallel targeted sequencing. *Nat Biotechnol, 27*(2), 182-189. doi:nbt.1523 [pii]
10.1038/nbt.1523

Gogolla, N., Takesian, A. E., Feng, G., Fagiolini, M., & Hensch, T. K. (2014). Sensory integration in mouse insular cortex reflects GABA circuit maturation. *Neuron, 83*(4), 894-905. doi:10.1016/j.neuron.2014.06.033

Grayton, H. M., Missler, M., Collier, D. A., & Fernandes, C. (2013). Altered social behaviours in neurexin 1alpha knockout mice resemble core symptoms in neurodevelopmental disorders. *PLoS One, 8*(6), e67114. doi:10.1371/journal.pone.0067114

Green, T. A., Alibhai, I. N., Unterberg, S., Neve, R. L., Ghose, S., Tamminga, C. A., & Nestler, E. J. (2008). Induction of activating transcription factors (ATFs) ATF2, ATF3, and ATF4 in the nucleus accumbens and their regulation of emotional behavior. *J Neurosci, 28*(9), 2025-2032. doi:10.1523/JNEUROSCI.5273-07.2008

Gronborg, T. K., Schendel, D. E., & Parner, E. T. (2013). Recurrence of autism spectrum disorders in full- and half-siblings and trends over time: a population-based cohort study. *JAMA Pediatr, 167*(10), 947-953. doi:10.1001/jamapediatrics.2013.2259

Guyenet, S. J., Furrer, S. A., Damian, V. M., Baughan, T. D., La Spada, A. R., & Garden, G. A. (2010). A simple composite phenotype scoring system for evaluating mouse models of cerebellar ataxia. *J Vis Exp*(39). doi:10.3791/1787

Han, S., Tai, C., Westenbroek, R. E., Yu, F. H., Cheah, C. S., Potter, G. B., . . . Catterall, W. A. (2012). Autistic-like behaviour in Scn1a+/- mice and rescue by enhanced GABA-mediated neurotransmission. *Nature, 489*(7416), 385-390. doi:10.1038/nature11356

Harony-Nicolas, H., Kay, M., Hoffmann, J. D., Klein, M. E., Bozdagi-Gunal, O., Riad, M., . . . Buxbaum, J. D. (2017). Oxytocin improves behavioral and electrophysiological deficits in a novel Shank3-deficient rat. *Elife, 6*. doi:10.7554/eLife.18904

Hattori, N. (2014). Cerebral organoids model human brain development and microcephaly. *Mov Disord, 29*(2), 185. doi:10.1002/mds.25740

Hazlett, H. C., Poe, M. D., Gerig, G., Styner, M., Chappell, C., Smith, R. G., . . . Piven, J. (2011). Early brain overgrowth in autism associated with an increase in cortical surface area before age 2 years. *Arch Gen Psychiatry, 68*(5), 467-476. doi:10.1001/archgenpsychiatry.2011.39

Henderson, L. B., Applegate, C. D., Wohler, E., Sheridan, M. B., Hoover-Fong, J., & Batista, D. A. (2014). The impact of chromosomal microarray on clinical management: a retrospective analysis. *Genet Med, 16*(9), 657-664. doi:10.1038/gim.2014.18

Hu, C., Chen, W., Myers, S. J., Yuan, H., & Traynelis, S. F. (2016). Human GRIN2B variants in neurodevelopmental disorders. *J Pharmacol Sci, 132*(2), 115-121. doi:10.1016/j.jphs.2016.10.002

Hulbert, S. W., & Jiang, Y. H. (2016). Monogenic mouse models of autism spectrum disorders: Common mechanisms and missing links. *Neuroscience, 321*, 3-23. doi:10.1016/j.neuroscience.2015.12.040

Insel, T. R. (2010). The challenge of translation in social neuroscience: a review of oxytocin, vasopressin, and affiliative behavior. *Neuron, 65*(6), 768-779. doi:10.1016/j.neuron.2010.03.005

Iossifov, I., O'Roak, B. J., Sanders, S. J., Ronemus, M., Krumm, N., Levy, D., . . . Wigler, M. (2014). The contribution of de novo coding mutations to autism spectrum disorder. *Nature, 515*(7526), 216-221. doi:10.1038/nature13908

Jiao, J., Yang, Y., Shi, Y., Chen, J., Gao, R., Fan, Y., . . . Gao, S. (2013). Modeling Dravet syndrome using induced pluripotent stem cells (iPSCs) and directly converted neurons. *Hum Mol Genet, 22*(21), 4241-4252. doi:10.1093/hmg/ddt275

Kandt, R. S., Haines, J. L., Smith, M., Northrup, H., Gardner, R. J., Short, M. P., . . . et al. (1992). Linkage of an important gene locus for tuberous sclerosis to a chromosome 16 marker for polycystic kidney disease. *Nat Genet, 2*(1), 37-41. doi:10.1038/ng0992-37

Kanner, L. (1968). Autistic disturbances of affective contact. *Acta Paedopsychiatr, 35*(4), 100-136.

Kelleher, R. J., 3rd, & Bear, M. F. (2008). The autistic neuron: troubled translation? *Cell, 135*(3), 401-406. doi:10.1016/j.cell.2008.10.017

Kilberg, M. S., Shan, J., & Su, N. (2009). ATF4-dependent transcription mediates signaling of amino acid limitation. *Trends Endocrinol Metab, 20*(9), 436-443. doi:10.1016/j.tem.2009.05.008

Kim, J. E., Lyoo, I. K., Estes, A. M., Renshaw, P. F., Shaw, D. W., Friedman, S. D., . . . Dager, S. R. (2010). Laterobasal amygdalar enlargement in 6- to 7-year-old children with autism spectrum disorder. *Arch Gen Psychiatry, 67*(11), 1187-1197. doi:10.1001/archgenpsychiatry.2010.148

Kim, Y. S., & Leventhal, B. L. (2015). Genetic epidemiology and insights into interactive genetic and environmental effects in autism spectrum disorders. *Biol Psychiatry, 77*(1), 66-74. doi:10.1016/j.biopsych.2014.11.001

Kindregan, D., Gallagher, L., & Gormley, J. (2015). Gait deviations in children with autism spectrum disorders: a review. *Autism Res Treat, 2015*, 741480. doi:10.1155/2015/741480

Kisanuki, Y. Y., Hammer, R. E., Miyazaki, J., Williams, S. C., Richardson, J. A., & Yanagisawa, M. (2001). Tie2-Cre transgenic mice: a new model for endothelial cell-lineage analysis in vivo. *Dev Biol, 230*(2), 230-242. doi:10.1006/dbio.2000.0106

Klein, S., Sharifi-Hannauer, P., & Martinez-Agosto, J. A. (2013). Macrocephaly as a clinical indicator of genetic subtypes in autism. *Autism Res, 6*(1), 51-56. doi:10.1002/aur.1266

Kline, D. D., Ogier, M., Kunze, D. L., & Katz, D. M. (2010). Exogenous brain-derived neurotrophic factor rescues synaptic dysfunction in Mecp2-null mice. *J Neurosci, 30*(15), 5303-5310. doi:10.1523/JNEUROSCI.5503-09.2010

Kohrman, M. H. (2012). Emerging treatments in the management of tuberous sclerosis complex. *Pediatr Neurol, 46*(5), 267-275. doi:10.1016/j.pediatrneurol.2012.02.015

Kolevzon, A., Bush, L., Wang, A. T., Halpern, D., Frank, Y., Grodberg, D., . . . Buxbaum, J. D. (2014). A pilot controlled trial of insulin-like growth factor-1 in children with Phelan-McDermid syndrome. *Mol Autism, 5*(1), 54. doi:10.1186/2040-2392-5-54

Krumm, N., Turner, T. N., Baker, C., Vives, L., Mohajeri, K., Witherspoon, K., . . . Eichler, E. E. (2015). Excess of rare, inherited truncating mutations in autism. *Nat Genet, 47*(6), 582-588. doi:10.1038/ng.3303

Krupp, D. R., Barnard, R. A., Duffourd, Y., Evans, S. A., Mulqueen, R. M., Bernier, R., . . . O'Roak, B. J. (2017). Exonic Mosaic Mutations Contribute Risk for Autism Spectrum Disorder. *Am J Hum Genet, 101*(3), 369-390. doi:10.1016/j.ajhg.2017.07.016

Kwon, C. H., Luikart, B. W., Powell, C. M., Zhou, J., Matheny, S. A., Zhang, W., . . . Parada, L. F. (2006). Pten regulates neuronal arborization and social interaction in mice. *Neuron, 50*(3), 377-388. doi:10.1016/j.neuron.2006.03.023

Lam, W. K., Cleary, M. A., Wraith, J. E., & Walter, J. H. (1996). Histidinaemia: a benign metabolic disorder. *Arch Dis Child, 74*(4), 343-346.

Lefauconnier, J. M., & Trouve, R. (1983). Developmental changes in the pattern of amino acid transport at the blood-brain barrier in rats. *Brain Res, 282*(2), 175-182.

Lenoir, P., Bodier, C., Desombre, H., Malvy, J., Abert, B., Ould Taleb, M., & Sauvage, D. (2009). [Prevalence of pervasive developmental disorders. A review]. *Encephale, 35*(1), 36-42. doi:10.1016/j.encep.2007.12.011

Li, J., Cai, T., Jiang, Y., Chen, H., He, X., Chen, C., . . . Wu, J. (2016). Genes with de novo mutations are shared by four neuropsychiatric disorders discovered from NPdenovo database. *Mol Psychiatry, 21*(2), 298. doi:10.1038/mp.2015.58

Lim, E. T., Uddin, M., De Rubeis, S., Chan, Y., Kamumbu, A. S., Zhang, X., . . . Walsh, C. A. (2017). Rates, distribution and implications of postzygotic mosaic mutations in autism spectrum disorder. *Nat Neurosci, 20*(9), 1217-1224. doi:10.1038/nn.4598

Lin, Z., Liu, Z., Li, X., Li, F., Hu, Y., Chen, B., . . . Liu, Y. (2017). Whole-exome sequencing identifies a novel de novo mutation in DYNC1H1 in epileptic encephalopathies. *Sci Rep, 7*(1), 258. doi:10.1038/s41598-017-00208-6

Loke, Y. J., Hannan, A. J., & Craig, J. M. (2015). The Role of Epigenetic Change in Autism Spectrum Disorders. *Front Neurol, 6*, 107. doi:10.3389/fneur.2015.00107

Lord, C., Risi, S., Lambrecht, L., Cook, E. H., Jr., Leventhal, B. L., DiLavore, P. C., . . . Rutter, M. (2000). The autism diagnostic observation schedule-generic: a standard measure of social and communication deficits associated with the spectrum of autism. *J Autism Dev Disord, 30*(3), 205-223.

Loth, E., Spooren, W., Ham, L. M., Isaac, M. B., Auriche-Benichou, C., Banaschewski, T., . . . Murphy, D. G. (2016). Identification and validation of biomarkers for autism spectrum disorders. *Nat Rev Drug Discov, 15*(1), 70-73. doi:10.1038/nrd.2015.7

Lozano, R., Martinez-Cerdeno, V., & Hagerman, R. J. (2015). Advances in the Understanding of the Gabaergic Neurobiology of FMR1 Expanded Alleles Leading to Targeted Treatments for Fragile X Spectrum Disorder. *Curr Pharm Des, 21*(34), 4972-4979.

Lu, A. T., & Cantor, R. M. (2012). Allowing for sex differences increases power in a GWAS of multiplex Autism families. *Mol Psychiatry, 17*(2), 215-222. doi:10.1038/mp.2010.127

Lynch, M. (2010). Rate, molecular spectrum, and consequences of human mutation. *Proc Natl Acad Sci U S A, 107*(3), 961-968. doi:10.1073/pnas.0912629107

Manning, M., Hudgins, L., Professional, P., & Guidelines, C. (2010). Array-based technology and recommendations for utilization in medical genetics practice for detection of chromosomal abnormalities. *Genet Med, 12*(11), 742-745. doi:10.1097/GIM.0b013e3181f8baad

Marchetto, M. C., Carromeu, C., Acab, A., Yu, D., Yeo, G. W., Mu, Y., . . . Muotri, A. R. (2010). A model for neural development and treatment of Rett syndrome using human induced pluripotent stem cells. *Cell, 143*(4), 527-539. doi:10.1016/j.cell.2010.10.016

Markram, K., & Markram, H. (2010). The intense world theory - a unifying theory of the neurobiology of autism. *Front Hum Neurosci, 4*, 224. doi:10.3389/fnhum.2010.00224

Mastroberardino, L., Spindler, B., Pfeiffer, R., Skelly, P. J., Loffing, J., Shoemaker, C. B., & Verrey, F. (1998). Amino-acid transport by heterodimers of 4F2hc/CD98 and members of a permease family. *Nature, 395*(6699), 288-291. doi:10.1038/26246

Matson, J. L., & Shoemaker, M. (2009). Intellectual disability and its relationship to autism spectrum disorders. *Res Dev Disabil, 30*(6), 1107-1114. doi:10.1016/j.ridd.2009.06.003

Matsuo, H., Tsukada, S., Nakata, T., Chairoungdua, A., Kim, D. K., Cha, S. H., . . . Kanai, Y. (2000). Expression of a system L neutral amino acid transporter at the blood-brain barrier. *Neuroreport, 11*(16), 3507-3511.

McBride, K. L., Varga, E. A., Pastore, M. T., Prior, T. W., Manickam, K., Atkin, J. F., & Herman, G. E. (2010). Confirmation study of PTEN mutations among individuals with autism or developmental delays/mental retardation and macrocephaly. *Autism Res, 3*(3), 137-141. doi:10.1002/aur.132

McCammon, J. M., & Sive, H. (2015). Addressing the Genetics of Human Mental Health Disorders in Model Organisms. *Annu Rev Genomics Hum Genet, 16*, 173-197. doi:10.1146/annurev-genom-090314-050048

Mefford, H. C., Batshaw, M. L., & Hoffman, E. P. (2012). Genomics, intellectual disability, and autism. *N Engl J Med, 366*(8), 733-743. doi:10.1056/NEJMra1114194

Meng, L., Ward, A. J., Chun, S., Bennett, C. F., Beaudet, A. L., & Rigo, F. (2015). Towards a therapy for Angelman syndrome by targeting a long non-coding RNA. *Nature, 518*(7539), 409-412. doi:10.1038/nature13975

Menkes, J. H., Hurst, P. L., & Craig, J. M. (1954). A new syndrome: progressive familial infantile cerebral dysfunction associated with an unusual urinary substance. *Pediatrics, 14*(5), 462-467.

Miles, J. H. (2011). Autism spectrum disorders--a genetics review. *Genet Med, 13*(4), 278-294. doi:10.1097/GIM.0b013e3181ff67ba

Mills, M., & Melhuish, E. (1974). Recognition of mother's voice in early infancy. *Nature, 252*(5479), 123-124.

Moy, S. S., Nadler, J. J., Young, N. B., Perez, A., Holloway, L. P., Barbaro, R. P., . . . Crawley, J. N. (2007). Mouse behavioral tasks relevant to autism: phenotypes of 10 inbred strains. *Behav Brain Res, 176*(1), 4-20. doi:10.1016/j.bbr.2006.07.030

Napolitano, L., Scalise, M., Galluccio, M., Pochini, L., Albanese, L. M., & Indiveri, C. (2015). LAT1 is the transport competent unit of the LAT1/CD98 heterodimeric amino acid transporter. *Int J Biochem Cell Biol, 67*, 25-33. doi:10.1016/j.biocel.2015.08.004

Nava, C., Dalle, C., Rastetter, A., Striano, P., de Kovel, C. G., Nabbout, R., . . . Depienne, C. (2014). De novo mutations in HCN1 cause early infantile epileptic encephalopathy. *Nat Genet, 46*(6), 640-645. doi:10.1038/ng.2952

Nelson, E. D., Kavalali, E. T., & Monteggia, L. M. (2006). MeCP2-dependent transcriptional repression regulates excitatory neurotransmission. *Curr Biol, 16*(7), 710-716. doi:10.1016/j.cub.2006.02.062

Nelson, S. B., & Valakh, V. (2015). Excitatory/Inhibitory Balance and Circuit Homeostasis in Autism Spectrum Disorders. *Neuron, 87*(4), 684-698. doi:10.1016/j.neuron.2015.07.033

Noebels, J. (2015). Pathway-driven discovery of epilepsy genes. *Nat Neurosci, 18*(3), 344-350. doi:10.1038/nn.3933

Novarino, G., El-Fishawy, P., Kayserili, H., Meguid, N. A., Scott, E. M., Schroth, J., . . . Gleeson, J. G. (2012a). Mutations in BCKD-kinase lead to a potentially treatable form of autism with epilepsy. *Science, 338*(6105), 394-397. doi:10.1126/science.1224631

Numis, A. L., Major, P., Montenegro, M. A., Muzykewicz, D. A., Pulsifer, M. B., & Thiele, E. A. (2011). Identification of risk factors for autism spectrum disorders in tuberous

sclerosis complex. *Neurology, 76*(11), 981-987. doi:10.1212/WNL.0b013e3182104347

Ogiwara, I., Miyamoto, H., Morita, N., Atapour, N., Mazaki, E., Inoue, I., . . . Yamakawa, K. (2007). Nav1.1 localizes to axons of parvalbumin-positive inhibitory interneurons: a circuit basis for epileptic seizures in mice carrying an Scn1a gene mutation. *J Neurosci, 27*(22), 5903-5914. doi:10.1523/JNEUROSCI.5270-06.2007

Oguro-Ando, A., Rosensweig, C., Herman, E., Nishimura, Y., Werling, D., Bill, B. R., . . . Geschwind, D. H. (2015). Increased CYFIP1 dosage alters cellular and dendritic morphology and dysregulates mTOR. *Mol Psychiatry, 20*(9), 1069-1078. doi:10.1038/mp.2014.124

Ooi, Y. P., Weng, S. J., Kossowsky, J., Gerger, H., & Sung, M. (2017). Oxytocin and Autism Spectrum Disorders: A Systematic Review and Meta-Analysis of Randomized Controlled Trials. *Pharmacopsychiatry, 50*(1), 5-13. doi:10.1055/s-0042-109400

Paquet, A., Olliac, B., Golse, B., & Vaivre-Douret, L. (2016). [Formula: see text]Current knowledge on motor disorders in children with autism spectrum disorder (ASD). *Child Neuropsychol, 22*(7), 763-794. doi:10.1080/09297049.2015.1085501

Pasca, A. M., Sloan, S. A., Clarke, L. E., Tian, Y., Makinson, C. D., Huber, N., . . . Pasca, S. P. (2015). Functional cortical neurons and astrocytes from human pluripotent stem cells in 3D culture. *Nat Methods, 12*(7), 671-678. doi:10.1038/nmeth.3415

Pasca, S. P., Portmann, T., Voineagu, I., Yazawa, M., Shcheglovitov, A., Pasca, A. M., . . . Dolmetsch, R. E. (2011). Using iPSC-derived neurons to uncover cellular phenotypes associated with Timothy syndrome. *Nat Med, 17*(12), 1657-1662. doi:10.1038/nm.2576

Phelan, K., & McDermid, H. E. (2012). The 22q13.3 Deletion Syndrome (Phelan-McDermid Syndrome). *Mol Syndromol, 2*(3-5), 186-201. doi:000334260

Pini, G., Congiu, L., Benincasa, A., DiMarco, P., Bigoni, S., Dyer, A. H., . . . Tropea, D. (2016). Illness Severity, Social and Cognitive Ability, and EEG Analysis of Ten Patients with Rett Syndrome Treated with Mecasermin (Recombinant Human IGF-1). *Autism Res Treat, 2016*, 5073078. doi:10.1155/2016/5073078

Pinto, D., Delaby, E., Merico, D., Barbosa, M., Merikangas, A., Klei, L., . . . Scherer, S. W. (2014). Convergence of genes and cellular pathways dysregulated in autism spectrum disorders. *Am J Hum Genet, 94*(5), 677-694. doi:10.1016/j.ajhg.2014.03.018

Poduri, A., Evrony, G. D., Cai, X., & Walsh, C. A. (2013). Somatic mutation, genomic variation, and neurological disease. *Science, 341*(6141), 1237758. doi:10.1126/science.1237758

Quadrato, G., Brown, J., & Arlotta, P. (2016). The promises and challenges of human brain organoids as models of neuropsychiatric disease. *Nat Med, 22*(11), 1220-1228. doi:10.1038/nm.4214

Redcay, E. (2008). The superior temporal sulcus performs a common function for social and speech perception: implications for the emergence of autism. *Neurosci Biobehav Rev, 32*(1), 123-142. doi:10.1016/j.neubiorev.2007.06.004

Reijnders, M. R. F., Kousi, M., van Woerden, G. M., Klein, M., Bralten, J., Mancini, G. M. S., . . . Brunner, H. G. (2017). Variation in a range of mTOR-related genes associates with intracranial volume and intellectual disability. *Nat Commun, 8*(1), 1052. doi:10.1038/s41467-017-00933-6

Richter, J. D., & Sonenberg, N. (2005). Regulation of cap-dependent translation by eIF4E inhibitory proteins. *Nature, 433*(7025), 477-480. doi:10.1038/nature03205

Rinehart, N. J., Tonge, B. J., Bradshaw, J. L., Iansek, R., Enticott, P. G., & McGinley, J. (2006). Gait function in high-functioning autism and Asperger's disorder : evidence for basal-ganglia and cerebellar involvement? *Eur Child Adolesc Psychiatry, 15*(5), 256-264. doi:10.1007/s00787-006-0530-y

Romano, E., Michetti, C., Caruso, A., Laviola, G., & Scattoni, M. L. (2013). Characterization of neonatal vocal and motor repertoire of reelin mutant mice. *PLoS One, 8*(5), e64407. doi:10.1371/journal.pone.0064407

Rothwell, P. E., Fuccillo, M. V., Maxeiner, S., Hayton, S. J., Gokce, O., Lim, B. K., . . . Sudhof, T. C. (2014). Autism-associated neuroligin-3 mutations commonly impair striatal circuits to boost repetitive behaviors. *Cell, 158*(1), 198-212. doi:10.1016/j.cell.2014.04.045

Rubenstein, J. L., & Merzenich, M. M. (2003). Model of autism: increased ratio of excitation/inhibition in key neural systems. *Genes Brain Behav, 2*(5), 255-267.

Saier, M. H., Jr., Yen, M. R., Noto, K., Tamang, D. G., & Elkan, C. (2009). The Transporter Classification Database: recent advances. *Nucleic Acids Res, 37*(Database issue), D274-278. doi:10.1093/nar/gkn862

Sanders, S. J., He, X., Willsey, A. J., Ercan-Sencicek, A. G., Samocha, K. E., Cicek, A. E., . . . State, M. W. (2015). Insights into Autism Spectrum Disorder Genomic Architecture and Biology from 71 Risk Loci. *Neuron, 87*(6), 1215-1233. doi:10.1016/j.neuron.2015.09.016

Sanders, S. J., Murtha, M. T., Gupta, A. R., Murdoch, J. D., Raubeson, M. J., Willsey, A. J., . . . State, M. W. (2012). De novo mutations revealed by whole-exome sequencing are strongly associated with autism. *Nature, 485*(7397), 237-241. doi:10.1038/nature10945

Santini, E., Huynh, T. N., MacAskill, A. F., Carter, A. G., Pierre, P., Ruggero, D., . . . Klann, E. (2013). Exaggerated translation causes synaptic and behavioural aberrations associated with autism. *Nature, 493*(7432), 411-415. doi:10.1038/nature11782

Sarachana, T., Xu, M., Wu, R. C., & Hu, V. W. (2011). Sex hormones in autism: androgens and estrogens differentially and reciprocally regulate RORA, a novel candidate gene for autism. *PLoS One, 6*(2), e17116. doi:10.1371/journal.pone.0017116

Scalise, M., Pochini, L., Panni, S., Pingitore, P., Hedfalk, K., & Indiveri, C. (2014). Transport mechanism and regulatory properties of the human amino acid transporter ASCT2 (SLC1A5). *Amino Acids, 46*(11), 2463-2475. doi:10.1007/s00726-014-1808-x

Scattoni, M. L., Crawley, J., & Ricceri, L. (2009). Ultrasonic vocalizations: a tool for behavioural phenotyping of mouse models of neurodevelopmental disorders. *Neurosci Biobehav Rev, 33*(4), 508-515. doi:10.1016/j.neubiorev.2008.08.003

Schmahmann, J. D., Rosene, D. L., & Pandya, D. N. (2004). Motor projections to the basis pontis in rhesus monkey. *J Comp Neurol, 478*(3), 248-268. doi:10.1002/cne.20286

Sharma, N., Mishra, R., & Mishra, D. (2015). The fifth edition of Diagnostic and Statistical Manual of Mental Disorders (DSM-5): what is new for the pediatrician? *Indian Pediatr, 52*(2), 141-143.

Shashi, V., McConkie-Rosell, A., Rosell, B., Schoch, K., Vellore, K., McDonald, M., . . . Goldstein, D. B. (2014). The utility of the traditional medical genetics diagnostic evaluation in the context of next-generation sequencing for undiagnosed genetic disorders. *Genet Med, 16*(2), 176-182. doi:10.1038/gim.2013.99

Shcheglovitov, A., Shcheglovitova, O., Yazawa, M., Portmann, T., Shu, R., Sebastiano, V., . . . Dolmetsch, R. E. (2013). SHANK3 and IGF1 restore synaptic deficits in neurons from

22q13 deletion syndrome patients. *Nature, 503*(7475), 267-271. doi:10.1038/nature12618

Silverman, J. L., Turner, S. M., Barkan, C. L., Tolu, S. S., Saxena, R., Hung, A. Y., . . . Crawley, J. N. (2011). Sociability and motor functions in Shank1 mutant mice. *Brain Res, 1380*, 120-137. doi:10.1016/j.brainres.2010.09.026

Sinclair, L. V., Rolf, J., Emslie, E., Shi, Y. B., Taylor, P. M., & Cantrell, D. A. (2013). Control of amino-acid transport by antigen receptors coordinates the metabolic reprogramming essential for T cell differentiation. *Nat Immunol, 14*(5), 500-508. doi:10.1038/ni.2556

Snyderman, S. E., Norton, P. M., Roitman, E., & Holt, L. E., Jr. (1964). Maple Syrup Urine Disease, with Particular Reference to Dietotherapy. *Pediatrics, 34*, 454-472.

Stone, J. L., Merriman, B., Cantor, R. M., Yonan, A. L., Gilliam, T. C., Geschwind, D. H., & Nelson, S. F. (2004). Evidence for sex-specific risk alleles in autism spectrum disorder. *Am J Hum Genet, 75*(6), 1117-1123. doi:10.1086/426034

Symonds, J. D., Zuberi, S. M., & Johnson, M. R. (2017). Advances in epilepsy gene discovery and implications for epilepsy diagnosis and treatment. *Curr Opin Neurol, 30*(2), 193-199. doi:10.1097/WCO.0000000000000433

Sztainberg, Y., Chen, H. M., Swann, J. W., Hao, S., Tang, B., Wu, Z., . . . Zoghbi, H. Y. (2015). Reversal of phenotypes in MECP2 duplication mice using genetic rescue or antisense oligonucleotides. *Nature, 528*(7580), 123-126. doi:10.1038/nature16159

Sztainberg, Y., & Zoghbi, H. Y. (2016). Lessons learned from studying syndromic autism spectrum disorders. *Nat Neurosci, 19*(11), 1408-1417. doi:10.1038/nn.4420

Tager-Flusberg, H., & Kasari, C. (2013). Minimally verbal school-aged children with autism spectrum disorder: the neglected end of the spectrum. *Autism Res, 6*(6), 468-478. doi:10.1002/aur.1329

Tai, C., Abe, Y., Westenbroek, R. E., Scheuer, T., & Catterall, W. A. (2014). Impaired excitability of somatostatin- and parvalbumin-expressing cortical interneurons in a mouse model of Dravet syndrome. *Proc Natl Acad Sci U S A, 111*(30), E3139-3148. doi:10.1073/pnas.1411131111

Thurman, D. J., Beghi, E., Begley, C. E., Berg, A. T., Buchhalter, J. R., Ding, D., . . . Epidemiology, I. C. o. (2011). Standards for epidemiologic studies and surveillance of epilepsy. *Epilepsia, 52 Suppl 7*, 2-26. doi:10.1111/j.1528-1167.2011.03121.x

Tick, B., Bolton, P., Happe, F., Rutter, M., & Rijsdijk, F. (2016). Heritability of autism spectrum disorders: a meta-analysis of twin studies. *J Child Psychol Psychiatry, 57*(5), 585-595. doi:10.1111/jcpp.12499

Tillotson, R., Selfridge, J., Koerner, M. V., Gadalla, K. K. E., Guy, J., De Sousa, D., . . . Bird, A. (2017). Radically truncated MeCP2 rescues Rett syndrome-like neurological defects. *Nature, 550*(7676), 398-401. doi:10.1038/nature24058

Tilot, A. K., Frazier, T. W., 2nd, & Eng, C. (2015). Balancing Proliferation and Connectivity in PTEN-associated Autism Spectrum Disorder. *Neurotherapeutics, 12*(3), 609-619. doi:10.1007/s13311-015-0356-8

Topper, S., Ober, C., & Das, S. (2011). Exome sequencing and the genetics of intellectual disability. *Clin Genet, 80*(2), 117-126. doi:10.1111/j.1399-0004.2011.01720.x

Trinh, M. A., Kaphzan, H., Wek, R. C., Pierre, P., Cavener, D. R., & Klann, E. (2012). Brain-specific disruption of the eIF2alpha kinase PERK decreases ATF4 expression and impairs behavioral flexibility. *Cell Rep, 1*(6), 676-688. doi:10.1016/j.celrep.2012.04.010

Tsai, P. T., Hull, C., Chu, Y., Greene-Colozzi, E., Sadowski, A. R., Leech, J. M., . . . Sahin, M. (2012). Autistic-like behaviour and cerebellar dysfunction in Purkinje cell Tsc1 mutant mice. *Nature, 488*(7413), 647-651. doi:10.1038/nature11310

Urbach, A., Bar-Nur, O., Daley, G. Q., & Benvenisty, N. (2010). Differential modeling of fragile X syndrome by human embryonic stem cells and induced pluripotent stem cells. *Cell Stem Cell, 6*(5), 407-411. doi:10.1016/j.stem.2010.04.005

Varoqueaux, F., Jamain, S., & Brose, N. (2004). Neuroligin 2 is exclusively localized to inhibitory synapses. *Eur J Cell Biol, 83*(9), 449-456. doi:10.1078/0171-9335-00410

Veenstra-VanderWeele, J., Cook, E. H., King, B. H., Zarevics, P., Cherubini, M., Walton-Bowen, K., . . . Carpenter, R. L. (2017). Arbaclofen in Children and Adolescents with Autism Spectrum Disorder: A Randomized, Controlled, Phase 2 Trial. *Neuropsychopharmacology, 42*(7), 1390-1398. doi:10.1038/npp.2016.237

Verkerk, A. J., Pieretti, M., Sutcliffe, J. S., Fu, Y. H., Kuhl, D. P., Pizzuti, A., . . . et al. (1991). Identification of a gene (FMR-1) containing a CGG repeat coincident with a breakpoint cluster region exhibiting length variation in fragile X syndrome. *Cell, 65*(5), 905-914.

Verrey, F. (2003). System L: heteromeric exchangers of large, neutral amino acids involved in directional transport. *Pflugers Arch, 445*(5), 529-533. doi:10.1007/s00424-002-0973-z

Vicidomini, C., Ponzoni, L., Lim, D., Schmeisser, M. J., Reim, D., Morello, N., . . . Verpelli, C. (2017). Pharmacological enhancement of mGlu5 receptors rescues behavioral deficits in SHANK3 knock-out mice. *Mol Psychiatry, 22*(5), 689-702. doi:10.1038/mp.2016.30

Vissers, L. E., de Ligt, J., Gilissen, C., Janssen, I., Steehouwer, M., de Vries, P., . . . Veltman, J. A. (2010). A de novo paradigm for mental retardation. *Nat Genet, 42*(12), 1109-1112. doi:10.1038/ng.712

Volkmar, F., Siegel, M., Woodbury-Smith, M., King, B., McCracken, J., State, M., . . . Adolescent Psychiatry Committee on Quality, I. (2014). Practice parameter for the assessment and treatment of children and adolescents with autism spectrum disorder. *J Am Acad Child Adolesc Psychiatry, 53*(2), 237-257. doi:10.1016/j.jaac.2013.10.013

Wang, X., Bey, A. L., Katz, B. M., Badea, A., Kim, N., David, L. K., . . . Jiang, Y. H. (2016). Altered mGluR5-Homer scaffolds and corticostriatal connectivity in a Shank3 complete knockout model of autism. *Nat Commun, 7*, 11459. doi:10.1038/ncomms11459

Wang, X., McCoy, P. A., Rodriguiz, R. M., Pan, Y., Je, H. S., Roberts, A. C., . . . Jiang, Y. H. (2011). Synaptic dysfunction and abnormal behaviors in mice lacking major isoforms of Shank3. *Hum Mol Genet, 20*(15), 3093-3108. doi:10.1093/hmg/ddr212

Warren, Z., McPheeters, M. L., Sathe, N., Foss-Feig, J. H., Glasser, A., & Veenstra-Vanderweele, J. (2011). A systematic review of early intensive intervention for autism spectrum disorders. *Pediatrics, 127*(5), e1303-1311. doi:10.1542/peds.2011-0426

Watson, K. K., & Platt, M. L. (2012). Of mice and monkeys: using non-human primate models to bridge mouse- and human-based investigations of autism spectrum disorders. *J Neurodev Disord, 4*(1), 21. doi:10.1186/1866-1955-4-21

Watson, R. E., Desesso, J. M., Hurtt, M. E., & Cappon, G. D. (2006). Postnatal growth and morphological development of the brain: a species comparison. *Birth Defects Res B Dev Reprod Toxicol, 77*(5), 471-484. doi:10.1002/bdrb.20090

Whitney, E. R., Kemper, T. L., Bauman, M. L., Rosene, D. L., & Blatt, G. J. (2008). Cerebellar Purkinje cells are reduced in a subpopulation of autistic brains: a stereological experiment using calbindin-D28k. *Cerebellum, 7*(3), 406-416. doi:10.1007/s12311-008-0043-y

Wolfson, R. L., Chantranupong, L., Saxton, R. A., Shen, K., Scaria, S. M., Cantor, J. R., & Sabatini, D. M. (2016). Sestrin2 is a leucine sensor for the mTORC1 pathway. *Science, 351*(6268), 43-48. doi:10.1126/science.aab2674

Wong, M., & Crino, P. B. (2012). Tuberous sclerosis and epilepsy: role of astrocytes. *Glia, 60*(8), 1244-1250. doi:10.1002/glia.22326

Wood, C. L., Warnell, F., Johnson, M., Hames, A., Pearce, M. S., McConachie, H., & Parr, J. R. (2015). Evidence for ASD recurrence rates and reproductive stoppage from large UK ASD research family databases. *Autism Res, 8*(1), 73-81. doi:10.1002/aur.1414

Yizhar, O., Fenno, L. E., Prigge, M., Schneider, F., Davidson, T. J., O'Shea, D. J., . . . Deisseroth, K. (2011). Neocortical excitation/inhibition balance in information processing and social dysfunction. *Nature, 477*(7363), 171-178. doi:10.1038/nature10360

Young, G. S., Merin, N., Rogers, S. J., & Ozonoff, S. (2009). Gaze behavior and affect at 6 months: predicting clinical outcomes and language development in typically developing infants and infants at risk for autism. *Dev Sci, 12*(5), 798-814. doi:10.1111/j.1467-7687.2009.00833.x

Yuen, R. K., Thiruvahindrapuram, B., Merico, D., Walker, S., Tammimies, K., Hoang, N., . . . Scherer, S. W. (2015). Whole-genome sequencing of quartet families with autism spectrum disorder. *Nat Med, 21*(2), 185-191. doi:10.1038/nm.3792

Zarafshan, H., Salmanian, M., Aghamohammadi, S., Mohammadi, M. R., & Mostafavi, S. A. (2017). Effectiveness of Non-Pharmacological Interventions on Stereotyped and Repetitive Behaviors of Pre-school Children With Autism: A Systematic Review. *Basic Clin Neurosci, 8*(2), 95-103. doi:10.18869/nirp.bcn.8.2.95

Zarei, M., Mataix-Cols, D., Heyman, I., Hough, M., Doherty, J., Burge, L., . . . James, A. (2011). Changes in gray matter volume and white matter microstructure in adolescents with obsessive-compulsive disorder. *Biol Psychiatry, 70*(11), 1083-1090. doi:10.1016/j.biopsych.2011.06.032

Zeisel, A., Munoz-Manchado, A. B., Codeluppi, S., Lonnerberg, P., La Manno, G., Jureus, A., . . . Linnarsson, S. (2015). Brain structure. Cell types in the mouse cortex and hippocampus revealed by single-cell RNA-seq. *Science, 347*(6226), 1138-1142. doi:10.1126/science.aaa1934

Zhou, J., Blundell, J., Ogawa, S., Kwon, C. H., Zhang, W., Sinton, C., . . . Parada, L. F. (2009). Pharmacological inhibition of mTORC1 suppresses anatomical, cellular, and behavioral abnormalities in neural-specific Pten knock-out mice. *J Neurosci, 29*(6), 1773-1783. doi:10.1523/JNEUROSCI.5685-08.2009

Zhubi, A., Cook, E. H., Guidotti, A., & Grayson, D. R. (2014). Epigenetic mechanisms in autism spectrum disorder. *Int Rev Neurobiol, 115*, 203-244. doi:10.1016/B978-0-12-801311-3.00006-8

Zinnanti, W. J., Lazovic, J., Griffin, K., Skvorak, K. J., Paul, H. S., Homanics, G. E., . . . Flanagan, J. M. (2009). Dual mechanism of brain injury and novel treatment strategy in maple syrup urine disease. *Brain, 132*(Pt 4), 903-918. doi:10.1093/brain/awp024

6 Appendix 1. Supplemental figures and tables

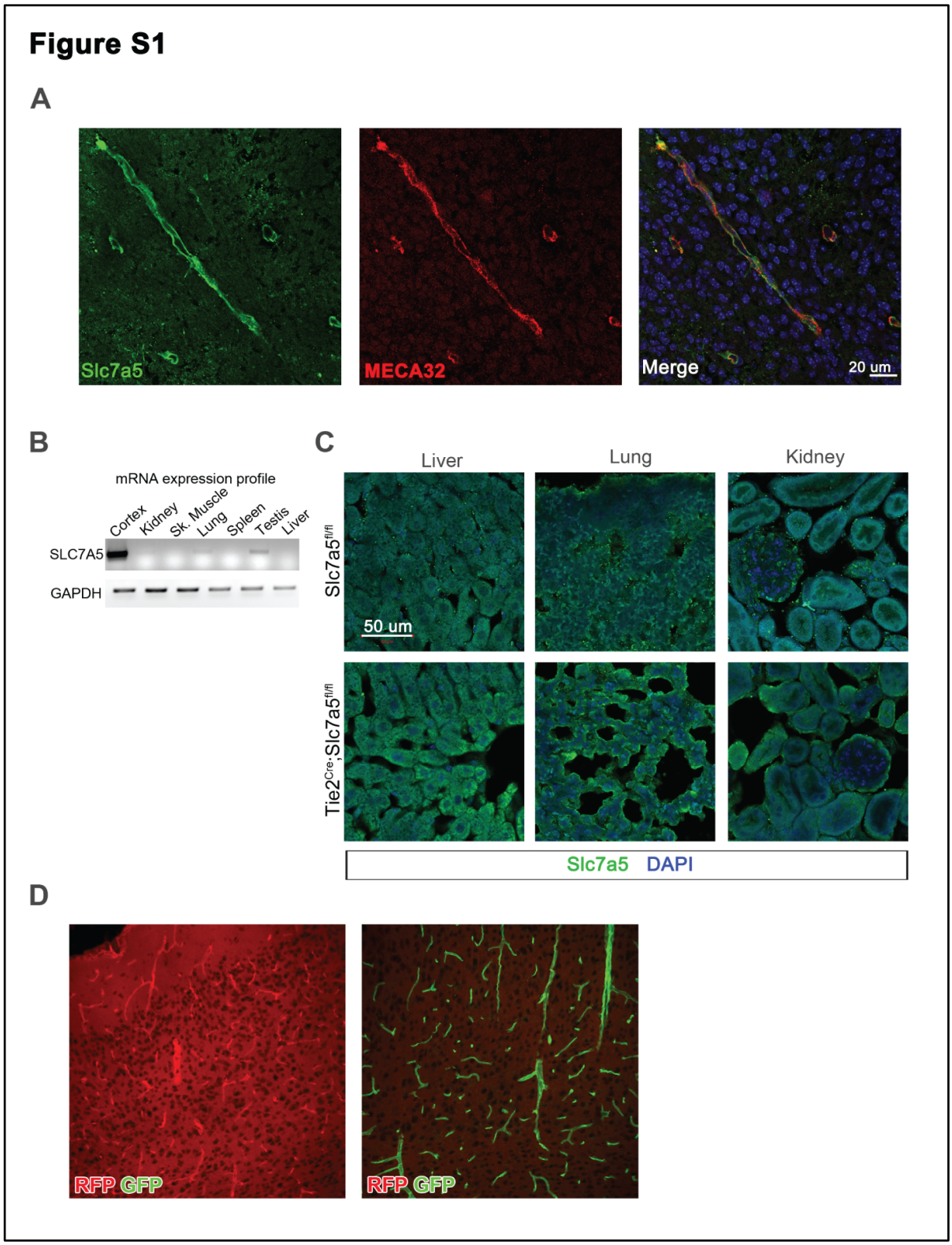

Figure S 1. Slc7a5 *and* Tie2Cre *expression at the BBB, Related to Figure 6*

(A) Representative images of cortical slices stained with Slc7a5 (left) and the endothelial cell marker MECA 32 (middle) antibodies. The merged image (right) displays the co-localization of the two markers in control animals.
(B) Human mRNA expression profile in different tissues (top) reveals almost exclusive expression of SLC7A5 in the cortex. Sampled tissues are: cortex, kidney, skeletal muscle, lung, spleen, testis, liver. GAPDH (bottom) was used as internal control.
(C) Representative Slc7a5 (green) immunostained mouse tissue slices from control *Slc7a5*$^{fl/fl}$ (top) and mutant *Tie2*^{Cre}*Slc7a5*$^{fl/fl}$ (bottom) animals. Tissues were sampled from adult (>P40) mice and they include: liver (left), lung (middle) and kidney (right). Nuclei were stained with DAPI (blue).
(D) Tie2-driven Cre recombinase expression in the BBB was verified by crossing *Tie2*^{Cre} mice with the reporter line Gt26Sor. Gt26Sor mice express cell-membrane localized red fluorescencent protein (RFP) in widespread cells and tissues prior to Cre recombinase exposure and cell membrane-localized green fluorescencent protein (GFP) in Cre recombinase expressing cells. Note GFP staining in the endothelial cells of the BBB (right). Images were obtained from the cerebral cortex of 2 days old (P2) mice. Immunohistochemical staining was done by Mike Liu.

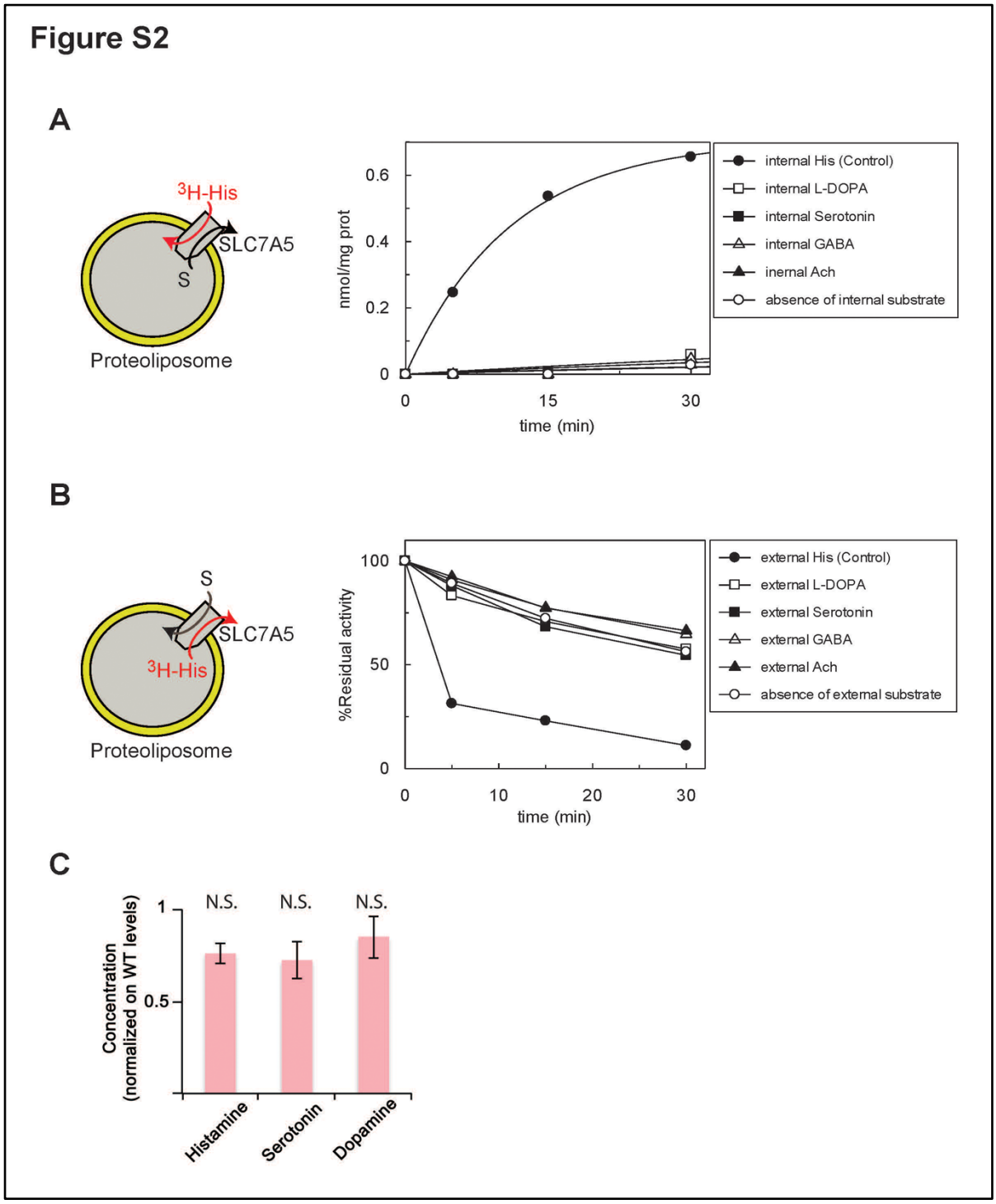

Figure S 2. Slc7a5 *does not transport neurotransmitters, Related to Figure 6*

(A-B) Left: Schematic of the in vitro transport assay - transport followed as uptake (A) of external [^{3}H]His in exchange to internal substrate (S) or as efflux (B) of internal [^{3}H]His in exchange with external substrate (S) in proteoliposomes with reconstituted SLC7A5 protein. Right: SLC7A5-mediated His uptake (A) and efflux (B) analysis indicates the inability of SLC7A5 to transport the tested neurotransmitters. Transport was started by adding 5 µM [^{3}H]His at time 0 to proteoliposomes containing 10 mM His, or the tested neurotransmitter, reconstituted with human SLC7A5 and stopped at the indicated times. Percentage of His efflux (B, % Residual activity) was calculated with respect to time 0 for each experimental condition. His-histidine; L-DOPA, L-3,4-dihydroxyphenylalanine; Ach-acethylcholine.

(C) Normal brain neurotransmitter levels in brain lysates of *Tie2^{Cre};Slc7a5$^{fl/fl}$* (red bars) mice. Neurotransmitter levels were quantified by HPLC and normalized on protein concentration and on control (*Tie2^{Cre};Slc7a5^{fl}/+*, grey bars) littermate levels (means ± SD; n=4 mice per genotype).
Proteoliposome study was done by Michele Galluccio, Mariafrancesca Scalise and Cesare Indiveri – University of Calabria.

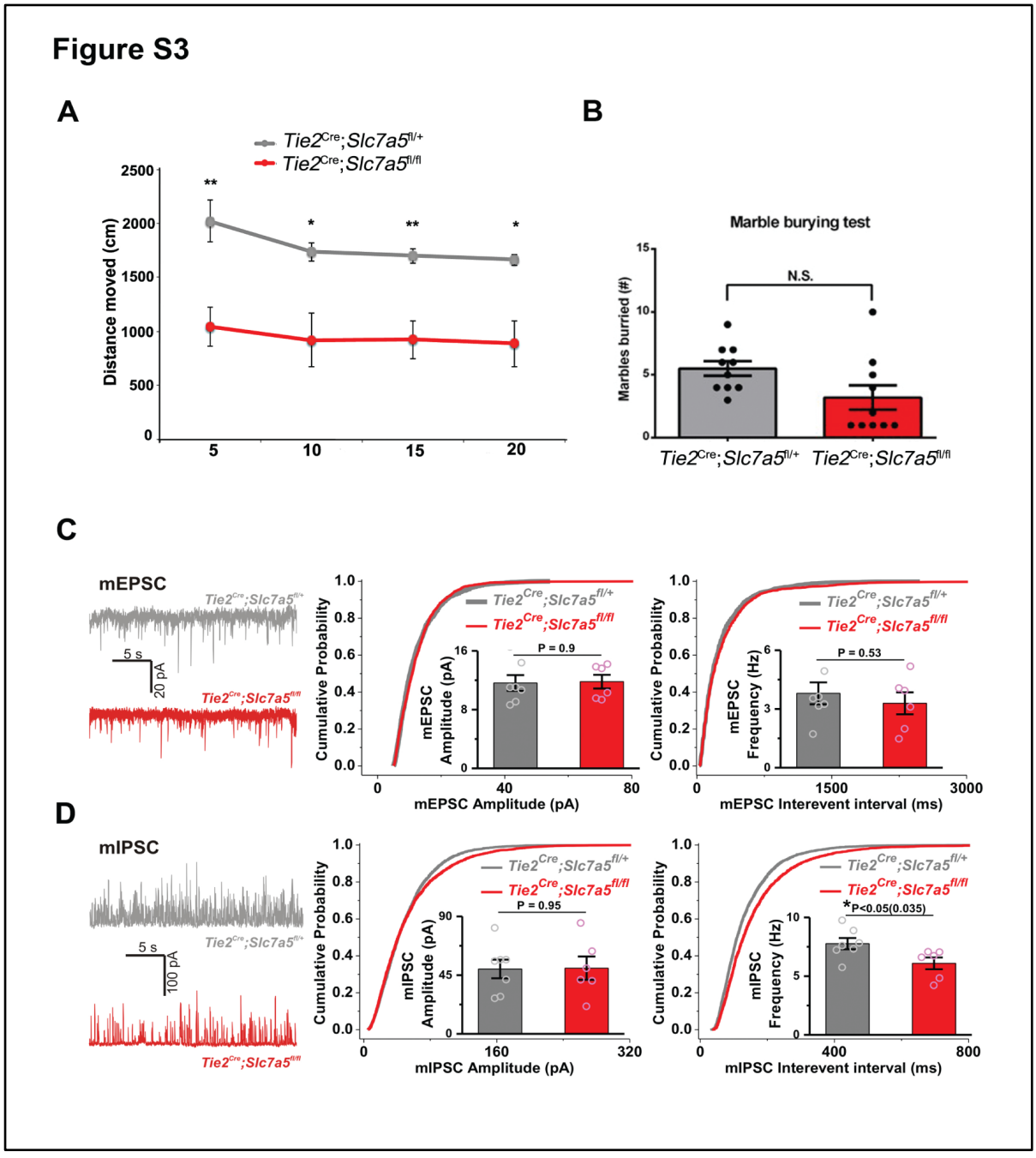

Figure S 3. Behavioral and electrophysiological alterations in Tie^{2Cre};Slc7a5$^{fl/fl}$ *mice, Related to Figure 8 and 9*

(A) *Tie2^{Cre};Slc7a5$^{fl/fl}$* (red) and *Tie2^{Cre};Slc7a5$^{fl/+}$* (grey) show similar habituation kinetics in the open field. Distance moved in the open field was analyzed in 5-minute bins over the course of 20 minutes. *Tie2^{Cre};Slc7a5$^{fl/fl}$* mice moved less at all given points *P<0.05, **P<0.01 (means ± SEM; n=10 mice per genotype).

(B) Marble burying test shows no significant difference between the number of marbles buried by the control *Tie2^{Cre};Slc7a5$^{fl/+}$* and the mutant *Tie2^{Cre};Slc7a5$^{fl/fl}$*; N.S., not significant (means ± SEM; n=10 mice per genotype; circles represent individual values).
(C-D) Left: Representative mEPSC (B) and mIPSC (C) recordings from *Tie2^{Cre};Slc7a5$^{fl/+}$* (grey) and *Tie2^{Cre};Slc7a5$^{fl/fl}$* (red) cerebellar Purkinje cells. Right: Cumulative probability distributions of peak amplitudes and interevent intervals of mEPSC (B) and mIPSC (C) in the two genotypes. Insets: quantifications of mean amplitudes and mean frequencies of the corresponding currents, along with absolute P values. Significant reduction in mIPSC mean frequency in mutants versus controls is indicated. Result confirmed by cumulative probability distribution analysis, Kolmogorov-Smirnov test: D=0.109; *P<0.05 (means ± SEM; $n_{cells}/n_{animals}$/genotype: 7/3/*Tie2^{Cre};Slc7a5$^{fl/+}$* and 6/3/*Tie^{2Cre};Slc7a5$^{fl/fl}$;* circles indicate individual values). mEPSCs and mIPSCs were recorded from the same cell. Elctrophysiological experiment was done by Elena Deliu – IST Austria.

Figure S4

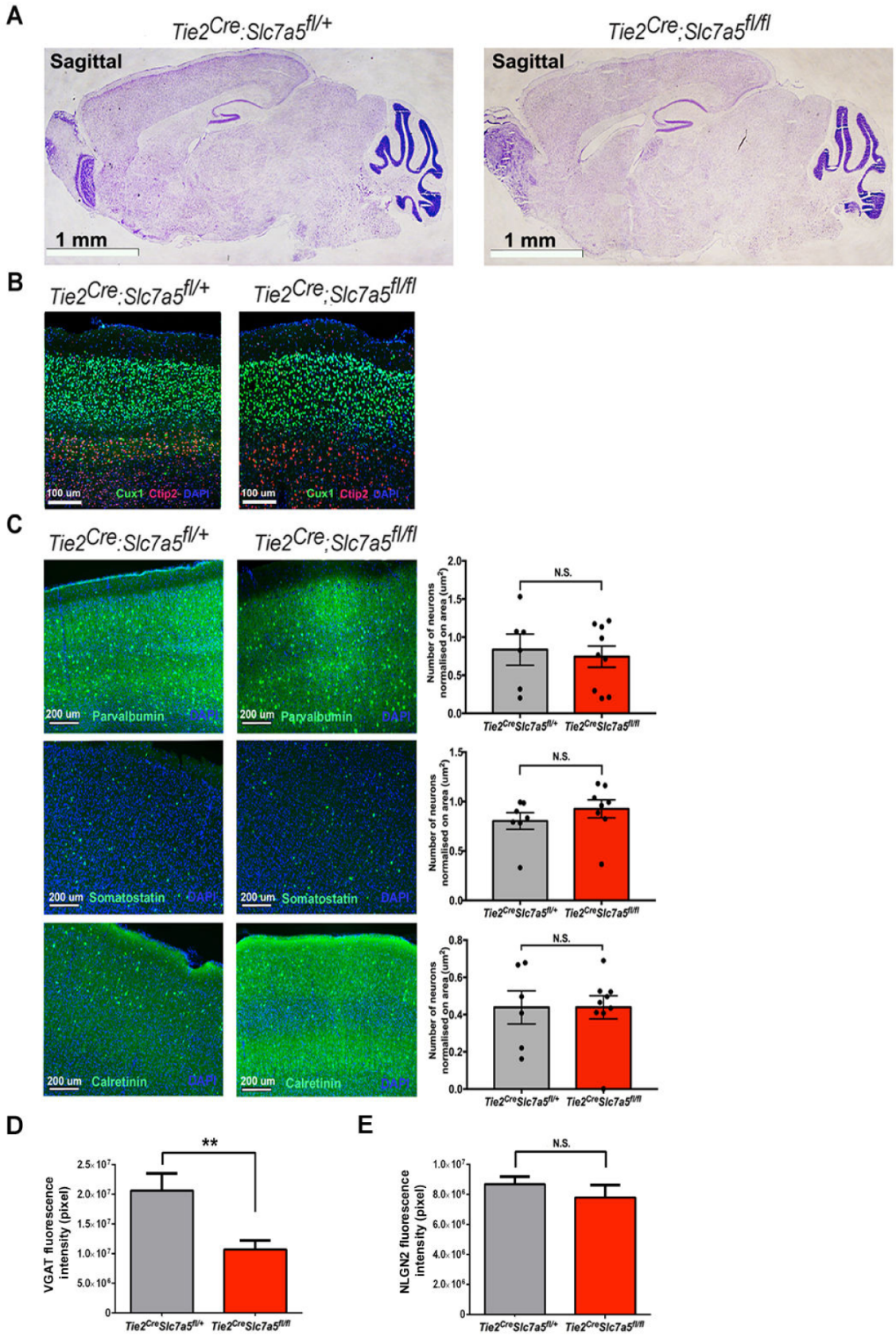
A
Tie2Cre:Slc7a5fl/+
Tie2Cre;Slc7a5fl/fl
Sagittal
Sagittal
1 mm
1 mm
B
Tie2Cre:Slc7a5fl/+
Tie2Cre;Slc7a5fl/fl
100 um Cux1 Ctip2 DAPI
100 um Cux1 Ctip2 DAPI
C
Tie2Cre:Slc7a5fl/+
Tie2Cre;Slc7a5fl/fl
200 um Parvalbumin DAPI
200 um Parvalbumin DAPI
200 um Somatostatin DAPI
200 um Somatostatin DAPI
200 um Calretinin DAPI
200 um Calretinin DAPI
Number of neurons normalised on area (um2)
N.S.
Tie2CreSlc7a5fl/+ Tie2CreSlc7a5fl/fl
D
VGAT fluorescence intensity (pixel)
**
E
NLGN2 fluorescence intensity (pixel)
N.S.

Figure S 4. Absence of gross alterations in brain architecture of $Tie^{2Cre};Slc7a5^{fl/fl}$ *mice, Related to Figure 9.*

(A) Nissl staining of sagittal sections of adult mouse brain indicating no differences in gross morphology between the control $Tie2^{Cre};Slc7a5^{fl/+}$ and mutant $Tie2^{Cre};Slc7a5^{fl/fl}$ mice. Scale bar = 1 mm.
(B) Immunostaining of Cux1 (green, upper layer neurons) and Ctip2 (red, lower layer neurons) shows similar cortical layer distribution in the two genotypes. Scale bar = 100 um.
(C) Representative images (left) and quantifications (right) indicating similar numbers of parvalbumin- (top), somatostatin- (middle) and calretinin- (bottom) positive interneurons in the cortices of wild-type and mutant mice; N. S., not significant (means ± SEM; n=3 mice per genotype; filled circles indicate individual values). Nuclei were stained with DAPI (blue). Scale bar = 200 um.
(D) Fluorescence intensity quantification of VGAT puncta in control $Tie2^{Cre};Slc7a5^{fl/+}$ compared to mutant $Tie2^{Cre};Slc7a5^{fl/fl}$ mice; **P<0.01 (means ± SEM; n=3 mice per genotype).
(E) Fluorescence intensity quantification of NLGN2 puncta displaying no difference between control $Tie2^{Cre};Slc7a5^{fl/+}$ and mutant $Tie2^{Cre};Slc7a5^{fl/fl}$ mice; N.S., not significant (means ± SEM; n=3 mice per genotype).

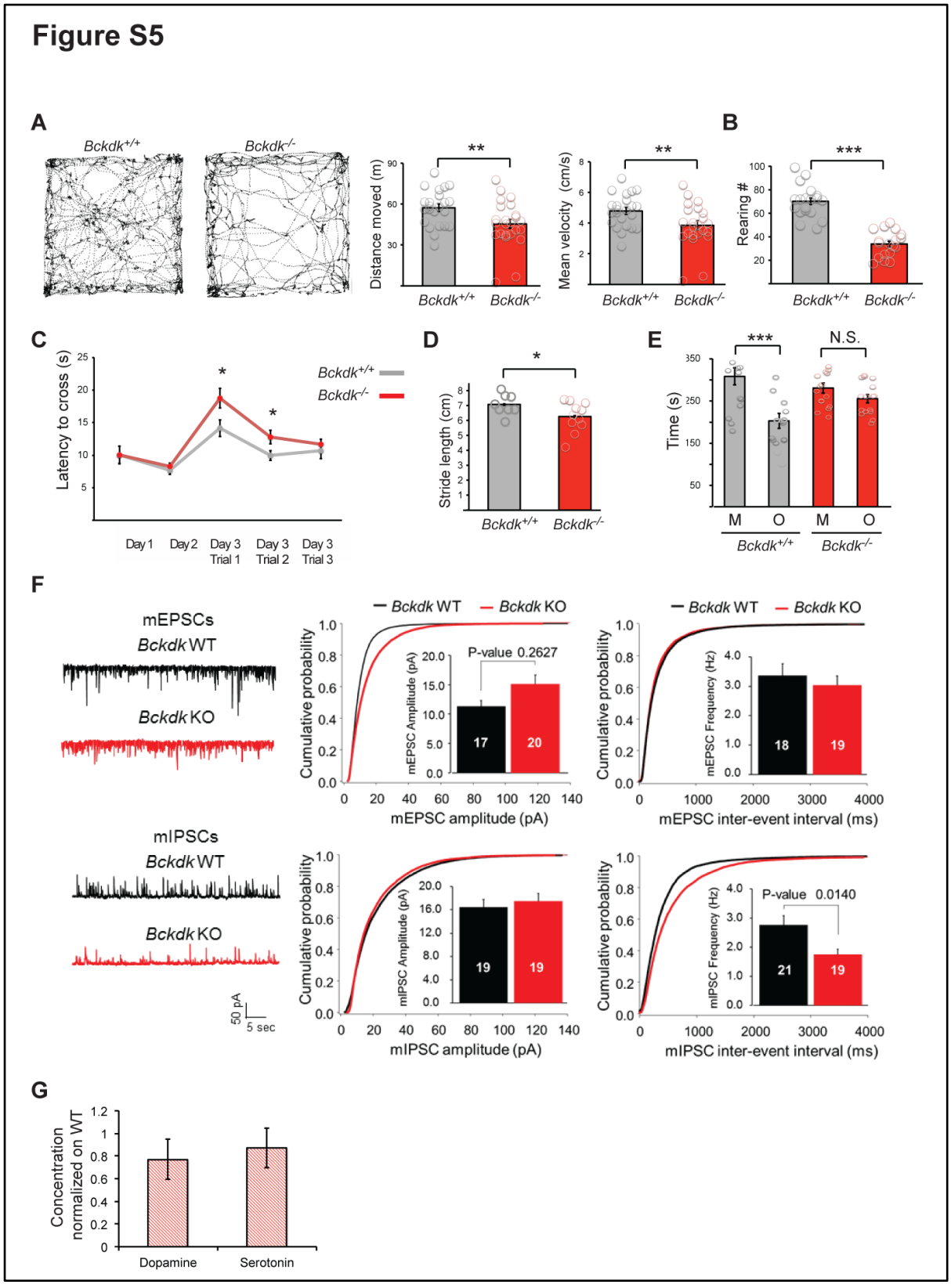

Figure S 5. Phenotypic characterization of Bckdk$^{-/-}$ *animals, Related to Figure 9.*

(A) Representative open field trajectories (left) and quantification of the total distance moved (middle) and the velocity during exploration (right); **P<0.01 (means ± SEM; n=25 mice per genotype; circles indicate individual values).

(B) Comparison of the number of rearings (anxiogenic forms of vertical exploration) of the two genotypes during the open field test, pointing out deficiencies in the mutants; ***P<0.001 (means ± SEM; n=18 mice per genotype; circles indicate individual values).
(C) Performance on the walking beam throughout the training days (Day1, Day2) and the three trials on the test day (Day3), showing elevated latency to cross the beam in the mutants; *P<0.05 (means ± SEM; n=23 mice per genotype).
(D) Stride length quantifications in the gait test reveal locomotor deficiencies in *Bckdk*$^{-/-}$ mice; *P<0.05 (means ± SEM; n=20 mice per genotype; circles indicate individual values).
(E) Bar graph quantifications of the number of contacts with the caged mouse (M) or with the caged object (O) in the three-chamber sociability test, revealing abnormal social interaction pattern in the mutant mice (mutants show no preference for the M over O, as opposed to controls); ***P<0.001, N.S., not significant (means ± SEM; n=16 mice per genotype; circles indicate individual values).
(F) Left: Representative mEPSC (top) and mIPSC (bottom) recordings from control *Bckdk*$^{+/+}$ (black) and *Bckdk*$^{-/-}$ (red) somatosensory cortex layers 2-3 pyramidal neurons; Right: Cumulative probability distributions of peak amplitudes and interevent intervals of mEPSC (top) and mIPSC (bottom) in the two genotypes. Insets: quantifications of mean amplitudes and mean frequencies of the corresponding currents. The significant reduction in mIPSC mean frequency detected in the mutants versus controls is indicated as absolute P value: *P<0.05 (means ± SEM; n>3 animals/genotype; number of recorded cells is noted on each column).
(G) Normal brain neurotransmitter levels in brain lysates of *Bckdk*$^{-/-}$ mice. Neurotransmitter levels were quantified by HPLC and normalized on protein concentration and on control littermate (*Bckdk*$^{+/+}$) levels; N.S., not significant (means ± SEM; n=4 mice per genotype).
Bckdk$^{-/-}$ experiments were done by Emanuela Morelli.

Figure S6

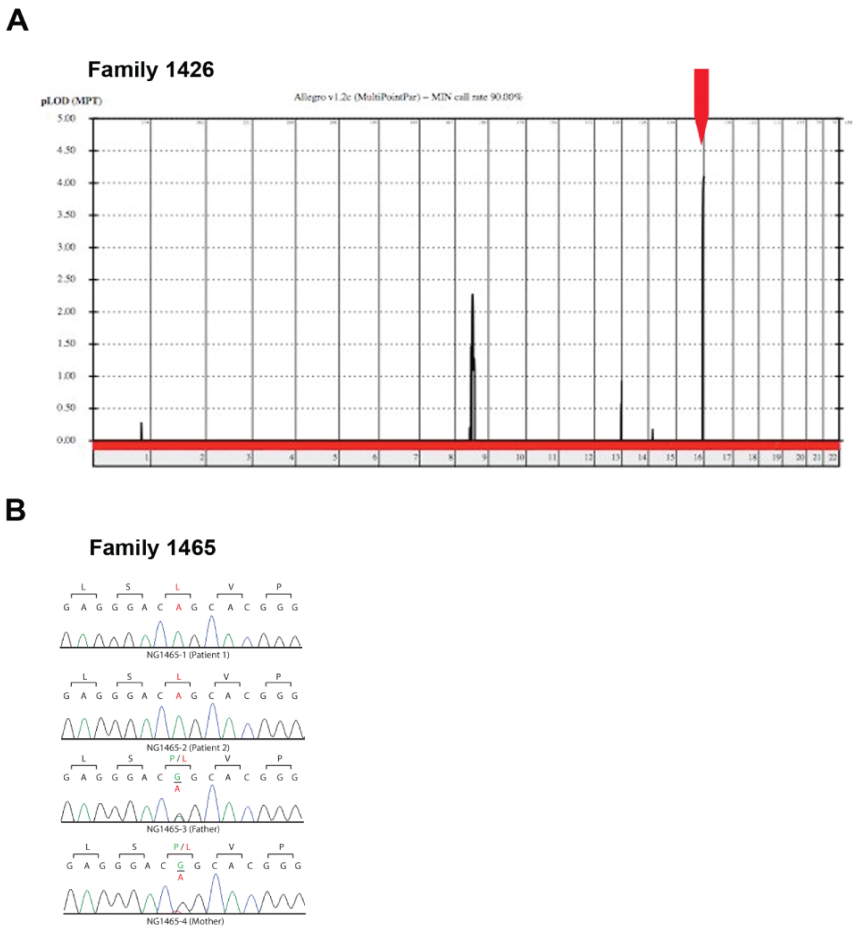

Figure S 6. Genotyping information of Family 1426 and 1465, Related to Figure 10.

(A) Homozygosity map for Family 1426. Blocks of homozygosity are depicted as peaks. The red arrow indicates the interval that includes *SLC7A5*.
(B) Sequence chromatograms of all members of Family 1465 including the affected siblings and the carrier parents.
WES was done by Ahmet Okay Caglayan and Gaia Novarino.

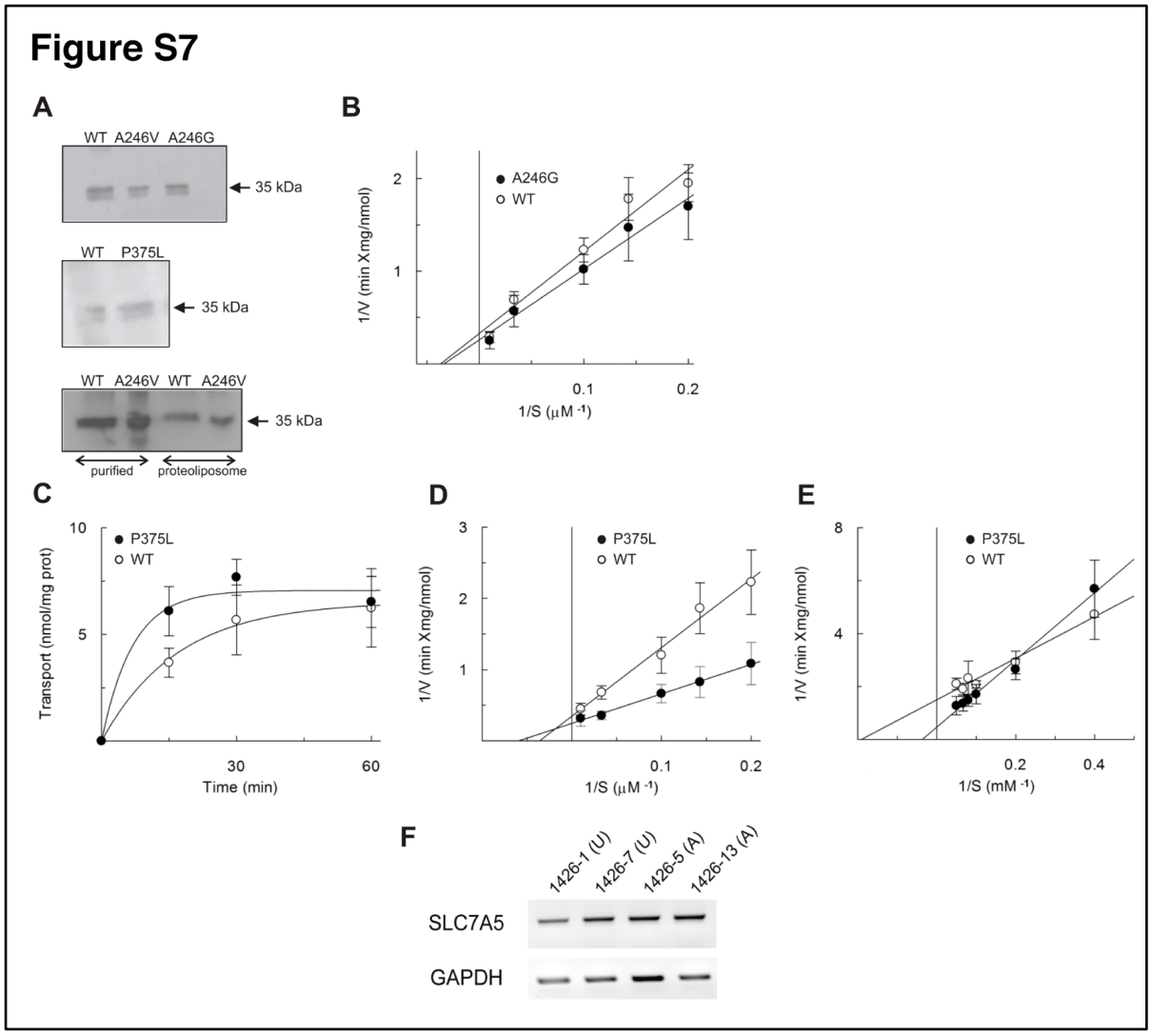

Figure S 7. Characterization of SLC7A5-A246V, -A246G and SLC7A5-P375L mutants, Related to Figure 11.

(A) Western blot analysis of the indicated SLC7A5 mutants in comparison with the WT protein reconstituted in proteoliposomes (top and middle panels). To evaluate the efficiency of reconstituted SLC7A5, proteoliposomes reconstituted with WT or SLC7A5 A246V were separated from liposomes (not containing reconstituted protein) by ultracentrifugation; blots of reconstituted proteins (proteoliposome) and of the purified protein before reconstitution (purified) are included in the bottom panel.

(B) SLC7A5-WT and SLC7A5-A246G-mediated transport rate (upon reconstitution in proteoliposomes) is dependent on external His concentration showing similar patterns for the two proteins. [^{3}H]-His was added at the indicated concentration to proteoliposomes containing 10 mM His, and transport stopped after 10 min (i.e. within the initial linear range of the time course). Data were fitted according to Lineweaver–Burk plot as reciprocal transport rate vs reciprocal His concentration (means ± SD; n=3 independent experiments).

(C) Time-course of the transport mediated by SLC7A5-WT and P375L reconstituted in proteoliposomes, showing that the P375L mutant protein is functional. Transport was started by adding 5 μM [^{3}H]His at time zero to proteoliposomes containing 10 mM His reconstituted with WT- or P375L- SLC7A5 and stopped at the indicated times as described in the Experimental Procedure (means ± SD; n=5 independent experiments).

(D) Rate of SLC7A5-mediated transport dependent on external His concentration. Transport rate was measured adding [^{3}H]His at the indicated concentration to proteoliposomes containing 10 mM His reconstituted with WT- or P375L-SLC7A5 protein. Transport was stopped after 10 min, i.e., within the initial linear range of the time course. Data were fitted according to Lineweaver–Burk plot as reciprocal transport rate vs reciprocal His concentration. (Means ± SD; n=3 independent experiments).

(E) Rate of SLC7A5-mediated transport dependent on internal His concentration. Transport rate was measured adding 50 μM [^{3}H]His to proteoliposomes, containing the indicated His concentrations, reconstituted with WT-

or P375L- SLC7A5 protein. Transport was stopped after 10 min, i.e., within the initial linear range of the time course. Data were fitted according to Lineweaver-Burk (or Michaelis-Menten) plot as reciprocal transport rate vs reciprocal His concentration. (Means ± SD; n=3 independent experiments).
(F) Representative immunoblot showing *SLC7A5* transcript expression in human dermal fibroblasts; expression level is not affected by the A246V missense mutation (n=3 independent experiments).
Proteoliposome study was done by Michele Galluccio, Mariafrancesca Scalise and Cesare Indiveri – University of Calabria, Italy.

Table S 1.

Table S1. Serum amino acid profile, Related to Figure 5

Amino acid	*Slc7a5*$^{fl/+}$;*Tie2*^{Cre}	*Slc7a5*$^{fl/fl}$;*Tie2*^{Cre}
4-AMINOBUTYRIC ACID	0,71 +/- 0,12	0,45 +/- 0,25
4-HYDROXYPROLINE	15,96 +/- 2,79	11,77 +/- 5,94
ALANINE	837,42 +/- 161,14	648,79 +/- 91,05
ARGININE	172,17 +/- 84,57	137,68 +/- 16,67
ASPARAGINE	37,98 +/- 11,83	31,15 +/- 7,23
ASPARTIC ACID	14,57 +/- 5,79	9,65 +/- 1,83
CITRULLINE	104,9 +/- 13,13	97,42 +/- 10,97
CYSTINE	5,15 +/- 1,81	2,12 +/- 0,55
GLUTAMIC ACID	125,52 +/- 36,6	124,86 +/- 39,36
GLUTAMIN	1072,97 +/- 191,3	1063,33 +/- 194,95
GLYCINE	440,03 +/- 55,91	402,34 +/- 47,3
HISTIDINE	84,98 +/- 9,92	82,67 +/- 7,19
ISOLEUCINE	81,69 +/- 19,26	85,29 +/- 9,76
LEUCINE	170,93 +/- 40,01	173,66 +/- 14,88
LYSINE	387,39 +/- 81,18	346,79 +/- 42,39
METHIONINE	76,58 +/- 17,9	63,54 +/- 8,17
ORNITHINE	105,02 +/- 33,1	68,11 +/- 8,79
PHENYLALANINE	104,88 +/- 25,57	98,44 +/- 7,53
PROLINE	155,95 +/- 67,36	96,76 +/- 20,59
SERINE	201,36 +/- 36,26	199,09 +/- 29,73
THREONINE	194,8 +/- 56,9	175,1 +/- 28,61
THYROSINE	100,41 +/- 26,39	84,72 +/- 18,65
TRYPTOPHAN	118,39 +/- 33,66	116,48 +/- 23,42
VALINE	305,33 +/- 77,64	266,69 +/- 24,86

Table S 2.

Table S2. Segregating, rare variants discovered in the affected individuals using whole-exome sequencing, Related to Figure 9

Family	Chr	Position	Ref Allele	Mut Allele	Gene	Function	AA Change	AA Position	Conservation	Allele Frequency	phast Cons	GERP
Family 1426												
	16	87874689	G	A	*SLC7A5*	missense	ALA/VAL	246/508	AAAAAAA-AAAAAAA-AA-AAAAAAAA-AA-A-AAAAA-AAAAAAA	0.001	1	4.72
Family 1465												
	2	111542319	CA	C	ACOXL	frameshift	T29	29/580	TTTTTTTT-TTT-TT-TRTRRTTTT-KTKM-TKK----------	0.0004	0.261	0.185
	16	89986498	A	G	MC1R TUBB3	missense	K278E	278/317	KK-KKKKK-/-KKQK-RK/KQKKQK-KK-KK-K-QQ/SSSNYRSRRR-/--	0.013	0.93	-0.119
	22	25131681	G	T	PIWIL3	missense	A543E	543/882	AAAAAA---/PAAG-----/-A---A---PA-------/---AA-A-AA-/PG	0.0064	0.004	0.716
	22	24226213	T	C	SLC2A11,	splice_donor	R259Q	259/496	RX-R--WLW/R--R-RWL/-R--RRR-Q-RR-R---/----KKKKKE-/--	0.0026	1	1.57
	16	87871467	G	A	SLC7A5	missense	P375L	375/508	PPPPP--P-/--PP---P/PPPPPPPPP-PP-P-PP/PPP-PPPPPPP/PP	0.0003	1	4.79

Table S 3.

Table S3. Brain amino acid levels after leucine and isoleucine i.c.v. administration, Related to Figure 11

	$Slc7a5^{fl/fl}$	$Tie2^{Cre};Slc7a5^{fl/fl}$
GLUTAMIN	1 ± 0.51	1.25 ± 0.20
CITRULLINE	1 ± 0.21	1.07 ± 0.15
SERINE	1 ± 0.39	2.66 ± 0.25 **
4-HYDROXYPROLINE	1 ± 0.55	0.96 ± 0.13
GLYCINE	1 ± 0.36	2.07 ± 0.18 **
THREONINE	1 ± 0.53	2.25 ± 0.14 **
GABA	1 ± 0.32	0.88 ± 0.08
PROLINE	1 ± 0.22	1.58 ± 0.11 **
HISTIDINE	1 ± 0.55	4.51 ± 0.60 **
VALINE	1 ± 0.32	0.94 ± 0.11
TRYPTOPHAN	1 ± 0.37	2.25 ± 0.43 **
PHENYLALANINE	1 ± 0.31	2.01 ± 0.15 **
LEUCINE	1 ± 0.23	0.96 ± 0.13
ISOLEUCINE	1 ± 0.25	1.09 ± 0.17
THYROSINE	1 ± 0.33	2.17 ± 0.18 **

Relevant brain amino acids were measured by HPLC. Levels measured in the mutant mice were normalized on control level.

Table S4. Mutagenesis primer sequences, Related to Methods

Primer name	Primer sequence
A246G Forward	GTGGGGAACATTGTGCTGGGCTTATACAGCGGCCTCTTTGC
A246V Forward	GTGGGGAACATTGTGCTGGTGTTATACAGCGGCCTCTTTGC
P375L Forward	CTCCTCACCCCCGTGCTGTCCCTCGTGTTCACG
A246G Reverse	GCAAAGAGGCCGCTGTATAAGCCCAGCACAATGTTCCCCAC
A246V Reverse	GCAAAGAGGCCGCTGTATAACACCAGCACAATGTTCCCCAC
P375L Reverse	CGTGAACACGAGGGACAGCACGGGGGTGAGGAG

Table S 5.

Table S5. Plasma amino acid levels from members of family 1426, Related to Methods (Human subjects)

Amino Acid	1426-12 (U)	1426-6 (A)	Normal range (2-18 years old)
Glycine	226.1	215.9	127-341
Ornithine	22.7	15.1	10-163
Arginine	0.9	0.5	10-140
Citrulline	10.2	11.7	1-46
Alanine	601.1	579.3	152-547
Serine	189.4	202.2	69-187
Valine	219.1	164.0	74-321
Threonine	48.7	50.4	35-226
Leucine+Isoleucine	189.3	148.8	N.A.
Methionine	20.1	18.6	7-47
Histidine	71.5	46.0	41-125
Phenylalanine	71.9	58.4	N.A.
Tyrosine	57.6	51.0	24-115
Aspartate	7.7	23.0	1-24
Glutamate	59.7	131.1	5-150

Plasma amino acids were quantified on bloodspot cards by FIA-MS or LC-MS/MS at the Mayo Clinic (Novarino et al. 2012). U, unaffected; A, affected. Values are expressed in nmol/ml.